INFLUENCE OF SIMPLIFICATIONS IN WATERSHED GEOMETRY IN SIMULATION OF SURFACE RUNOFF

by
L. J. Lane,
D. A. Woolhiser,
and
V. Yevjevich

December 1975

HYDROLOGY PAPERS
COLORADO STATE UNIVERSITY
Fort Collins, Colorado

81

INFLUENCE OF SIMPLIFICATIONS IN WATERSHED GEOMETRY IN SIMULATION OF SURFACE RUNOFF

by
L. J. Lane,*
D. A. Woolhiser,**
and
V. Yevjevich***

HYDROLOGY PAPERS
COLORADO STATE UNIVERSITY
FORT COLLINS, COLORADO 80521

*Hydrologist, USDA, ARS, Tucson, Arizona
**Research Hydraulic Engineer, USDA, ARS, Fort Collins, Colorado
***Professor of Civil Engineering, Colorado State University, Fort Collins, Colorado

December 1975

No. 81

TABLE OF CONTENTS

Chapter		Page
	ACKNOWLEDGMENTS	iv
	ABSTRACT	iv
I	INTRODUCTION	1
	1.1 General Statements	1
	1.2 Scope and Objectives	1
	1.3 Brief Review of Relevant Literature	1
II	BASIC MODELS	5
	2.1 Watershed Geometry: Cascade of Planes and Channels	5
	2.2 Rainfall Excess-Surface Runoff: Kinematic Cascade	6
	2.3 Summary of Modeling Procedure	6
III	ANALYSIS OF OVERLAND FLOW OVER UNIFORM AND COMPLEX SLOPES	8
	3.1 Equations for Description of Overland Flow Surfaces	8
	3.2 Determination of Characteristic Time for a Plane	8
	3.3 Storage at Equilibrium	11
	3.4 Kinematic Impulse Response	12
	3.5 Pulse Response	20
	3.6 Response to Complex Input	21
IV	RUNOFF FROM COMPLEX WATERSHEDS	23
	4.1 Geometric Simplification	23
	4.2 Goodness-of-Fit Statistics for the Simplified Geometry	30
	4.3 Goodness-of-Fit Statistics for Hydrograph Fitting	31
	4.4 Relating Statistics of the Simplified Geometry to Statistics of the Fitted Hydrographs	35
	4.5 Relation Between Combined Goodness-of-Fit Statistics and Hydraulic Roughness Parameters	39
V	PARAMETER ESTIMATION AND MODEL TESTING	41
	5.1 Selection Criteria for Simplified Geometry	41
	5.2 Determination of Roughness Parameters	42
	5.3 Model Testing	42
VI	CONCLUSIONS AND RECOMMENDATIONS	47
	6.1 Conclusions	47
	6.2 Recommendations for Further Research	47
	REFERENCES	49

ACKNOWLEDGMENTS

This paper is based on the Ph.D. thesis by L. J. Lane at Colorado State University. The support of the Agricultural Research Service of the United States Department of Agriculture is gratefully acknowledged. Particular thanks are due K. G. Renard and the staff of the Southwest Watershed Research Center of the Agricultural Research Service at Tucson, Arizona, and to the Colorado-Wyoming Area, Agricultural Research Service at Fort Collins, Colorado.

The encouragement and assistance given by S. A. Schumm, M. M. Siddiqui, and D. B. McWhorter are thankfully acknowledged.

Vijay Singh provided several computer programs and a great bulk of hydrologic data. Randy Parker generously provided data from his experimental work and Professor Freeman Smith provided information from the Pawnee Site.

The publication of this paper is partially supported by Colorado State University Experiment Station Project 1372-1114(Mathematical Modeling of Small Watersheds).

ABSTRACT

In formulating the equations describing the flow of water on the surface of a watershed, geometric simplifications (the substitution of a simple geometry for a more complex one) must be made. The problem is to examine techniques for and consequences of such simplifications; and thereby to develop objective procedures for geometric simplification of complex watersheds. Watershed geometry is represented by a series of planes and channels in cascade. When overland flow and open channel flow in the cascade are described by the kinematic wave equations the resulting mathematical model is called the "kinematic cascade model."

Planes are fitted to coordinate data from topographic maps by a least squares procedure. Residuals of this fit form a geometric goodness-of-fit statistic as the improvement over using the mean elevation. Channel elements are determined using Gray's method, as the slope of the hypotenuse of a right triangle with the same area as that under the observed stream profile. The ratio of the altitude of this right triangle to the total relief of a stream is the index of concavity, a channel goodness-of-fit statistic. An overall goodness-of-fit statistic is the drainage density ratio (the ratio of drainage density in the cascade of planes and channels to drainage density of the watershed).

The kinematic impulse response is the solution of the kinematic cascade model for an impulse (instantaneous) input. For overland flow, peak discharge of the impulse response is affected more by the shape of the overland flow surface than is the characteristic time. Peak discharge of the kinematic impulse response is greater for parabolic than for uniform slope surfaces. These differences in peak discharge are greater for laminar than for turbulent flow. A goodness-of-fit statistic measuring how well a cascade of planes fits a parabolic slope is related to the resulting peak discharge of the impulse response from the parabolic surface and from the cascade of planes approximation. This statistic can also be used to determine the number of planes in cascade necessary to approximate the kinematic impulse response from a parabolic surface.

For a concave channel, the index of concavity is related to the error in peak discharge of a routed hydrograph when the channel slope is assumed uniform. Using the equivalent, or Gray's slope, results in less error than using a uniform slope estimated as the total channel relief over the length. For a channel system, underestimating the drainage density results in overestimated time characteristics and underestimated peak discharge. Moreover, lag time, as the first moment of a linear instantaneous unit hydrograph, decreases as drainage density increases. The degree of apparent nonlinearity is affected by drainage density as a measure of the relative proportions of laminar and turbulent flow.

The mean value of a hydrograph goodness-of-fit statistic, as the improvement over using the mean discharge, increases as the geometric goodness-of-fit statistic increases but decreases as the drainage density increases.

A combined goodness-of-fit statistic, the product of the drainage density ratio and the geometric goodness-of-fit statistic, is related to the degree of distortion in optimal-hydraulic roughness parameters. Distortions in watershed geometry result in optimal roughness parameters smaller than the corresponding empirically derived values for simple watersheds where less distortion is involved.

Given rainfall, runoff, and topographic data for a small watershed, it is possible to define the simplest kinematic cascade geometry which when used in simulation will, on the average, preserve selected hydrograph characteristics to a given degree of accuracy.

Chapter I
INTRODUCTION

1.1 General Statements

To address the problem of surface runoff as related to watershed features one must study fundamentals of the past as well as current research. How can the hydrologic processes be understood? One way is to investigate the properties of simple mathematical models constructed to simulate the operation of nature with respect to specific quantities of interest. If the model is understood, then one attempts to infer properties of its prototype. This method is a standard tool, a mathematical model. The method can be summarized as an oversimplification in the following sequence: Nature - Questions - Mathematical Model - Understanding - Inference. There is a great deal of mire between each element in the sequence. Unfortunately, the sturdy links are for the most part based on experience and judgment and (for want of more precise terms) creativity, cleverness, and insight. Fortunately, there is a partial solution by way of observed data--supportive or negative empirical evidence, i.e., observed data provide the means of testability.

Considering surface runoff, the thesis is that mathematical models can be strengthened by systematically incorporating more basin or watershed characteristics into them. By this means, the links between the phases discussed above are strengthened so that they become more objective. By constructing the models based upon theory and by testing them with data the result is a procedure with systematic and empirical import, i.e., the theory helps to distinguish laws from accidental generalizations and the observed data provide the basis for testing hypothesized relationships. Thus, theories are introduced to explain a system of regularities but they must be definite enough to allow testing.

Before proceeding, we would like to define some terms basic to this discussion. The terms "watershed," "drainage basin," and "catchment" are synonymous. "Watershed" means an area above a specified point on a stream enclosed by a perimeter. The "watershed perimeter" is an area in which surface runoff will move into the stream or its tributaries above the specified point. Thus, "watershed" connotes a physical entity for which statements of continuity can be made. With respect to surface runoff, the watershed boundaries are, except for the stream outlet, the locus of points where there is no mass flux of water.

If attention is limited to stream channels that are conceptualized as single lines, then the resulting line diagram is called a "channel network." A simple concept of the surface of a watershed is that it consists of the channel network and the interchannel areas of overland flow within the watershed perimeter. Flow from this surface is called "surface runoff."

1.2 Scope and Objectives

Although many of the concepts discussed here may have wider applicability, the study excludes urban watersheds. Emphasis is on rainfall excess-surface runoff relationships on small rural watersheds. Data from artificial watersheds are used in developing relationships, but the main interest is in natural and cultivated agricultural watersheds.

Before the analyses, the basic models are presented and discussed. Then the theory of overland flow over complex surfaces. Next, the analyses are extended to natural watersheds, and, finally, to parameter estimation and model testing.

The four preliminary or auxiliary objectives are:

1. To select hydrograph characteristics which should be preserved in simulating surface runoff from small agricultural watersheds.

2. To develop statistics which can be used to determine when the selected hydrograph characteristics have been preserved to a given degree in a surface runoff simulation.

3. To select a set of watershed characteristics which should be preserved in simulating surface runoff from small agricultural watersheds.

4. To develop statistics which can be used to judge when the selected watershed characteristics have been preserved to a given degree in a simplified geometrical representation of the watershed.

With these objectives as prerequisites, the major objective in this study is then to relate statistics of the simplified geometry to watershed characteristics and to hydrograph characteristics to define the simplest geometry which when used in simulation will preserve the selected hydrograph characteristics to a given degree of accuracy.

1.3 Brief Review of Relevant Literature

Only a few representative or typical articles are reviewed. Of the many papers read, only those directly relevant (explicitly used) to this study are cited. Obviously, these references are only a small portion of the extensive body of excellent literature available. This review is intended to provide a short list of select quality sources that should provide both a starting point for introduction to the literature and an overview of sources influential in the present endeavor.

Three areas of fundamental import here are kinematic wave theory, unit hydrograph theory, and the theory of incorporating basin characteristics in surface runoff models. Kinematic wave theory via the kinematic cascade model is the basic tool for surface runoff simulation used here. References chosen are those which show the development of this theory. Although the flow of papers on unit hydrographs is seemingly endless, the noteworthy steps in its development can be traced in a few sources. The literature on incorporating basin characteristics in surface runoff models is enormous, but relevant ones are implicitly defined by the conceptual form of the kinematic and unit hydrograph models. For the kinematic wave theory, characteristics distributed over the basin are relevant, while for the unit hydrograph theory lumped parameters can be used.

Under conditions where the momentum equation can be approximated to a good degree by maintaining only terms expressing bottom slope and friction slope, flow is called "kinematic." Under these conditions,

local depth and discharge on a plane have a simple functional relation

$$Q = \alpha h^n \tag{1.1}$$

where: Q = local discharge, h = local depth, α = coefficient incorporating slope and roughness, and n = exponent reflecting flow type (laminar or turbulent). These definitions are for flow over a hydraulically smooth plane. However, the same form can be used for irregular surfaces where the mean flux per unit width is proportional to the storage in an incremental area. An early reference (Lighthill and Whitham, 1955) presented the theory of kinematic waves. The next step is to sources developing the kinematic cascade.

Henderson and Wooding (1964) applied the theory to flow over a plane and compared their results to data with a good reproduction of observations. Then Wooding (1965a, 1965b, and 1966) extended the theory to a watershed model, discussed numerical solutions, and compared results with observed runoff data. This extension was an important step in developing a general watershed model based upon kinematic flow. A complex watershed was modeled as two symmetric lateral planes contributing to a channel bisecting the area. Schematically the model could be compared to an open book with the channel in the center so that there is a lateral slope for the planes but also a down channel slope for the channel and planes. This model is referred to as the Wooding model and will serve as a standard for comparison as well as a first approximation throughout this study.

Brakensiek (1967) made the essential step from Wooding's model to the kinematic cascade model. This step is fundamental because rather than a single plane discharging into a channel--a lumped nonlinear model--Brakensiek broke the lateral flow portion into a sequential series (cascade) of planes. With this cascade formulation an obvious extension was to let each plane have its own characteristics resulting in a distributed model. Kibler and Woolhiser (1970, p. vii) defined a kinematic cascade as: "...a sequence of n discrete overland flow planes or channel segments in which the kinematic wave equations are used to describe the unsteady flow. Each plane or channel is characterized by a length, l_k, width, w_k, and a roughness-slope factor, α_k."

Thus, the kinematic cascade is a distributed (since each element may have different characteristics, including rainfall excess) model with lumped parameters in the subelements. It is nonlinear since values for n in Eq. 1.1 are generally not equal to one. For examples of recent applications in urban and rural agricultural watersheds, see Harley, et al., (1970) and Singh (1974).

A great many papers have been published on unit hydrographs. Many papers are repetitive or merely familiar applications on a new or slightly different watershed. However, because the concept is so elegantly simple and historically and practically basic to rainfall-runoff studies, it is also used as a standard for comparison as well as a first approximation in this study. In all of the following the instantaneous unit hydrograph (IUH), rather than finite duration unit hydrographs, are used. The reason for this is that the IUH or linear impulse response characterizes a linear, time-invariant system.

Define a delta function or impulse as a function so that

$$\delta(t-t_o) = 0 \quad \text{when} \quad t \neq t_o \tag{1.2}$$

and

$$\int_{-\infty}^{+\infty} \delta(t-t_o)dt = 1.0 \tag{1.3}$$

i.e., an impulse or delta function is a function with some properties, such as homogeneity, so that

$$a\ \delta(t-t_o) = 0, \quad t \neq t_o \tag{1.4}$$

and

$$\int_{-\infty}^{+\infty} a\ \delta(t-t_o)dt = a \tag{1.5}$$

where a is a real constant. A delta function also has the sifting property

$$\int_{-\infty}^{+\infty} \phi(t)\ \delta(t-t_o)dt = \phi(t_o) \tag{1.6}$$

where $\phi(t)$ is a function of time.

Consider a linear time-invariant system which has the properties of superposition, time invariance, and homogeneity. Superposition requires that if an input to the system, x_i, produces an output, y_i, and an input of x_j produces y_j, then $x_i + x_j$ produces $y_i + y_j$. "Time invariance" means that x_i produces y_i without regard to time, and "homogeneity" means that ax_i as input produces ay_i as output. The linear system response to a delta or impulse input denotes the linear impulse response or the instantaneous unit hydrograph (IUH).

Let h(t) be the linear impulse response, x(t) be an arbitrary input or rainfall excess function, and y(t) be the surface runoff response to this arbitrary input.

$$\delta(t) \quad \text{produces} \quad h(t) \tag{1.7}$$

by definition,

$$\delta(t-\tau) \quad \text{produces} \quad h(t-\tau) \tag{1.8}$$

by time invariance,

$$x(\tau)\ \delta(t-\tau) \quad \text{produces} \quad x(\tau)\ h(t-\tau) \tag{1.9}$$

by homogeneity, and

$$\int_{-\infty}^{+\infty} x(\tau)\ \delta(t-\tau)\ d\tau \quad \text{produces} \quad \int_{-\infty}^{+\infty} x(\tau)\ h(t-\tau)\ d\tau \tag{1.10}$$

by superposition. By substituting Eq. 1.6 in the left side of Eq. 1.10 is then $x(\tau)$, the arbitrary input producing y(t) as the response. Therefore, the right side of Eq. 1.10 is identically y(t), the response. Hence

$$y(t) = \int_{-\infty}^{+\infty} x(\tau)\ h(t-\tau)\ d\tau. \tag{1.11}$$

as the familiar convolution integral. Gupta (1966) developed Eq. 1.11 on which the above is based. Dooge (1973) is a complete and excellent source on linear theory in hydrology.

Obvious questions are how well does the linear model conform with observed data from watersheds and how to obtain h(t). Dooge (1973) discussed the second question, and the first question will be investigated in a later chapter.

A much more difficult question is how are basin characteristics incorporated into rainfall-runoff models? First one might ask, why is it necessary to incorporate basin characteristics into the models? Many models are used to simulate surface runoff, given parameters for the model, input data, and initial conditions. Efficients methods for a priori estimation of parameters are fewer. Surface runoff on ungaged basins must be estimated, and unlike the situation for gaged basins (where parameters may be obtained by optimization), parameter estimates for ungaged basins are not based on observed rainfall-runoff data for the basin in question. Hence, the desire to develop relationships between basin characteristics and surface water response. Also the hydrologic consequences of changing land use on small watersheds must be estimated. Hopefully, geomorphic parameters can be a useful means of quantifying these changes in ways that will be logically reflected in hydrologic models.

Significant Geomorphic Parameters Which May Be Incorporated into Specific Mathematical Models. Geomorphic parameters of interest here can be classified into four main groups: (1) Linear factors of channel systems, (2) Areal factors of channel systems, (3) Relief factors of basins, (4) Energy factors on the watershed surface. The last category includes both potential and dissipative factors. Judging which parameters are significant is a subjective matter, however, aside from those parameters necessary for description in a classical sense, only those parameters which can be incorporated into a specific model are judged significant with respect to that model. Markovic (1966) gives an excellent description of many geomorphic parameters and is a primary source for much of the following.

1. Linear Factors of Channel Systems.

Stream Order, u. In the Horton-Strahler system (Horton, 1945; Strahler, 1952) a first-order stream is the smallest unbranched stream. Two first-order streams join to form a second-order stream, etc. The order of the main stream is the highest and is also the order of the basin at that point on the main stream. Strahler (1964, pp. 4-43) gives a summary of the reasoning in judging the importance of stream order: "Usefulness of the stream-order system depends on the premise that, on the average, if a sufficiently large sample is treated, order number is directly proportional to size of the contributing watershed, to channel dimensions, and to stream discharge at that place in the system. Because order number is dimensionless, two drainage networks differing greatly in linear scale can be compared with respect to corresponding points in their geometry through use of order number."

Number of Streams of a Given Order u, N_u. The number of streams of each order is counted up to $N_u = 1$, where u is the basin order. Since a watershed of order u may be modeled as a collection of subelements of lower order, the number of streams of each order is an important concept. A parameter derived from N_u is the bifurcation ratio

$$R_b = \frac{N_u}{N_{u+1}} \tag{1.12}$$

which may be used as one index of hydrograph shape, given two basins similar in other respects (Strahler, 1964).

Stream Lengths of Order u, L_u. The total length of all streams of order u is the stream length, L_u, which can be used to define the mean stream length of order u as

$$\bar{L}_u = \frac{L_u}{N_u} \tag{1.13}$$

This term is also important in describing components of a watershed.

Length of Main Stream, L_c. The length of the main stream is the length of the highest order stream projected back to the watershed divide. This parameter is important in determining hydrograph time characteristics (Gray, 1961).

Length of Overland Flow, L_o. The length over which water must flow to reach a stream channel is the length of the overland flow. Horton (1945) has a good discussion of its importance. It is important to note that perhaps in nature and certainly in many hydrologic models the length of overland flow determines the flow type.

2. Areal Factors of Channel Systems.

Watershed Area, A. The area enclosed by the watershed perimeter projected on a horizontal plane is the watershed area. Nearly all geomorphic parameters in a basin are related to basin or watershed area.

Drainage Density, D_d. The ratio of the total length of all streams in a watershed to the watershed area is the drainage density. This is an important parameter in hydrology because it is an index of drainage efficiency and length of overland flow. The average length of overland flow is approximately equal to one over twice the drainage density (Horton, 1932). Thus, drainage density is important as an index of the relative proportion of overland and open channel flow. Moreover, recent observations point to the importance of the areal distribution of drainage density within a watershed to the hydrologic response of that watershed. The apparent nonlinearity of the surface response varies with the drainage density and areal distribution of drainage density.

Watershed Shape. There are several parameters expressing watershed shape, such as circularity or elongation. These parameters may be important in drainage efficiency or travel time characteristics. Just how to assess these influences due to form is not yet known. Recent regression studies have indicated their importance, but perhaps a calibrated hydrologic model could be used to analyze the influence of basin shape.

3. Relief Factors of Basins.

Slope of the Main Channel, S_c. The main channel of length, L_c, is the highest order stream projected to the basin divide. Define S_c (Gray, 1961) as the slope of the right triangle hypotenuse with the same length and the same area as the area under the stream profile. This slope is important in calculating main channel velocity.

Average Watershed Slope, S_w. If a plane is fit to watershed coordinate data by least squares, then this slope of the best-fit plane is a measure of the overall watershed slope. Moreover, this is one objective method of fitting planes to subareas of a drainage basin.

Total Relief, H. The total or basin relief is the difference between the lowest (outlet) and the highest (divide) points in the watershed. The total relief provides a maximum elevation drop of surface water.

Hypsometric Curve, f(x). The hypsometric curve relates relative basin height to relative basin area and is thus a measure of the distribution of elevation with respect to area. The hypsometric integral is the area under this curve.

Average Watershed Elevation, $\bar{h}$. The average watershed elevation can be defined in several ways. We define average elevation as the mean of the vertical coordinates of distance above base level.

4. Energy Factors of the Watershed Surface.

Potential Energy, U. The total potential energy of a uniform depth of water on the watershed surface is equivalent to the amount of work required to raise that volume of water to the given elevation above base level. The total potential energy is related to the hypsometric integral as shown below.

Drainage basin area is related to elevation by the hypsometric curve, f(x). If A is total basin area and H is total basin height, then a/A and h/H define relative area and relative height. The hypsometric (area-altitude) curve is expressed as a function.

The hypsometric integral is then expressed as

$$I_h = \int_{x=0}^{1} [f(x)dx] = \int_{a/A=0}^{1} [h/H\ d(a/A)] = \frac{1}{AH} \int_{a=0}^{A} [hda] \tag{1.14}$$

as the relative area below the hypsometric curve.

The potential energy, dU, of a differential volume of specific weight, γ, at an elevation, h, above base level is

$$dU = \gamma h dv = \gamma h z da \tag{1.15}$$

where dv is differential volume, equal to zda; z is depth of differential element, and da is differential area (projected area).

The total potential energy of a sheet of water of uniform depth over the projected watershed area is then

$$U = \int dU = \int_A \gamma z h da \tag{1.16}$$

where h is a function of position in the basin.

Relation of Potential Energy to Hypsometric Integral. If Eq. 1.14 is multiplied by A and H, basin area and relief, we have

$$AH\ I_h = AH \int_0^1 f(x)\ dx = AH \int_0^1 h/H\ d(a/A) = \int_{a=0}^{A} hda \tag{1.17}$$

If Eq. 1.17 is multiplied by γz then

$$AHI_h \gamma z = \int_A \gamma z h da = U, \tag{1.18}$$

which demonstrates that the total potential energy of a uniform input of depth, z, to a basin of area A is

$$U = AH\gamma z I_h \tag{1.19}$$

as stated above.

Topographic Roughness, B_f. One measure of topographic roughness (as opposed to hydraulic roughness) is derived from fitting a plane to coordinate data from the watershed surface. Define B_f as the standard deviation of the watershed surface from the plane and consider its distribution. A very small variance would indicate a relatively good fit by the plane, while a large variance would indicate the opposite. Deviations from the plane produce an objective criterion in fitting planes to subareas of the watershed in modeling its components.

Hydraulic Roughness. Roughness coefficients are such as C in the Chezy formula or n in the Manning formula. These coefficients relate flow velocity and friction losses in overland and open channel flow. Thus, the potential energy is dissipated by flow over the watershed surface.

Chapter II
BASIC MODELS

2.1 Watershed Geometry: Cascade of Planes and Channels

In the simplest terms a watershed is modeled as a channel network and the interchannel areas of overland flow. The elements (planes and channels) are arranged in a cascade with a logical plane to plane, plane to channel, and channel to channel system of flow.

Each interchannel (including upland) area is modeled as a plane or as a cascade of planes. Each plane is characterized by an area, length and width, a slope, and a roughness. If any of these factors vary excessively within an area, the area is modeled as a cascade of planes containing a sufficient number of elements to distribute the factors to the extent necessary to preserve their areal variability.

One way of estimating the slope of each plane is by deriving a least squares estimate of the slope by fitting a plane to coordinate data from topographic maps. Hobson (1967) has taken such an approach in trying to describe surface shape in a topographic sense. The reasoning is that the deviations from the plane can be analyzed to characterize the goodness-of-fit of the least squares plane. Hobson's procedure has been modified to provide estimates of the slope of each element and to provide a measure of how well the plane or cascade of planes fits the original coordinate data. Thus, there seems to be an objective means of estimating overland flow-plane slope, as well as an objective means of determining the number of planes necessary to model an area.

A topographic map defines a watershed perimeter and channel network. Moreover each point on and within the perimeter is defined by its coordinates (x, y, z). Similar to Hobson's (1967) notation, e_i is an elevation point corresponding to (u_i, v_i) as the corresponding x and y coordinates. The coefficients of the least squares fitted plane are b_i. In matrix form

$$B = [UV]^{-1} E \tag{2.1}$$

where

$$B = \begin{bmatrix} b_1 \\ b_2 \\ b_3 \end{bmatrix} \tag{2.2}$$

is the coefficient vector,

$$E = \begin{bmatrix} \sum e_i \\ \sum u_i\ e_i \\ \sum v_i\ e_i \end{bmatrix} \tag{2.3}$$

is called the "elevation vector," and

$$[UV] = \begin{bmatrix} N & \sum u_i & \sum v_i \\ \sum u_i & \sum u_i^2 & \sum u_i\ v_i \\ \sum v_i & \sum u_i\ v_i & \sum v_i^2 \end{bmatrix} \tag{2.4}$$

with this notation a computed elevation value is

$$\hat{z}_i = b_1 + (b_2\ u_i + b_3\ v_i). \tag{2.5}$$

A deviation from the observed elevation is then $e_i - \hat{z}_i$ or $z_i - \hat{z}_i$; where the hat denotes an estimated value. A goodness-of-fit statistic based upon these deviations is derived in Chapter IV.

The general procedure for fitting a cascade of planes and channels to watershed data from topographic maps is to select coordinate data over the watershed area with each point representing nearly the same area within the perimeter. A single plane fit to the coordinate data is the simplest cascade. The next cascade would be one channel and two lateral planes--the Wooding model. The procedure is then to include successively more planes and channels in the cascade to form more complex models. Throughout the procedure certain watershed properties are preserved. Each of the successively more complex models has the same total drainage area. If the length of the main channel, L_c, is also preserved, then the area and length specify the width for a single plane. For the Wooding model, the main channel is located and thus this length specifies the width of the lateral planes. As the complexity of the kinematic cascade increases, the freedom in choosing the arrangement and size of the elements also increases. This procedure is discussed in more detail in Chapter IV.

Gray (1961) defined slope of the main stream, S_c, as the slope of a line drawn along the measured profile which has the same area under it as is under the observed profile. This slope is the slope of the hypotenuse of a right triangle with the same area, A, and length, L_c, as the observed profile. These slopes are illustrated in Fig. 2.1. With respect to the triangle, the area is

$$A = 1/2\ L_c\ h \tag{2.6}$$

and the slope is

$$S_c = h/L_c \tag{2.7}$$

If Eq. 2.6 is solved for h and this is substituted in Eq. 2.7, then

$$S_c = 2A/L_c^2 \tag{2.8}$$

as the equivalent channel slope. With respect to the observed stream profile

$$A = \int_{y=0}^{H_c} (L_c - x)\ dy \tag{2.9}$$

where if the slope is S(x), then

$$dy = S(x)\ dx \tag{2.10}$$

in Eq. 2.9.

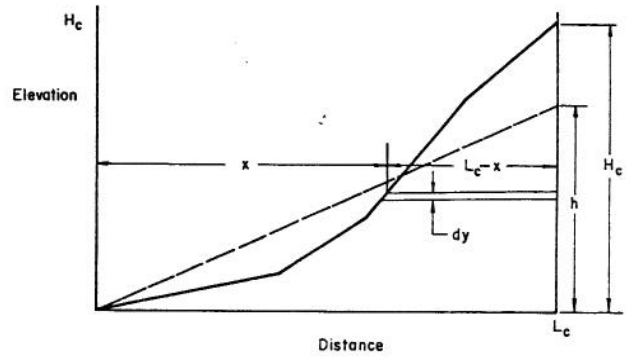

Fig. 2.1. Definition sketch of main channel slope determination. Solid line represents the measured stream profile and dashed line the right triangle.

With this value of dy, Eq. 2.9 is

$$A = \int_{x=0}^{L_c} (L_c - x)\, S(x)\, dx, \qquad (2.11)$$

and then Eq. 2.8 becomes

$$S_c = 2 \int_{x=0}^{L_c} \frac{(L_c - x)}{L_c^2} S(x)\, dx, \qquad (2.12)$$

where $(L_c-x)/L_c^2$ can be considered a weighting factor (Lane, 1974). For example, this factor is zero at $x = L_c$ and a maximum at $x = 0$. Therefore, Gray's method produces a channel slope which is weighted by distance from the headwaters of the main stream. The highest weight is given to the slope at the outlet.

If H_c is the total relief of the stream and h is the altitude of the above right triangle, then their ratio, h/H_c, can be used as an index of concavity so that a value less than one (the usual case) corresponds to an overall concave profile while a value greater than one indicates an overall convex profile. This index is used as a measure of how well the channel slope is represented by a straight line.

Assuming that a given watershed with drainage density, D_d, is modeled as a simplified cascade of planes and channels with drainage density, d_d, then the ratio d_d/D_d is a measure of how well the channel network is modeled with respect to total length. This ratio and the index of concavity provide measures of the goodness-of-fit of the model's channels with respect to the linear dimensions of the channels in the watershed. Subsequent analyses investigate the hydraulic import of these indices.

2.2 Rainfall Excess-Surface Runoff: Kinematic Cascade

Recall the kinematic wave theory wherein the continuity equation is

$$\frac{\partial h}{\partial t} + \frac{\partial (uh)}{\partial x} = q(x,t) \qquad (2.13)$$

with the stage-discharge equation as

$$Q = \alpha h^n \qquad (2.14)$$

where: h = depth of flow, u = velocity, t = time, x = distance in direction of flow, q = lateral inflow, Q = discharge rate, α = coefficient, and n = exponent. The kinematic cascade model is the above equations for the cascade of planes and channels. Kibler and Woolhiser (1970) presented a finite-difference method of solution known as the single-step Lax-Wendroff method. This method, from Houghton and Kasahara (1968), was compared with two other finite-difference schemes given by Kibler and Woolhiser (1970). Their results are summarized in their Table 3 on p. 14. Briefly, the Lax-Wendroff scheme is second order and produced less numerical distortion in peak discharge rates than the other finite-difference schemes. The basic tool in this study is a general program for the kinematic cascade using the Lax-Wendroff method. As programmed by Woolhiser, channel flow is turbulent and the Chezy relationship is assumed. Flow over the planes begins as laminar flow with a transition to turbulent flow if a transitional Reynolds number is reached.

2.3 Summary of Modeling Procedure

The modeling procedure can be summarized by showing how watershed geometry is combined with kinematic wave theory in the kinematic cascade model. The basic tool used here is the finite difference program for the kinematic cascade. Input to this program consists of the geometry from topographic analysis and rainfall-runoff data from hydrologic analysis.

The modeling procedure is summarized in the form of a block diagram in Fig. 2.2. The left portion of

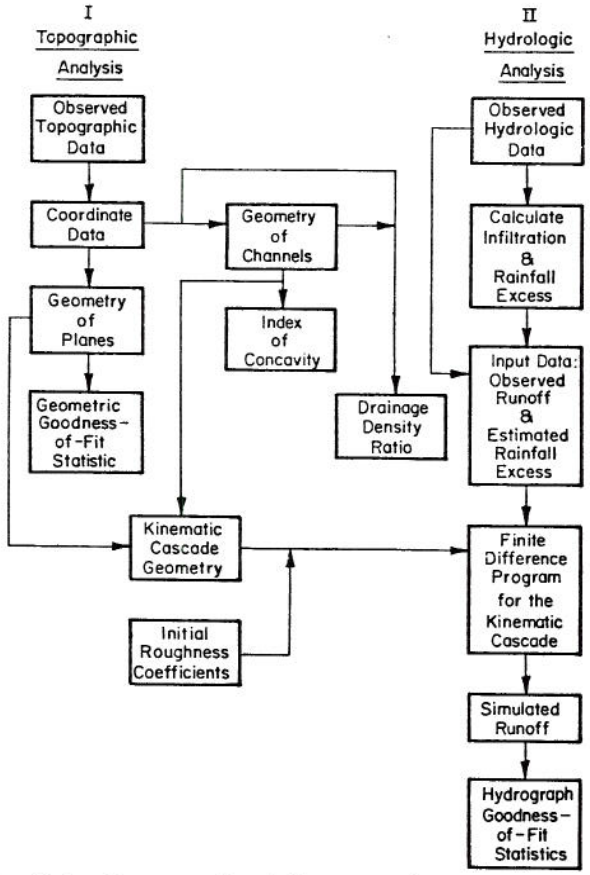

Fig. 2.2. Summary of modeling procedure.

this figure deals with topographic analysis and the right portion shows the sequence of hydrologic analysis. Topographic maps are used to provide coordinate data defining the watershed perimeter, channel network, and interior points on the watershed surface. These data are used to determine the geometry of planes and a geometric goodness-of-fit statistic as a measure of how well the cascade of planes fits the original coordinate data. Here the term goodness-of-fit statistic is used to describe how well a watershed component is represented in a mathematical model. Thus, the term has a slightly different connotation than its classical statistical one.

The original coordinate data are also used to determine the channel network. The index of concavity is a goodness-of-fit statistic for an individual channel and the drainage density ratio is a goodness-of-fit statistic for the entire channel network.

The channel geometry and geometry of the planes define the kinematic cascade geometry. Topographic input to the finite difference program consists of the cascade geometry and initial estimates of the roughness coefficients. The goodness-of-fit statistics are described in Chapter IV, and the roughness coefficients are described in Chapter V.

Observed hydrologic data consist of rainfall and runoff data. The latter are used to estimate rainfall excess from rainfall data and to define the runoff objective function for optimization. Rainfall excess and runoff data are input to the finite difference program which produces simulated runoff hydrographs and thus hydrograph goodness-of-fit statistics. The hydrograph goodness-of-fit statistic is a measure of how well the simulated runoff corresponds to observed runoff. The above description is brief, but additional material is presented in later chapters after overland flow analysis presented in the next chapter.

Chapter III
ANALYSIS OF OVERLAND FLOW OVER UNIFORM AND COMPLEX SLOPES

3.1 Equations for Description of Overland Flow Surfaces

Before proceeding to an analysis of complex watersheds consisting of interchannel areas (areas of overland flow) and the channel network, overland flow must be examined as a first step in watershed simulation. In addition to the effects of slope, length, and roughness, the influence of slope shape upon overland flow must be examined.

Kibler and Woolhiser (1970) developed a procedure to approximate a two-plane cascade as a single plane. In a step closer to actual slope shapes, slopes can be modeled with a cubic equation with parabolic and plane shapes as simplifications or special cases.

Let $y(x)$ be the elevation of the overland flow surface. Assume a function of the following form:

$$y(x) = a_o + a_1 x + a_2 x^2 + a_3 x^3 \tag{3.1}$$

where: y = elevation of the surface, x = distance, and a_i = coefficients to be determined.

A third degree equation can be fit to four points $(x_i, y_i)(i = 1, 2, 3, 4)$, using the Lagrange form (Conte, 1965) as

$$y(x) = \sum_{k=0}^{3} L_k(x)\, y_k, \tag{3.2}$$

where

$$L_k(x) = \prod_{\substack{j=0 \\ j\neq k}}^{3} (x-x_j) \Bigg/ \prod_{\substack{j=0 \\ j\neq k}}^{3} (x_k-x_j) \tag{3.3}$$

$L_k(x)$ are third degree polynomials whose parameters depend only on the chosen values of x_i. If x is scaled by dividing it by the length of flow, L_o, then

$$x_* = x/L_o \tag{3.4}$$

and four convenient points for x_* on [0, 1] are 0.0, 0.25, 0.50, and 1.0. With these values the corresponding polynomials are

$$L_0(x) = 1-7x + 14x^2 - 8x^3, \tag{3.5}$$

$$L_1(x) = 10.66x - 32x^2 + 21.33x^3, \tag{3.6}$$

$$L_2(x) = -4x + 20x^2 - 16x^3, \text{ and} \tag{3.7}$$

$$L_3(x) = 0.333x - 2x^2 + 2.667x^3, \tag{3.8}$$

where the subscript has been dropped. The equation of the surface is then found by choosing the y_k values and substituting them and equations 3.5 to 3.8 into Eq. 3.2. Constraints relevant to the problem are that y_k must be chosen so that there are no extrema on the interval [0, 1]. That is, the slope function

$$s(x) = y'(x) = a_1 + 2a_2 x + 3a_3 x^2 \tag{3.9}$$

must not have roots on [0, 1], or, it must be that

$$p = \frac{-2a_2 \pm \sqrt{4a_2^2 - 12a_1a_3}}{6a_3} \tag{3.10}$$

so that $p \notin [0, 1]$.

As derived in Chapter I, the hypsometric integral is a measure of the potential energy of a uniform input to a surface. In anticipation of testing the significance of potential energy in overland flow, the hypsometric integral is derived for surfaces described by Eq. 3.1. For a unit width of an arbitrary surface, then the product of elevation (with respect to Y_o) and differential area (in projection on a horizontal plane) becomes the product of elevation and differential distance per unit width, i.e.

$$(Y_o-y)dA = (Y_o-y)dx \tag{3.11}$$

Integrating over x(scaled) the result is the integral of the area-altitude curve or the hypsometric curve. If y is scaled by Y_o, $y_* = y/Y_o$, but used without the subscript, the hypsometric integral becomes

$$I_h = \int_{x=0}^{1} (1-y(x))\, dx \tag{3.12}$$

The area per unit width is L_o and the total relief is Y_o, so that the potential energy of a uniform input of depth h_o is

$$U = \gamma A H I_h h_o \tag{3.13}$$

which becomes

$$U = \gamma L_o Y_o I_h h_o \tag{3.14}$$

where U is potential energy and γ is the specific weight of water.

3.2 Determination of Characteristic Time for a Plane

Before examining overland flow on arbitrary surfaces, overland flow on a plane must be considered. Characteristic time (time to equilibrium, time of concentration) is defined in terms of length and velocity at steady state.

For a discussion of characteristic times for more complex configurations see Golany and Larson (1971). For a nomograph for time of concentration in turbulent flow, see Ragan and Duru (1972). In contrast, the study described here considers laminar flow and situations where the overland flow is laminar and turbulent at the same time at different positions on the plane. Moreover, the equations presented incorporate the transition Reynolds number into the equations for calculating characteristic time.

In considering flow over a plane the following parameters are necessary to determine the characteristic time; length, slope and roughness of the plane, as well as the Reynolds number for transition from laminar to turbulent flow. In addition, a pulse input of magnitude P is assumed uniform over the plane. Finally, kinematic flow is assumed.

Let Q be the equilibrium discharge per foot of width at the downstream boundary corresponding to the uniform rainfall excess rate, P. Let V be the normal velocity at the downstream boundary corresponding to the equilibrium discharge. The length of the plane is L, and the characteristic time is T. The Darcy-Weisbach friction factor is f, where

$$f = K/R_e \tag{3.15}$$

for laminar flow, and

$$f = 8g/C^2 \tag{3.16}$$

for turbulent flow; where: f = Darcy-Weisbach friction factor, K = roughness coefficient, R_e = Reynolds number, g = gravity constant, and C = Chezy C. Furthermore, R_c is the Reynolds number above which flow is turbulent so that

$$C = \sqrt{8g/f} \tag{3.17}$$

and then to match friction factor at $R_e = R_c$

$$C = \sqrt{8gR_c/K}\ . \tag{3.18}$$

Thus, the roughness is described by the parameter K and a transition Reynolds number.

Recall the kinematic stage-discharge equation

$$Q = \alpha h^n \tag{3.19}$$

where $n = 3.0$ for laminar flow and $n = 1.5$ (Chezy form) for turbulent flow. The coefficient α for laminar flow is

$$\alpha = \frac{8gS}{K\nu} \tag{3.20}$$

where S is the slope and ν is the kinematic viscosity. For turbulent flow,

$$\alpha = C\sqrt{S} \tag{3.21}$$

where C is determined by Eq. 3.18.

From Eq. 3.19 the steady state depth H is

$$H = (Q/\alpha)^{1/n} \tag{3.22}$$

so that the steady state velocity

$$V = \alpha H^{n-1} \tag{3.23}$$

becomes

$$V = \alpha(Q/\alpha)^{\frac{n-1}{n}}\ . \tag{3.24}$$

Since

$$1 - \frac{n-1}{n} = 1/n \quad \text{then}$$

$$V = \alpha^{1/n} Q^{\frac{n-1}{n}}\ . \tag{3.25}$$

To convert P (in in./hr) to Q (in cfs/ft) to use in Eq. 3.25,

$$Q = P(L/43200). \tag{3.26}$$

Substituting Eq. 3.26 into 3.25, the result is

$$V = \alpha^{\frac{1}{n}} P^{\frac{n-1}{n}} \left(\frac{L}{43200}\right)^{\frac{n-1}{n}} \tag{3.27}$$

as the velocity (in ft/sec). Since

$$T = L/V \tag{3.28}$$

the characteristic time in sec is

$$T = (43200)^{+\left(\frac{n-1}{n}\right) - \frac{1}{n}} \alpha^{-\left(\frac{n-1}{n}\right)} P^{\frac{1}{n}} L\ . \tag{3.29}$$

Equation 3.29 is valid if the flow is all laminar. However if there is a transition to turbulent flow then

$$T = T_L + T_T \tag{3.30}$$

where T_L is the time corresponding to laminar flow and T_T is the time corresponding to turbulent flow. To evaluate Eq. 3.30 whether there is a transition to turbulent flow must be determined, and if so, the two lengths of flow of each type. At any point on the plane (in the direction of flow and with respect to discharge per unit width) the Reynolds number is

$$R_e = Q/\nu \tag{3.31}$$

which by Eq. 3.26 is

$$R_e = \frac{PL}{43200\nu}\ . \tag{3.32}$$

Now if Eq. 3.32 is solved for L at the transition

$$L_L = (43200\nu)\ R_c/P \tag{3.33}$$

is the length of laminar flow before the transition. Two cases arise: (1) the length of the plane is less than L_L, so that Eq. 3.30 becomes

$$T = T_L \tag{3.34}$$

where $T_T = 0$; and (2) the length of the plane is greater than L_L so that

$$L_T = L - L_L. \tag{3.35}$$

In this case T_T is evaluated by Eq. 3.29 and then corrected for the nonzero upstream boundary condition. That is, the turbulent portion of the plane is equivalent to a plane of length, L_T, with an upstream boundary condition corresponding to the point of transition from laminar to turbulent flow. Moreover, by Eq. 3.29 T_T varies as the 2/3 power of L. Therefore, the combined characteristic time for the entire plane is

$$T = T_L + \left(\frac{L_T}{L_L + L_T}\right)^{2/3} T_T \qquad (3.36)$$

The Reynolds number, as defined by Eq. 3.32, is for various values of L and P shown in Fig. 3.1A. The length of laminar flow, L_L, from Eq. 3.33 is shown in Fig. 3.1B. For example, for an input rate of P = 1.0 in./hr and a transition number of R_c = 500, the length of laminar flow from Fig. 3.1B is approximately 270 ft.

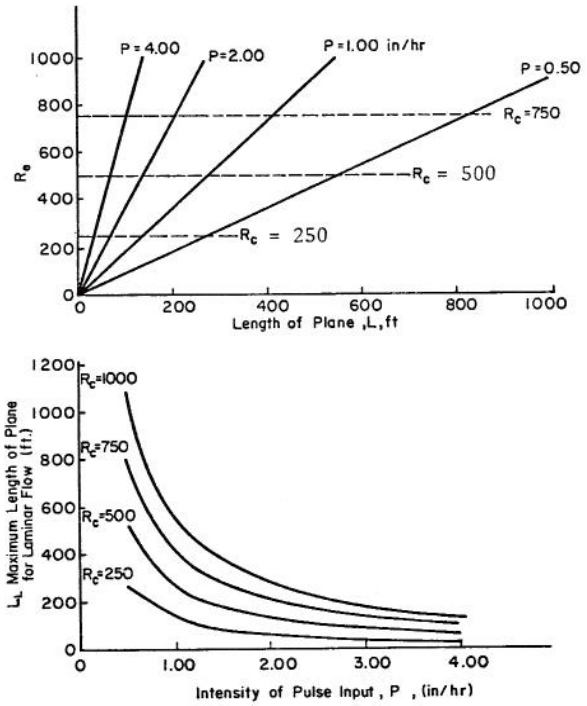

Fig. 3.1. Reynolds number and length of laminar flow as functions of input rate and length of the plane. (A) Reynolds number R_e, at equilibrium discharge. (B) Maximum length of plane for laminar flow.

Using the length of laminar flow, L_L, Fig. 3.2 can be used to give an approximate solution to Eq. 3.29 for T_L (in sec). Now, if $L_L < L$ then the length of turbulent flow, L_T, is greater than zero. With the positive value of L_T, Fig. 3.3 can be used to estimate the characteristic time for turbulent flow, T_T. Finally, the values of L_L, L_T, T_L, and T_T are entered in Eq. 3.36 to estimate the composite characteristic time.

To test the above procedure, 10 simulation runs were made using the finite-difference program and assuming that equilibrium discharge was equal to 95 percent of the input rate. Properties of the 10 planes as well as the times are given in Table 3.1. Test cases no. 2, 6, 7 and 8 are examples of transitions to turbulent flow, while for the others flow was entirely laminar. The extent to which calculated and simulated characteristic times correspond is shown in Fig. 3.4.

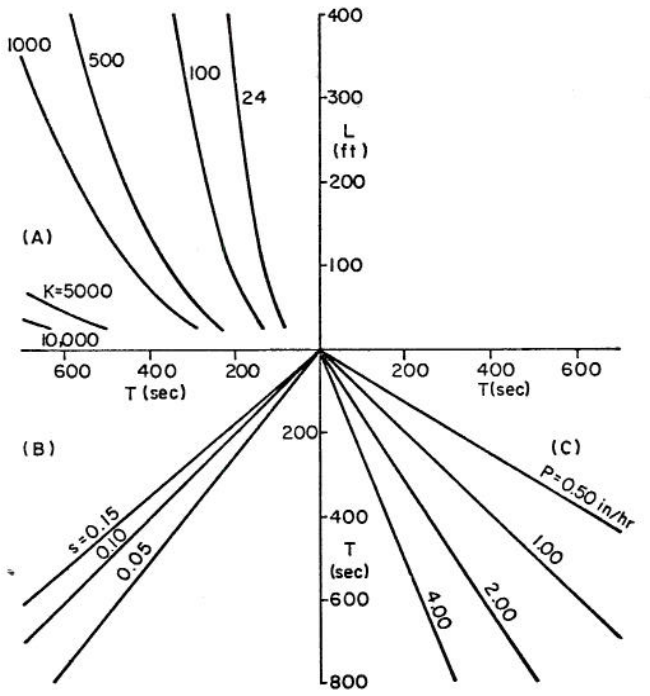

Fig. 3.2. Characteristic time for laminar flow, T_L, over a plane: (A) As a function of length, L, and roughness coefficient, K; (B) As a function of slope, S, and (C) As a function of intensity of pulse input, P.

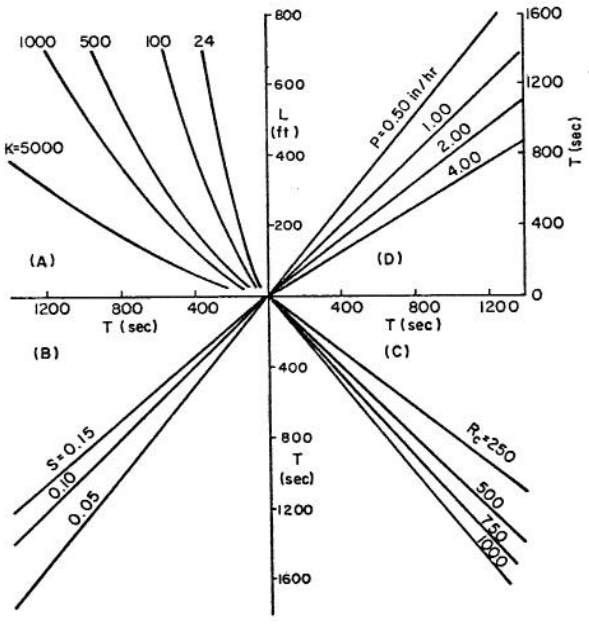

Fig. 3.3. Characteristic time for turbulent flow, T_T, over a plane: (A) As a function of length, L, and roughness coefficient, K; (B) As a function of slope, S; (C) As a function of transition Reynolds number, R_c, and (D) As a function of intensity of pulse input, P.

Table 3.1. Simulation Results for Equilibrium Times on Selected Planes.

Test Case No.	Length of Plane L (ft)	Roughness Coefficient K	Slope S	Transition Reynolds Number	Intensity of Pulse Input P (in./hr)	Calculated Characteristic Time T (sec)	Simulated Time to Equilibrium T_e (sec)
1	25.	24.	.05	500.	2.0	67.	63.
2	250.	24.	.05	500.	2.0	177.	170.*
3	100.	500.	.10	500.	1.0	365.	356.
4	100.	500.	.15	500.	1.0	318.	308.
5	250.	500.	.10	500.	1.0	492.	488.
6	250.	500.	.10	250.	1.0	607.	595.*
7	250.	500.	.10	500.	2.0	385.	377.*
8	250.	500.	.10	750.	2.0	322.	326.*
9	250.	500.	.10	1000.	2.0	310.	302.
10	25.	500.	.05	500.	2.0	185.	173.

*Laminar and Turbulent Flow.

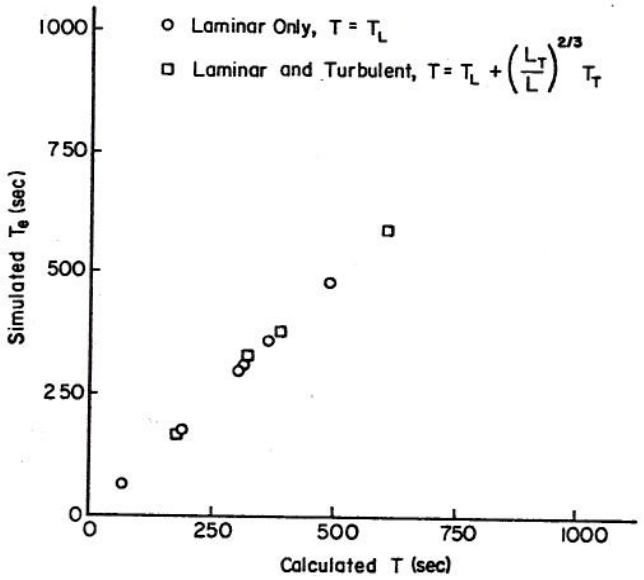

Fig 3.4. Comparison of simulated times to equilibrium and calculated values for 10 test cases.

3.3 Storage at Equilibrium

In addition to the characteristic time derived above, the storage on the surface at equilibrium is proposed as a characteristic number. The reasoning is that this storage represents the overall system performance at equilibrium. The storage per unit width on a plane surface at equilibrium is

$$S_e = \bar{H}L \tag{3.37}$$

where $\bar{H}$ is the average equilibrium or steady state depth, and L is the length of the plane. Considering the depth at an arbitrary distance, x, from the upstream boundary, steady state discharge is

$$q(x) = \alpha\, h(x)^n \tag{3.38}$$

where α and n have values corresponding to the flow type at the point x. Solving Eq. 3.38 for the steady state depth with $q(x)$ determined as in Eq. 3.26 for an arbitrary x instead of L, the result is

$$h(x) = \left[\frac{Px}{43200\ \alpha}\right]^{\frac{1}{n}} \tag{3.39}$$

for $0 \le x \le L$. The average depth is then

$$\bar{H} = \left(\int_0^L h(x)dx\right) \Big/ L, \tag{3.40}$$

where a possible transition from laminar to turbulent flow is accounted for by adopting the proper values of α and n in Eq. 3.39. The resulting equation is

$$\bar{H} = \left(\int_0^{L_L} h(x)dx + \int_{L_L}^{L} h(x)dx\right) \Big/ L \tag{3.41}$$

where the length of laminar flow, L_L, is determined by Eq. 3.33. If L_L is greater than or equal to the length of the plane, L, then the second integral in Eq. 3.41 is zero.

To illustrate the application of the average storage concept to specific planes, again consider the 10 test cases given in Table 3.1. The average depth at equilibrium discharge is calculated using Eq. 3.41 for each of the 10 cases. These results are summarized in Table 3.2.

The relation between average depth and depth at the downstream boundary is shown in Fig. 3.5. From Eqs. 3.39 and 3.40, the depths should be related by the factor $n/(n+1)$, the coefficient due to integration, equal to 0.75 for laminar and 0.60 for turbulent flow. The cases with mixed laminar and turbulent flow fall between these extremes. The equilibrium storage

Table 3.2. Summary of Storage at Equilibrium for Uniform Input to Planes with Kinematic Flow, for 10 Test Cases from Table 3.1.

Test Case No.	Intensity of Pulse Input, P (in./hr)	Length of Plane L (ft)	Length of Flow		Coefficient		Average Depth H (ft)	Depth at Downstream Boundary h(L) (ft)	Storage S_e (ft^3/ft)
			Laminar L_L (ft)	Turbulent L_T (ft)	α (Laminar)	α (Turbulent)			
1	2.0	25.	25.	-	44700.	-	.0022	.0030	.056
2	2.0	250.	130.	120.	44700.	16.38	.0052	.0079	1.290
3	1.0	100.	100.	-	4293.	-	.0061	.0081	.611
4	1.0	100.	100.	-	6440.	-	.0053	.0071	.533
5	1.0	250.	250.	-	4293.	-	.0083	.0110	2.072
6	1.0	250.	130.	120.	4293.	3.59	.0089	.0138	2.233
7	2.0	250.	130.	120.	4293.	5.08	.0113	.0173	2.818
8	2.0	250.	194.	56.	4293.	6.22	.0106	.0151	2.643
9	2.0	250.	250.	-	4293.	-	.0104	.0139	2.610
10	2.0	25.	25.	-	2147.	-	.0061	.0081	.152

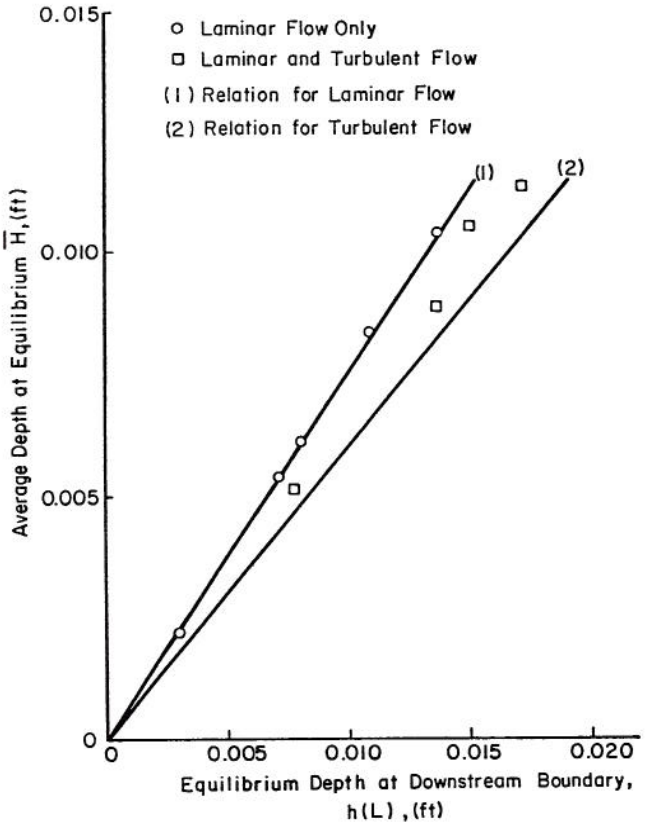

Fig. 3.5. Relation between downstream boundary and average depths at equilibrium, uniform, constant input on planes.

can be estimated from the equilibrium depth at the downstream boundary as well as from the average equilibrium depth as derived above.

In Section 3.2 characteristic time for a plane is derived and in this section equilibrium storage or characteristic depth which determines storage is derived. Both factors reflect the hydraulic performance of a plane in response to a pulse input (uniform and constant) of magnitude P.

3.4 Kinematic Impulse Response

As in the previous two sections, the intent here is to examine overland flow on arbitrary surfaces and to see how the characteristics of the surfaces are reflected in the flow characteristics. However, in the previous sections the analyses were restricted to equilibrium or steady state conditions. Is there a similar theory for dynamic conditions? The extreme contrast is the impulse response. A pulse input is an input of finite magnitude beginning at time zero and continuing at a constant rate. An impulse input is an input of finite depth occurring instantaneously. A pulse input is also known as a "step function" while an impulse input is also known as a "delta function." In contrast with the linear impulse response, or instantaneous unit hydrograph, the kinematic impulse response is nonlinear; i.e., the response varies with the magnitude of the impulse input. In spite of this, the nonlinear impulse response is proposed as an efficient means of representing the combined effects of several factors in a functional form. The reasoning is that the nonlinear impulse response is a function characterizing a particular dynamic response of a complex nonlinear system. By using the impulse input, the space and time variabilities of the input are eliminated. Thus the influence of the surface configuration is emphasized.

The kinematic impulse response was used as a kernel function by Eagleson (1967) to allow superposition in a study of the influence of spatial variability of the rainfall. Harley, et al., (1970) obtained impulse responses for a single plane and derived a minimum sampling interval for the input in terms of the time of concentration. The following sections examine the kinematic impulse response for planes (see above references) and for surfaces described by second order (parabolic) equations.

Recall the kinematic wave equations:

$$\frac{\partial h}{\partial t} + \frac{\partial (uh)}{\partial x} = q(x,t) \qquad (3.42)$$

and

$$u = \alpha h^{n-1}, \tag{3.43}$$

where the variables are as defined previously. If Eq. 3.43 is substituted into Eq. 3.42 the result is:

$$\frac{\partial h}{\partial t} + n\,\alpha(x)h^{n-1}\frac{\partial h}{\partial x} = q - \alpha'(x)h^{n} \tag{3.44}$$

where

$$\alpha'(x) = \partial\alpha(x)/\partial x.$$

An impulse input is equivalent to an initial condition of

$$h(o) = h_o \tag{3.45}$$

for the partial differential equation, Eq. 3.44.

3.4.1 Plane Surface

For a plane surface, the equation for the slope, Eq. 3.9 is $S(x) = S_o$, a constant. Evaluation of the coefficient $\alpha(x)$ reduces to the case of α as a constant, so that $\alpha'(x) = 0$ and Eq. 3.44 reduces to

$$\frac{\partial h}{\partial t} + n\alpha h^{n-1}\frac{\partial h}{\partial x} = q. \tag{3.46}$$

To obtain a solution to Eq. 3.46, consider the equation of the characteristic defined by dx/dt. So we must first solve for h as a function of x.

Take the total derivative of h with respect to time, which produces

$$\frac{dh}{dt} = \frac{\partial h}{\partial x}\frac{dx}{dt} + \frac{\partial h}{\partial t} \tag{3.47}$$

which is the same as the left side of Eq. 3.46, if

$$\frac{dx}{dt} = n\alpha h^{n-1}. \tag{3.48}$$

Therefore,

$$\frac{dh}{dt} = \frac{\partial h}{\partial t} + n\alpha h^{n-1}\frac{\partial h}{\partial x} = q \tag{3.49}$$

so that from Eq. 3.49

$$\frac{dh}{dt} = q \tag{3.50}$$

and from Eqs. 3.48 and 3.50

$$\frac{dh}{dx} = \frac{dh/dt}{dx/dt} = \frac{q}{n\alpha h^{n-1}} \tag{3.51}$$

which must be solved to obtain h as a function of x. Rearranging Eq. 3.51,

$$\frac{dh}{h} = \frac{q\,dx}{n\alpha h^{n}} \tag{3.52}$$

which produces

$$\ln h = \int \frac{q}{n\alpha h^{n}}\,dx + \ln C_1 \tag{3.53}$$

with $h(x)$ as its solution.

The solution to Eq. 3.53, $h(x)$, can be substituted into Eq. 3.48 to give

$$\frac{dx}{dt} = n\alpha[h(x)]^{n-1}, \tag{3.54}$$

with its solution $t(x)$ as a function of x.

Before obtaining the impulse response, it is desirable to consider some of its features qualitatively. As discussed previously, the usual sequence of events for a pulse response is for overland flow to begin as laminar flow with transition to turbulent flow, if the flow depth reaches the transition depth for the given conditions. With an impulse input the situation is reversed. Flow begins with an initial depth which may or may not exceed the transition depth. If it does, flow begins as turbulent and will revert to laminar flow somewhere on the recession. If the initial depth is less than the transition depth, the flow will begin and remain laminar. This transition depth is

$$h_T = (R_c\nu/\alpha)^{1/3} \tag{3.55}$$

which is compared with h_o to determine the initial flow type.

For an impulse input, q in Eq. 3.42 is zero, so that Eq. 3.53 becomes

$$\ln h = \ln c_1 \tag{3.56}$$

and

$$h(x) = c_1. \tag{3.57}$$

For $t \le t_c$, the time of concentration or characteristic time defined earlier, it must be that $c_1 = h_o$, the uniform impulse input. With this solution, Eq. 3.54 becomes

$$\frac{dx}{dt} = n\alpha h_o^{n-1} \tag{3.58}$$

and

$$dt = \frac{dx}{n\alpha h_o^{n-1}} \tag{3.59}$$

with solution

$$t(x) = \frac{x}{n\alpha h_o^{n-1}} + c_2 \tag{3.60}$$

which defines characteristics in the x-t plane as straight lines.

To show how the above method is used in calculating the impulse response, assume that only laminar flow exists. Furthermore, assume a plane as described in Tables 3.1 and 3.2 as Test Case No. 5. Therefore, $L = 250$ ft; $K = 500$; $S = 0.10$, and from Eq. 3.55 the transition depth is $h_T = 0.0112$ ft. Thus, assume an impulse input of $h_o = 0.01$ ft which insures laminar flow, then Eq. 3.60 takes the form

$$t(x) = \frac{x}{3\alpha h_o^{2}} \tag{3.61}$$

where α is computed by Eq. 3.20 and then, as in Table 3.2, $\alpha = 4293$. Therefore,

$$t(x) = 0.776x, \tag{3.62}$$

which is 194 sec at the downstream boundary, or the time of concentration is $t_c = 194$ sec. Characteristics for this example are shown in Fig. 3.6. The

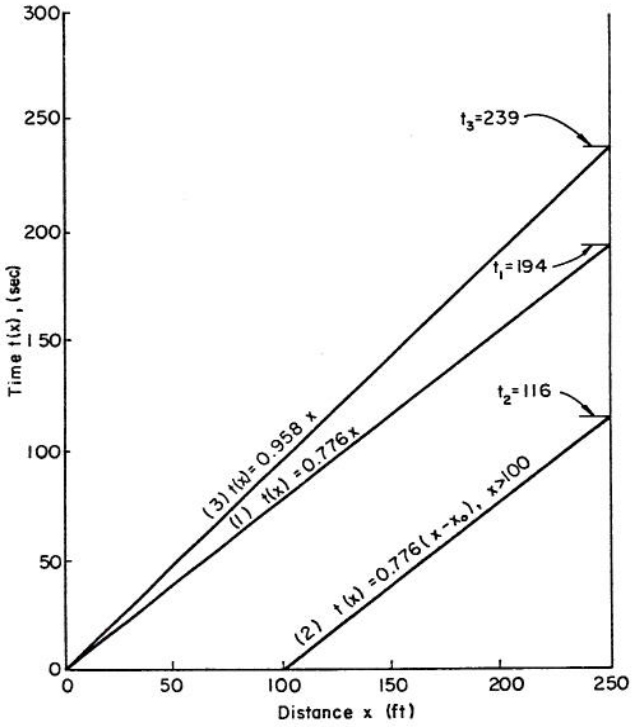

Fig. 3.6. Characteristics in x-t plane, (1) h_o=0.01 ft, x_o=0.0, (2) h_o=0.01, x_o=100. ft, (3) h_o= 0.009 ft, x_o=0.0.

curve (1) is for $x_o = 0$ and $h_o = 0.01$ ft. All characteristics below this are straight and parallel for the same h_o but for different x_o values (see curve (2)). Curve (3) above, is for $x_o = 0$, but at a smaller depth (0.009 ft). If $x = L$, downstream boundary, then for $h_o = 0.01$ each x_o, so that $0 \le x_o \le L$, determines a point on the impulse response, between $t = 0$ and $t = t_c$, as follows:

$$t(h_o,x) = 0.0000776(x-x_o)/h_o^2 \tag{3.63}$$

and

$$Q = 4293\, h_o^3 . \tag{3.64}$$

For $t > t_c$, each h less than h_o produces a point on the recession of the impulse response as follows

$$t(h,x) = 0.0000776\, x/h^2, \quad 0 \le h \le .01 \tag{3.65}$$

and

$$Q = 4293\, h^3. \tag{3.66}$$

Thus, Eqs. 3.63 to 3.66 determine each point (t,Q) on the impulse response. If the flow were entirely turbulent, a similar procedure, with appropriate values of α and n, could be used to compute the impulse response. Values of Q in Eqs. 3.64 and 3.66 are in ft^3/sec-ft. To convert to inches per hour, it is necessary to multiply by 43200/L. Rather than assuming various values of x_o in Eq. 3.63 and various values of $h < h_o$ in Eq. 3.65 it is possible to express the impulse response in terms of the time of concentration, t_c, from Eq. 3.60 with $x = L$, and the impulse h_o (see Harley, et al., 1970). If discharge is expressed in cubic feet per second per foot of width, and

$$t_c = \frac{L}{n\alpha\, h_o^{n-1}} \tag{3.67}$$

then the impulse response for flow of a single type is

$$Q = \begin{cases} \alpha\, h_o^{\,n}, & o \le t \le t_c, \\ \alpha\left(\frac{L}{n\alpha t}\right)^{\frac{n}{n-1}}, & t > t_c \end{cases} . \tag{3.68}$$

In inches per hour, the equation is

$$Q = \begin{cases} (43200./L)\alpha h_o^{\,n}, & o \le t \le t_c, \\ (43200./L)\ \alpha\left(\frac{L}{n\alpha t}\right)^{\frac{n}{n-1}}, & t > t_c. \end{cases} \tag{3.69}$$

A relevant question is how to account for a transition from turbulent to laminar flow in the recession when the flow is initially turbulent. An abrupt transition (negative shock, see Woolhiser, et al., 1971) is shown in Fig. 3.7A. The continuity equation for a region as shown over an interval, dt, is

$$(Q_T - Q_L)dt = \Delta h\, dx \tag{3.70}$$

per unit width. Dividing by dt and with Δh as $h_T - h_L$, the result is

$$(Q_T - Q_L) = \frac{dx}{dt}\,(h_T - h_L) \tag{3.71}$$

so that the shock velocity as shown in Fig. 3.7B is

$$\frac{dx}{dt} = \frac{Q_T - Q_L}{h_T - h_L} \tag{3.72}$$

where T and L represent turbulent and laminar flow. In addition, if Eq. 3.72 must agree with similar calculations for laminar and turbulent flow, then

$$\frac{dx}{dt} = \frac{Q_T - Q_L}{h_T - h_L} = \frac{\alpha_T h_T^{1.5} - \alpha_L h_L^{3}}{h_T - h_L} \tag{3.73}$$

which is also equal to $\frac{1}{n}\,(dx/dt)$ as calculated by Eq. 3.48 for turbulent and laminar flow. Thus, by equating these values

$$h_L = \sqrt{\frac{1}{2}\,\frac{\alpha_T}{\alpha_L}}\; h_T^{1/2} . \tag{3.74}$$

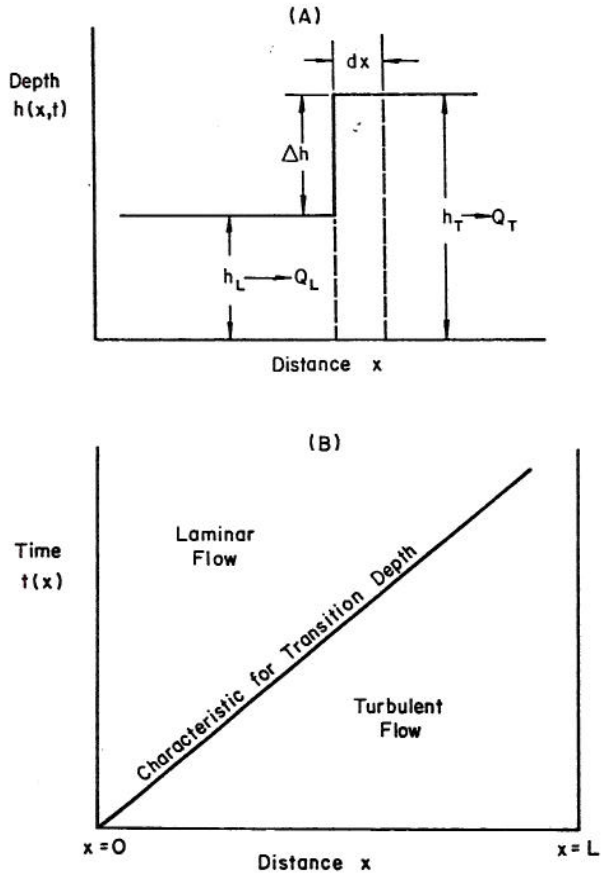

Fig. 3.7. Schematic description of abrupt transition from turbulent flow to laminar flow in the impulse response recession. (A) Schematic of abrupt transition from laminar to turbulent flow; and (B) Schematic for characteristic of the transition depth.

If such a recessional transition to laminar flow is assumed, then after a sufficiently large time, the flow will be laminar.

In anticipation of relating nonlinear and linear impulse responses, consider calculating moments of the nonlinear impulse response using Eq. 3.68 for laminar flow. To calculate the first moment $tQ(t)$ must be integrated for a laminar recession. Consider the time from beginning of laminar flow, and the integral

$$\int_{t_t}^{\infty} tQ(t)dt \tag{3.75}$$

which becomes

$$\int_{t_t}^{\infty} t\alpha\left(\frac{L}{n\alpha t}\right)^{3/2} dt \tag{3.76}$$

for $t_t > t_c$, the time of concentration. Therefore, Eq. 3.76 is of the form

$$C \int_{t_t}^{\infty} t^{-1/2}\, dt \tag{3.77}$$

which is

$$\left[2Ct^{1/2}\right]_{t_t}^{\infty} \tag{3.78}$$

and thus the moments do not exist. If the flow were entirely turbulent, then the first moment would exist but higher ones would not. Finally, moments could be calculated by approximating Eq. 3.75 by a summation with numerical values for t and $Q(t)$.

Figure 3.8 shows an impulse response beginning as turbulent flow with a transition to laminar flow for Test Case No. 5 (Table 3.1) with an impulsive input of magnitude 0.25 in., and the solution as given by Eq. 3.69. Several properties of the nonlinear impulse response of a plane are illustrated in this figure.

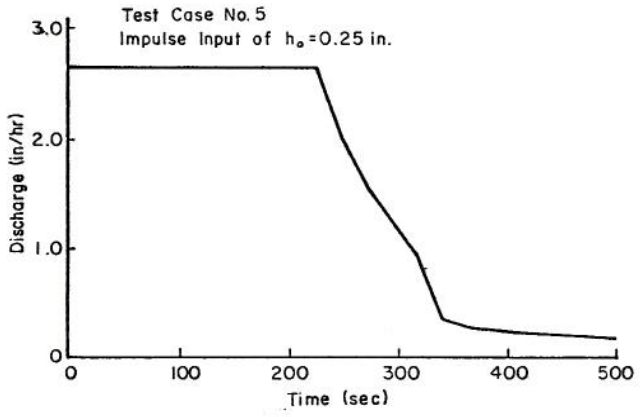

Fig. 3.8. Example of nonlinear impulse response starting as turbulent flow with a transition to laminar flow in the recession for a plane as described as Test Case No. 5 in Table 3.1.

The initial rate is constant up until the time of concentration; then there is a portion of turbulent recession, followed by a transition to laminar flow. In contrast with the linear impulse response, physical features of the system are reflected in the nonlinear impulse response. In the next sections the kinematic impulse response is used to examine the influence of slope shape upon overland flow.

3.4.2 Parabolic Surface

A parabolic surface is next examined. In this case the elevation of the surface is $y(x)$ as given by Eq. 3.1 with $a_3 = 0$, so that

$$s(x) = y'(x) = a_1 + 2a_2x \tag{3.79}$$

Eq. 3.44 becomes

$$\frac{\partial h}{\partial t} + n\alpha(x)\, h^{n-1} \frac{\partial h}{\partial x} = q - \alpha'(x)h^n \tag{3.80}$$

where

$$\alpha(x) = \frac{8g}{K\nu} S(x) = \frac{8g}{K\nu} (a_1 + 2a_2 x) \qquad (3.81)$$

for laminar flow and

$$\alpha(x) = \left(\frac{8gR_c}{K}\right)^{1/2} S(x)^{1/2}$$

$$= \left(\frac{8gR_c}{K}\right)^{1/2} (a_1 + 2a_2 x)^{1/2} \qquad (3.82)$$

for turbulent flow. Let $c_1 = 8g/K\nu$ and $c_2 = (8gR_c/K)^{1/2}$ so that

$$\alpha(x) = c_1 (a_1 + 2a_2 x) \qquad (3.83)$$

for laminar flow, and

$$\alpha(x) = c_2 (a_1 + 2a_2 x)^{1/2} \qquad (3.84)$$

for turbulent flow. The derivative of α is now no longer zero; in fact:

$$\alpha'(x) = 2c_1 a_2 \qquad (3.85)$$

for laminar flow, and

$$\alpha'(x) = c_2 a_2 (a_1 + 2a_2 x)^{-1/2} \qquad (3.86)$$

for turbulent flow.

Recall that the total derivative

$$\frac{dh}{dt} = \frac{\partial h}{\partial x}\frac{dx}{dt} + \frac{\partial h}{\partial t} \qquad (3.87)$$

is equal to the left side of Eq. 3.81, if

$$\frac{dx}{dt} = n\alpha(x)\, h^{n-1} \qquad (3.88)$$

and then

$$\frac{dh}{dt} = \frac{\partial h}{\partial t} + n\alpha(x)\, h^{n-1} \qquad (3.89)$$

as before. From Eq. 3.89

$$\frac{dh}{dt} = q - \alpha'(x) h^n \qquad (3.90)$$

and then from Eq. 3.88

$$\frac{dh}{dx} = \frac{dh/dt}{dx/dt} = \frac{q - \alpha'(x)h^n}{n\alpha(x)h^{n-1}} \qquad (3.91)$$

which reduces to

$$\frac{dh}{h} = \frac{q}{n\alpha(x)h^n}\, dx - \frac{\alpha'(x)}{n\alpha(x)}\, dx. \qquad (3.92)$$

For an impulsive input $q = 0$, and

$$\frac{dh}{h} = -\frac{1}{n}\,\frac{\alpha'(x)}{\alpha(x)}\, dx \qquad (3.93)$$

which has its solution,

$$\ln h = -\frac{1}{n} \ln \alpha(x) + \ln c_3 \qquad (3.94)$$

and thus,

$$h(x) = \frac{c_3}{\alpha(x)^{\frac{1}{n}}} \qquad (3.95)$$

where c_3 must be evaluated. Require that $h(x_o)$ at time zero equal h_o the impulsive input. Therefore,

$$c_3 = \alpha(x_o)^{\frac{1}{n}} h_o . \qquad (3.96)$$

Substitute $h(x)$ into Eq. 3.88 to produce:

$$\frac{dx}{dt} = n\alpha(x)\, h(x)^{n-1} \qquad (3.97)$$

which simplifies to;

$$dt = \frac{dx}{n\alpha(x)\, h(x)^{n-1}} \qquad (3.98)$$

which has the solution

$$t(x) = \int \frac{dx}{n\alpha(x)\, h(x)^{n-1}} + c_4 \qquad (3.99)$$

where c_4 must be evaluated. Substituting for $h(x)$, as given by Eq. 3.95, the result is

$$t(x) = \int \frac{dx}{nc_3^{n-1}\, \alpha(x)^{\frac{1}{n}}} + c_4 \qquad (3.100)$$

where c_3 is given by Eq. 3.96. Now, solving for $t(x)$:

$$t(x) = \frac{1}{4a_2 c_1 c_3^2}\, \alpha(x)^{2/3} + c_4 + c_5 \qquad (3.101)$$

for laminar flow, and

$$t(x) = \frac{1}{2a_2 c_2^2 c_3^{1/2}}\, \alpha(x)^{4/3} + c_4 + c_5 \qquad (3.102)$$

for turbulent flow. Let $c_6 = c_4 + c_5$, and require that $t(x_o) = 0$ so that

$$c_6 = \frac{-\alpha(x_o)^{2/3}}{4a_2 c_1 c_3^2} \qquad (3.103)$$

for laminar flow and

$$c_6 = -\frac{\alpha(x_o)^{4/3}}{2a_2 c_2^2 c_3^{1/2}} \qquad (3.104)$$

for turbulent flow.

Since $\alpha(x)$ is proportional to x for laminar flow and $x^{1/2}$ for turbulent flow, $t(x)$ is proportional to $x^{2/3}$ in Eqs. 3.101 and 3.102. From Eq. 3.95, $h(x)$ is proportional to $x^{-1/3}$ for both flow types.

Before considering a specific example, impulse responses from parabolic surfaces must be examined qualitatively. Consider an impulse input so that the plane response is entirely laminar, and assume a similar but concave surface and the possibility that there might be a transition to turbulent flow. If attention is limited to flow at the downstream boundary, then the transition will occur if q/ν exceeds R_c, the transition Reynolds number. The procedure would be to start with an x_o slightly less than L, the length of the surface, and apply Eqs. 3.95 and 3.99 for decreasing x_o until the transition discharge is reached. At this point the equations for turbulent flow would apply until the recessional transition.

As examples, consider two parabolic surfaces with other properties as in Test Case No. 5 (Table 3.1, Fig. 3.8). Slope profiles for these examples and the plane are shown in Fig. 3.9. For the concave surface

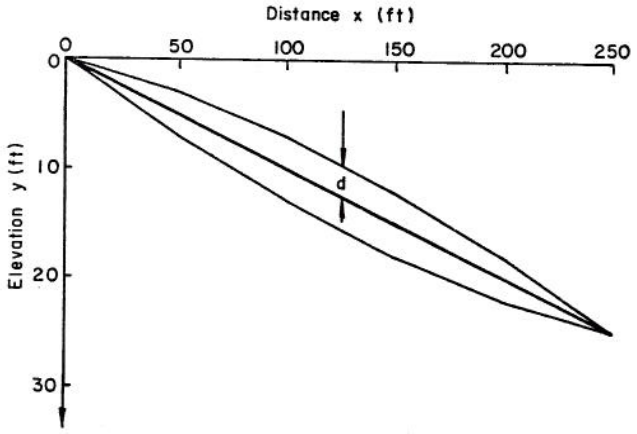

Fig. 3.9. Slope profiles for uniform and parabolic surfaces.

$a_o = 0$, $a_1 = 0.15$, and $a_2 = -0.0002$, so that Eq. 3.79 is

$$y(x) = 0.15x - 0.0002x^2 \qquad (3.105)$$

and for the convex surface $a_o = 0$, $a_1 = 0.05$, and $a_2 = 0.0002$ so that

$$y(x) = 0.05x + 0.0002x^2 \ . \qquad (3.106)$$

The impulse responses for the plane, concave, and convex surfaces are shown in Figs. 3.10 and 3.11. Figure 3.10 shows the three hydrographs for initially turbulent flow, and Figure 3.11 is for initially laminar flow. The concave and convex surfaces are symmetrical (but opposite) in their deviations from the uniform slope plane (Fig. 3.9). For parabolic surfaces, such as shown in Fig. 3.9, a measure of the degree of departure from a uniform slope (plane) is the difference in elevations. If L is the length of the surface (in projection on a horizontal plane) and S_o is the average slope, then

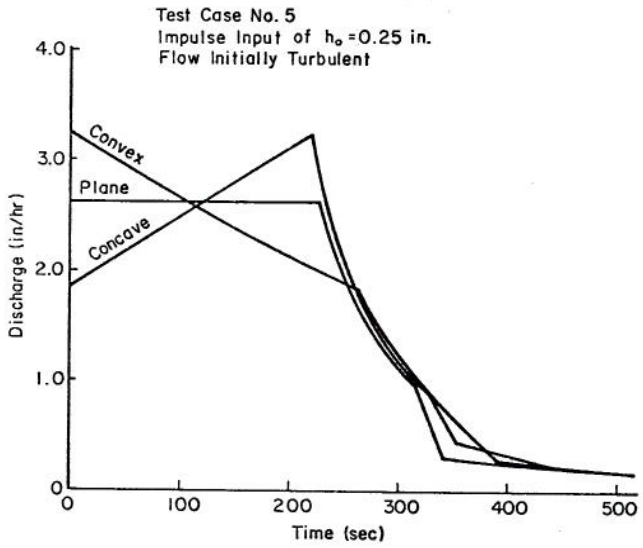

Fig. 3.10. Impulse responses for uniform and parabolic slopes, flow initially turbulent.

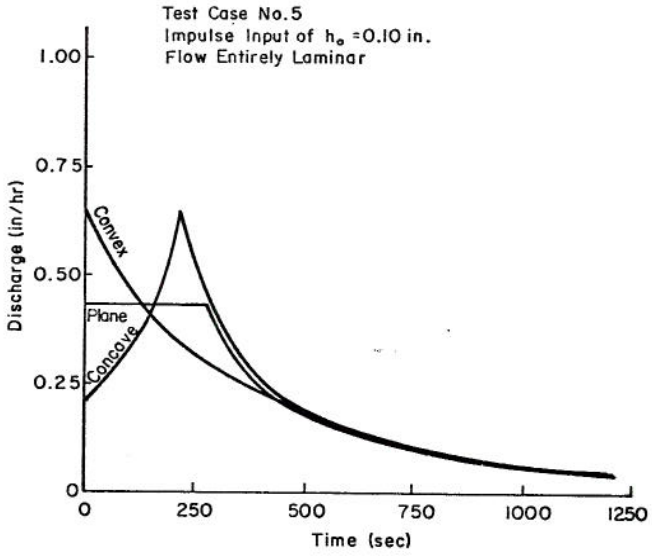

Fig. 3.11. Impulse responses for uniform and parabolic slopes, flow initially laminar.

$$d(x) = S_o x - a_1 x - a_2 x^2 \qquad (3.107)$$

is the departure as a function of distance.

Now, in anticipation of using a similar statistic in modeling complex watersheds, consider the integral of $[d(x)]^2$ divided by the integral of $(S_o x)^2$. That is,

$$r^2 = 1.0 - \frac{\int_o^L [d(x)]^2 \, dx}{\int_o^L S_o^2 x^2 \, dx} \qquad (3.108)$$

is the proposed statistic. The next step is to relate this statistic to characteristics of the impulse response.

From Eq. 3.68 the peak discharge of the impulse response for a plane is

$$q_p = \alpha h_o^n \tag{3.109}$$

and for a concave parabola,

$$q_p = \alpha(o)\ h_o^n \tag{3.110}$$

(from Eqs. 3.95 and 3.96, for $x_o = 0$, and at $t = t_c = t(L)$ as in Eqs. 3.101 and 3.102). For the convex parabola the peak is at $t = 0$ so that

$$q_p = \alpha(L)\ h_o^n \tag{3.111}$$

where h_o is the magnitude of the impulse input and $\alpha(x)$ is a function of x. Recall that $\alpha(x)$ is a function of slope (assuming constant roughness) as given by Eqs. 3.83 and 3.84

$$\alpha(x) = c\ S(x)^{n/3} \tag{3.112}$$

where the coefficient c and exponent n depend upon the flow type. Now, the ratio of the peak of the impulse response from the concave surface to the peak of the impulse response from the plane is

$$\frac{q_p(\text{concave})}{q_p(\text{plane})} = \frac{\alpha(o)\ h_o^n}{\alpha\ h_o^n} = \left(\frac{S(0)}{S_o}\right)^{n/3} \tag{3.113}$$

where S_o is the slope of the plane or the average slope and $S(0)$ is the initial (maximum) slope of the concave surface. The corresponding ratio for the convex parabolic surface is

$$\frac{q_p(\text{convex})}{q_p(\text{plane})} = \frac{\alpha(L)\ h_o^n}{\alpha\ h_o^n} = \left(\frac{S(L)}{S_o}\right)^{n/3} \tag{3.114}$$

where $S(L)$ is the slope of the convex surface at the downstream boundary (the maximum slope). Therefore, the ratios then become (S_{max}/S_o) for laminar flow and $(S_{max}/S_o)^{1/2}$ for turbulent flow.

The relation between these peak ratios and the corresponding values of r^2 is shown in Fig. 3.12. The circle points correspond to entirely laminar flow and the square points are for initially turbulent flow. Since $n = 3.0$ for laminar flow and $n = 1.5$ for turbulent flow in Eqs. 3.113 and 3.114, the effects of slope shape upon the peak rate of runoff is more pronounced for laminar flow.

In subsequent analysis, a cascade of planes will be used to model complex slope shapes. The statistic of deviations, r^2, of the planes from the complex slope will be used as a measure of how well the slope is being modeled with respect to peak discharge of the impulse response.

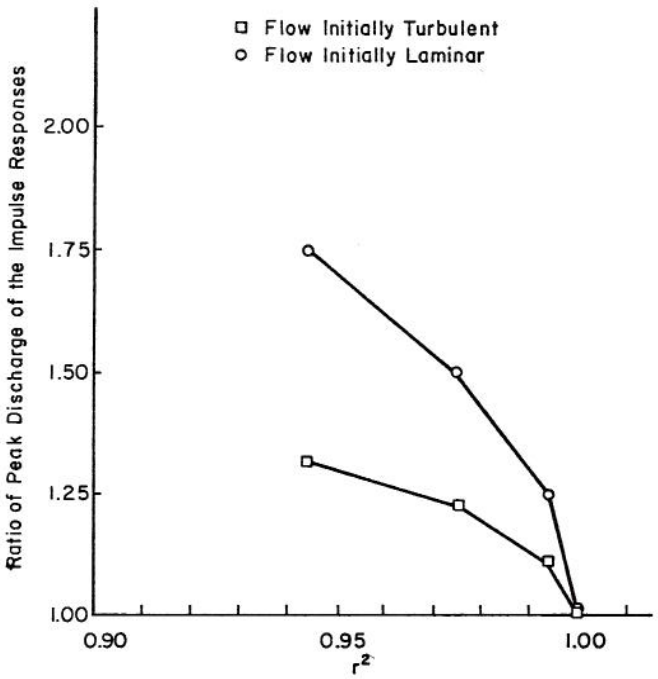

Fig. 3.12. Relation between the statistic of deviations, r^2, and ratio of peak discharge of the impulse response from concave parabolic and plane surfaces.

3.4.3 Complex Surfaces

To examine the influence of complex slope shape upon overland flow, assume that geometrically simpler surfaces than those found on natural hillslopes could reproduce some essential properties. For example, parabolic surfaces were used to investigate concave and convex slope shapes. As discussed earlier, a cubic equation is a simple representation of a complex surface with both convex and concave portions. For cubic surfaces, the slope function is now quadratic. Equation 3.80 could be solved as in the previous section. However, because of the trade-off between analytic and numerical methods when the former becomes more involved and because of the necessity of examining a cascade of planes approximation to complex slopes, numerical methods are used in this section. The procedure is to use a cascade of planes and the finite difference program for a kinematic cascade.

Cascade of Planes Approximation. For example, consider Test Case No. 5 (Table 3.1) with a concave parabolic surface as the lower curve in Fig. 3.9. The procedure is to model the concave surface as a plane, a cascade of two planes, three planes, and so on. Then, the goodness-of-fit statistic (r^2 or $1-r^2$) is compared with the corresponding impulse responses. Again, r^2 is defined by Eq. 3.108, where $d(x)$ is the difference between the cascade of planes and the concave parabolic surface.

Table 3.3 presents the results of simulation, using the finite difference program. The first four rows of the table are for laminar flow and the last four rows are for turbulent flow. Moreover, the

Table 3.3. Surface Characteristics of the Cascade of Planes Approximations to Parabolic Surfaces Versus Peak Discharge of the Impulse Responses. Test Case No. 5 as Given in Table 3.1.

Number of Planes in Cascade	Goodness of Fit Statistic r^2	Transformed Statistic $(1-r^2)^{5/12}$	Peak Discharge of Impulse Response (in./hr)		Ratio of Peak Discharge of Impulse Responses to: Peak from Plane Y_1	Peak from Parabolic Surface Y_2	Logarithmic Transformed Ratios of Peaks $\ln Y_1$	$\ln Y_2$
			Concave	Convex	Concave	Concave	Concave	Concave
Laminar								
2	.9906	.1429	.7124	.6440	1.659	1.106	.5062	.1007
3	.9966	.09358	.6640	.6440	1.547	1.031	.4363	.0305
4	.9982	.07150	.6445	.6440	1.501	1.001	.4061	.0010
∞*	1.00	0.0	.6440	.6440	1.500	1.000	.4055	0.0
Turbulent								
2	.9906	.1429	3.379	3.230	1.281	1.046	.2476	.0450
3	.9966	.09358	3.268	3.230	1.239	1.012	.2143	.0119
4	.9982	.07150	3.232	3.230	1.226	1.001	.2038	.0010
∞*	1.00	0.0	3.230	3.230	1.225	1.000	.2029	0.0

*Infinite number of planes corresponds to the parabolic surfaces, see curves labeled "concave/convex" in Figs. 3.10 and 3.11.

impulsive inputs are identical to those used in producing hydrographs (Figs. 3.10 and 3.11). The columns labeled Y_2 shows the ratio of the cascade of planes peak discharge to the parabolic surface peak discharge. For the convex surface two planes are sufficient to duplicate the peak discharge from the parabolic surface because the discharge for an impulse response peaks at time zero and is thus a function of h_o and α at the downstream boundary. However, the hydrograph shape is not well reproduced. For the concave surface, the peak discharge comes closer to the theoretical value as the number of planes in the cascade increases. For example, a cascade of three planes has a peak discharge differing only by 3 percent from the theoretical value for laminar flow and only about 1 percent for turbulent flow. There seems to be a linear relation between $\ln Y_2$ and $(1-r^2)^{5/12}$ for the concave cascades.

As an index of how time properties are preserved in the cascade approximation to the concave surface, the time to peak discharge (equal to the time of concentration for the concave parabolic surface) is plotted in Fig. 3.13. Since time to peak, T_p, is undefined for the impulse response, it is represented as 0, $t_c/2$, and t_c; where t_c is the time of concentration for a plane. These three points are shown in the vertical axis in Fig. 3.13. The horizontal line in Fig. 3.13 represents the time of concentration or the characteristic time for the parabolic surface. The percent errors in characteristic time for the two, three and four plane cascades are -22, -14, and -11, respectively. For example of the overall correspondence of the impulse response from a similar parabolic surface, hydrographs for a three-plane cascade and for the parabolic surface are shown in Fig. 3.14. The peak values, time to peak, and later recession values are in excellent agreement.

While it is perhaps premature to discuss some implications of the above analyses due to the lack of extension of the above results to complex watersheds

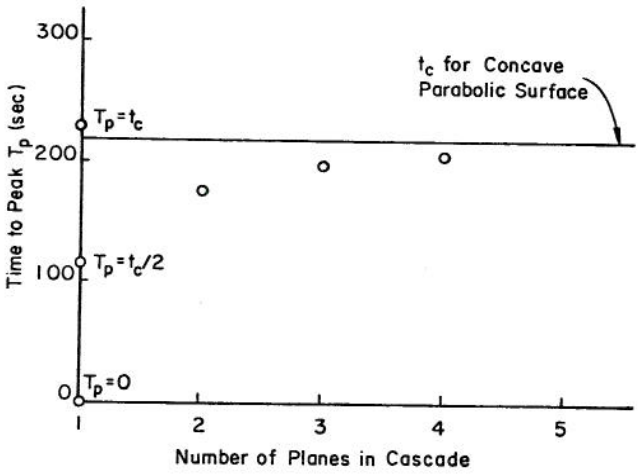

Fig. 3.13. Relation between number of planes in cascade and time to peak of impulse response as an approximate characteristic time. Test Case No. 5 as described in Tables 3.1 and 3.3.

and for complex inputs, let us proceed to do so. First, it is established that overland flow is affected by slope shape and that the effects on peak discharge and time characteristics of the impulse response can be related to statistics of the surface as related to uniform slopes. Moreover, the impulse response of complex slopes can be simulated by a cascade of planes. The goodness-of-fit of the geometric approximation via a cascade of planes can in turn be related to goodness-of-fit measures of the impulse responses. These basic relationships provide hints as to methods of analyzing complex watersheds, i.e., they provide clues as to possible relationships between geometric and hydrologic goodness-of-fit statistics for complex watersheds. Before this development, however, responses to inputs other than impulse inputs must be examined.

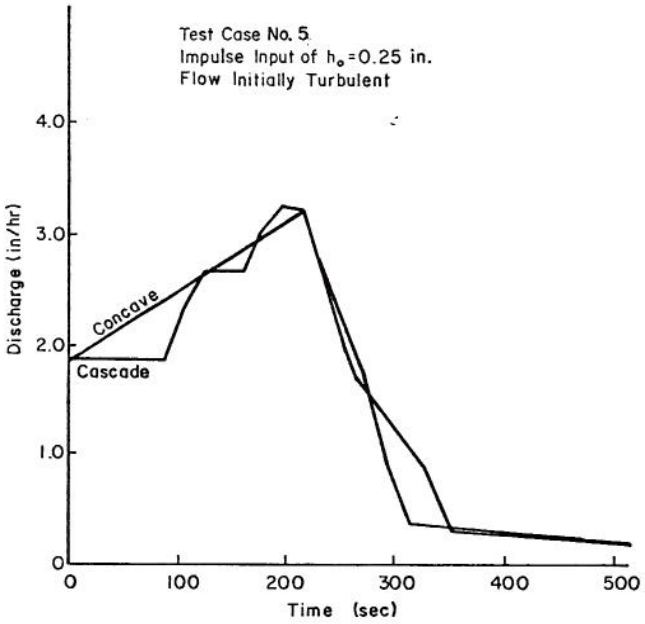

Fig. 3.14. Impulse responses for a concave parabolic surface and for a three-plane cascade approximation to that surface.

3.5 Pulse Response

In the previous section it was noted that as the analytic solution became more complex numerical methods became more attractive. The situation is similar when the input pattern becomes more complex. This section presents an analytic solution for constant, uniform input (pulse input) to a plane. Numerical methods are used for more complex input to planes and for pulse (uniform and constant) input on concave slopes.

3.5.1 Plane Surface

As with the impulse response, the pulse response of a plane is well-known. For example, see Henderson and Wooding (1964) for analysis and plots of pulse responses; for a general discussion, see Chapter 15 of Eagleson (1970), for discussion in terms of nonlinear systems, see Dooge (1967) and Singh (1974) for plane and converging surfaces.

The basic equation (Eq. 3.44) is solved in two parts; the rising and recession limbs. For a pulse input of duration equal to the time to equilibrium, T, the rising hydrograph is given as

$$Q = Q_e (t/T)^n \qquad (3.115)$$

where T is given as

$$T = \alpha^{-\frac{1}{n}} Q_e^{-(\frac{n-1}{n})} L \qquad (3.116)$$

or since $Q_e = P(L/43200.)$, T is also given by Eq. 3.29. Thus, from Eq. 3.115 the discharge on the rising hydrograph is related to t^3 for laminar flow and $t^{1.5}$ for turbulent flow. The recession from equilibrium is given as

$$\left(\frac{Q_e}{Q} - 1\right)\left(Q/Q_e\right)^{\frac{1}{n}} = \alpha(t/T) \qquad (3.117)$$

where Q is discharge; Q_e is the equilibrium discharge, and t is elapsed time after cessation of input. If the pulse input ends before time T, then the response is called a "partial equilibrium response." The rising hydrograph is given by Eq. 3.115 until, D, the duration of input, then constant at the rate Q(D) for a period of time given by

$$t' = T\, n^{-1}\, (Q(D)/Q_e)^{\frac{1}{n}}\, (Q_e/Q(D)-1) \qquad (3.118)$$

until recession begins as described by Eq. 3.117 starting from equilibrium at time D.

3.5.2 Parabolic Surface

As described in Section 3.4.3, parabolic surfaces are modeled as cascades of planes for analysis using the finite difference program. As before, the goodness-of-fit statistic, r^2, is used to judge the number of planes necessary. The procedure is to derive a relation as shown in Table 3.3 and Fig. 3.13 and then use the runoff from the resulting cascade of planes as an approximation to the pulse response of the parabolic surface. Rather than examine pulse responses separately, the responses of a plane and a concave cascade of three planes are considered.

3.5.3 Comparison of Partial Equilibrium Hydrographs

The 10 test cases as described in Tables 3.1 and 3.2 were used for comparison. Each plane was compared with a concave cascade of three planes with similar characteristics, except the slope of the uppermost plane in the cascade had 1.5 times the average slope, the second plane had the average slope (same as the uniform plane described in Table 3.1), and the lowest plane had 0.5 the average slope. Characteristic times, T, were derived by simulation for each case. The results of this simulation are shown in Fig. 3.15 where corresponding times are shown for

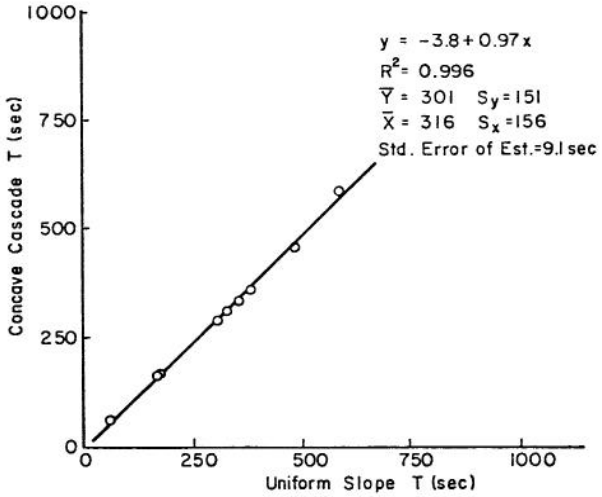

Fig. 3.15. Relation between equilibrium times, T, on uniform slope and corresponding concave cascade. Equilibrium discharge as 95 percent of input rate.

the uniform slope and concave slope surfaces. The differences are small, about 5 percent.

Dimensionless rising hydrographs for a plane are shown in Fig. 3.16 as the solid lines. The upper

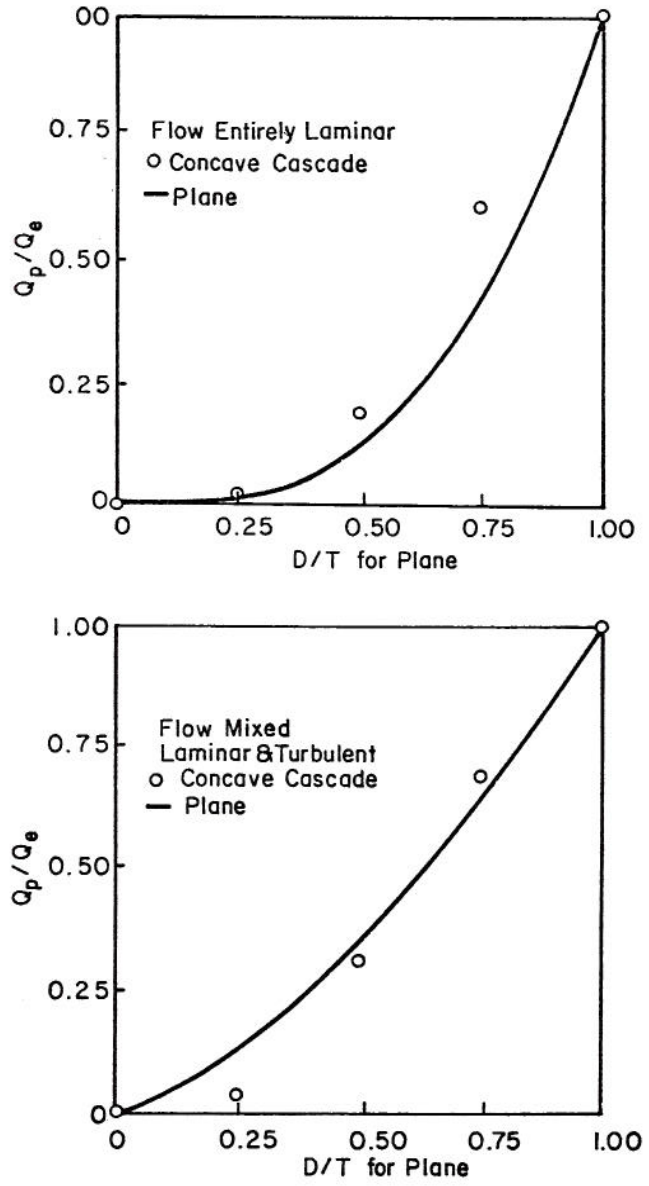

Fig. 3.16. Comparison of partial equilibrium hydrographs from uniform (plane) slopes and from concave cascades of three planes. Test Cases Nos. 1 to 10, as in Tables 3.1 and 3.2.

graph is for entirely laminar flow and the solid curve in the lower graph is for entirely turbulent flow. The circled points in the upper portion of Fig. 3.16 are simulation results for the concave cascade with T as calculated from the uniform slope. The ratio of Q_p/Q_e for the cascade to Q_p/Q_e for the uniform slope is nearly 1.5 as predicted by Eq. 3.113, for the points at 0.25, 0.50, and 0.75 on the D/T axis. The least squares fit to these points has an exponent of 2.77 as compared with the 3.0 value for laminar flow on a plane. The circled points in the lower portion of Fig. 3.16 are for those cases where there was both laminar and turbulent flow on the plane for $D = T$. For D/T values less than 0.5, flow was almost entirely laminar; hence, the points fall below the line for turbulent flow. This suggests that under conditions where flow becomes turbulent on the uniform slope but remains laminar on the cascade that peak discharge from the plane would exceed the peak discharge on the concave surface.

As in the case of impulse inputs, pulse responses for inputs of duration less than equilibrium are significantly influenced by characteristics of the overland flow surface. For laminar sheet flow, the results are straightforward--concavity increases peak discharge. For mixed-flow type, if there is a difference in the flow types, peak discharge from the concave surface can be less than or greater than the corresponding peak discharge from a plane.

3.6 Response to Complex Input

As used here, complex input means rainfall excess that can vary in time and space. If the input varies in time but not in space it is uniform, varying. If it varies in space but not time, it is nonuniform, constant. Finally, if the rainfall excess varies in time and space, it is varying, nonuniform.

If the above concepts of complex input are considered in light of laminar and turbulent flow, as well as uniform slope and complex slope surfaces, the problem becomes complex. This section will consider a specific example to accomplish two objectives. First, to demonstrate cognizance of the problems in assuming uniform constant input to a plane surface, as representative of all overland flow situations. Second, to illustrate the power of simulation and to suggest a procedure for simulation studies to sort out the influence of the various factors.

This discussion is limited to two input patterns, as shown in Fig. 3.17. In the upper portion of the graph, $P_1 = 0.5\ \overline{P}$ and $P_2 = 1.5\ \overline{P}$, where $\overline{P}$ is the average rainfall excess rate. In the lower portion of Fig. 3.17, $P_1 = 1.5\ \overline{P}$, and $P_2 = 0.5\ \overline{P}$. For example, consider Test Case No. 5 as described in Table 3.1. The average rainfall excess $\overline{P}$, is 1.0 in./hr for a duration equal to the time to equilibrium.

Overland flow hydrographs corresponding to the input patterns shown in Fig. 3.17 are shown in Fig. 3.18. For these hydrographs the average input rates are equal as are the durations. There is a difference in the rising portions of the hydrographs and in the peak discharge which in a qualitative sense, are large due to the large variations in the input-variations in rate and to the large time interval, $D/2$, as compared with the duration.

Every hydrologist seriously considering surface runoff on natural watersheds is aware of space-time variability of rainfall and rainfall excess. In spite of this, spatial variability of rainfall excess and the resulting runoff are described as "partial area response" or some other term which suggests a new concept. The concept is not new nor does it require special attention. Models which admit distributed parameters and distributed input implicitly and explicitly account for this concept. For example, just as a cascade of planes can adequately represent a complex slope, the number of planes can be increased--each with a different rainfall excess--to account for spatial variability of rainfall excess.

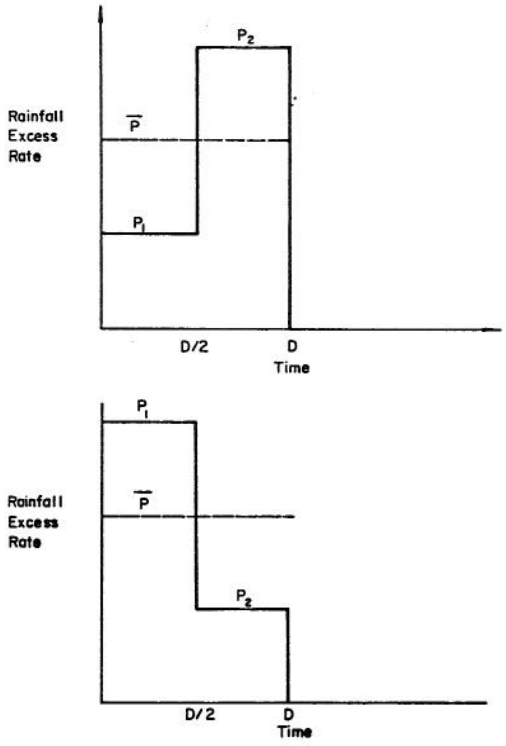

Fig. 3.17. Rainfall excess input patterns for uniform, time varying input.

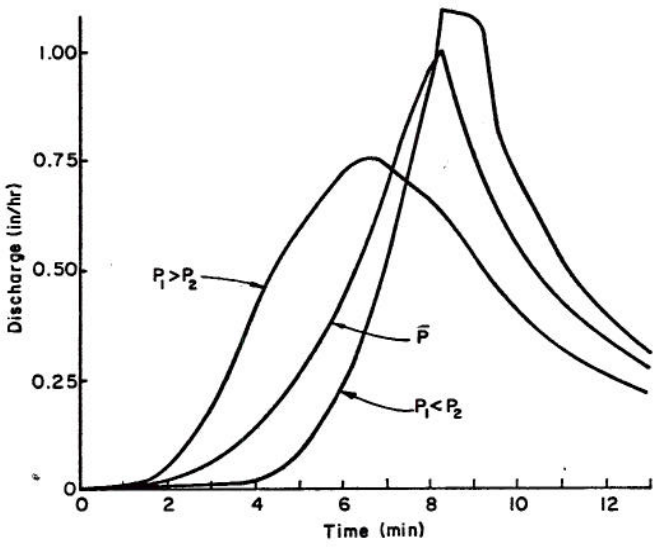

Fig. 3.18. Overland flow hydrographs for input patterns shown in Fig. 3.17. Example of uniform time varying input. Test Case No. 5.

Chapter IV
RUNOFF FROM COMPLEX WATERSHEDS

4.1 Geometric Simplification

The term "complex watershed" as used here denotes situations where a one-to-one correspondence between geometrical elements in the model and in the real system cannot be maintained. Thus, the term connotes overland flow over natural surfaces and open channel flow in natural channels as opposed to hypothetical flow situations.

Before more involved discussions of simplification techniques, the reasons for geometric simplification are discussed. Geometric simplification is the substitution of a rather simple geometry for a more complex one; i.e., a complex watershed is modeled as a simple cascade of planes and channels. To model surface runoff from a complex watershed (i.e., to formulate and solve the equations describing the process) one must assume a simplified geometry. Moreover, there is a tradeoff between network complexity and accuracy, on the one hand, and computational ease and data requirements on the other. Finally, to sort out the influence of specific components within the system, these components must be isolated and computationally separate enough to allow sensitivity analysis. Assuming the need to adopt simplified geometric representations of complex watersheds, now it is possible to examine techniques for and consequences of such simplifications.

4.1.1 Characteristics Which Are Preserved

In adopting the kinematic cascade model for surface runoff, several watershed characteristics should be preserved. A watershed characteristic is preserved if its value remains unchanged in the simplified geometry. As discussed in the Introduction, watershed area is the single most important geomorphic parameter. To preserve mass continuity, watershed area must be preserved. Also, nearly all geomorphic characteristics are related to area. The length and equivalent (Gray's) slope of the main channel is preserved. By fitting planes by least squares, the average watershed slope (as calculated from coordinate data) is also preserved. The total relief, average elevation and hypsometric integral may be nearly preserved or slightly distorted. Finally, by preserving the above characteristics, the potential energy is nearly preserved.

Suppose that some of the above geomorphic parameters (see column 1 of Table 4.1) were not preserved in the surface runoff model. Many peak discharge equations have been developed, and most of them contain area. For example, Jarvis (1926) plotted $A^{1/2}$ versus peak discharge for a large number of drainage basins. The rational formula is used for estimating peak discharge as

$$Q = CIA \qquad (4.1)$$

where C is a coefficient, I is rainfall intensity, and A is drainage area. Thus, a misrepresentation of the area is likely to result in errors in runoff estimates. As shown by Gray (1961) and confirmed by Murphey et al., (1974) the length and slope of the main channel are correlated with hydrograph time characteristics. As shown by Hickok et al., (1959) average watershed slope (along with other geomorphic parameters) is important in estimating lag time. Finally, if the total relief, average elevation, and hypsometric integral are not preserved then neither is the potential energy of a uniform input to the watershed.

4.1.2 Some Characteristics Which Are Distorted in the Simplified Geometry

The third column of Table 4.1 is a list of some geomorphic parameters which are distorted in the simplified geometry. Stream order and drainage density are not preserved in modeling complex watersheds. However, it may be possible to preserve stream order, but by modeling only a portion of all streams, the drainage density may not be preserved. The effects of a modified drainage density will be discussed in detail later. Topographic roughness will always be distorted in fitting planes to irregular coordinate data. If complex slopes are poorly modeled by a plane, then the measure of topographic roughness will be large. If an irregular area containing many channels is modeled as a plane, then the topographic roughness will not be preserved nor will the drainage density be preserved. In the kinematic cascade model used here, channel cross sections are assumed trapezoidal or triangular. However, in the absence of detailed data, assumptions can be made based upon relationships between hydraulic factors and channel geometry. A primary source in this area for ephemeral streams is the paper by Leopold and Miller (1956) who present extensive data--photographs, tables, and graphs. An excellent review of the state-of-the-art and a good bibliography are presented by Chitale (1973).

Given observed rainfall-runoff data and an assumed model, it is possible to derive optimal roughness coefficients. Any errors in the data as well as geometric distortions will be reflected in these estimated roughness coefficients. Therefore, it is reasonable to expect distortions in estimated (optimized) roughness parameters when there are distortions in other watershed characteristics. A detailed analysis is postponed until after the effects of distortions in channel characteristics and in drainage density are examined.

Before considering the effects of the above distortions, why distortions are needed must be discussed. From Eq. 1.12, the number of first order streams seems to increase with the bifurcation ratio to a power of u-1, where u is the basin order. For higher order basins, the number of streams becomes so large that the trade-off (previously discussed) favors distorting the total number of channels and thus the drainage density. That is, there is a point where the return from including more channels in the model is overcome by the added cost and effort of doing so. How this point is quantified is a major portion of this study and is discussed and analyzed subsequently.

4.1.3 Effects of Distortions

Effects of distortions considered here are limited to those which are reflected in the surface runoff. For example, in Chapter III the influence of overland flow-surface shape upon peak discharge was examined in detail. Slope shape affects the magnitude and time of occurrence of peak discharge of the overland flow hydrograph. Since slope shape was analyzed in Chapter III and drainage density is a measure of

Table 4.1. Some Watershed Characteristics Affected by Geometric Simplifications Adopted in Model Formulation in This Study.

Characteristics Essentially Preserved		Characteristics Slightly Changed		Characteristics Distorted	
A,	Area	F(x),	Hypsometric curve	u,	Stream order
L_c,	Main Channel Length	H,	Total relief	D_d,	Drainage density
S_c,	Main Channel Slope	$\bar{h}$,	Mean watershed elevation	B_f,	Topographic roughness
S_w,	Mean Watershed Slope	I_h,	Hypsometric integral	C, K,	Hydraulic roughness coefficients
		U,	Potential energy	-	Channel characteristics such as cross sections, concavity, etc.
				-	Watershed shape

stream order and topographic roughness, the following discussions will be limited to the effects of distortions in channel characteristics, drainage density, and hydraulic roughness coefficients.

Effects of Distortions in Main Channel Characteristics. If the channel cross section is adequately represented, then the depth area relation for the stream is preserved. If the cross section is not preserved, then the distortions will be reflected in the depth-area and depth-discharge relations. In situations where such data are available, the cross sections are modeled as accurately as possible; when data are not available it is necessary to assume a cross-sectional configuration.

A common conception (e.g. Eagleson, 1970) is that in the absence of lateral inflow, kinematic flood routing results in a steepening of the hydrograph rise, a lengthening of the recession, but no attenuation of peak discharge. The routed hydrograph does change shape as described above and there is a decrease in peak discharge. As an example, consider a rectangular channel with the impulse response of a plane 250 ft long by 100 ft wide as the input hydrograph at the upstream boundary. This input hydrograph is described in Table 3.1 as Test Case No. 5 and is shown in Fig. 3.8. The method of characteristics as described in Chapter III is used to route this hydrograph in a channel. The original calculations were with dimensionless variables, but for this example assume a 1500 ft long channel with a 25 ft wide rectangular cross section. The assumed channel has an average slope of 0.02 and a Chezy C of 40.

At the upstream boundary there is an abrupt rise to rate of Q_o at time zero. The discharge is then constant from $t = 0$ to $t = t_c$, the time concentration of the plane. The characteristic for this constant depth is

$$\frac{dx}{dt_c} = \alpha n h^{n-1} \tag{4.2}$$

where the subscript c denotes characteristic.

The corresponding equation for the shock is

$$\frac{dx}{dt_s} = \alpha h^{n-1} \tag{4.3}$$

where the subscript s denotes shock. Consider the characteristic originating at $x = 0$ and $t = t_c$, that is at the upstream boundary at the end of the period of constant discharge. Since this characteristic is n-times faster than the shock, the two will intercept at a point (t_s, x_s). The situation is as follows: (1) for (t, x) less than (t_s, x_s) there is no reduction in peak discharge but the duration of constant discharge is decreasing, (2) for (t, x) beyond (t_s, x_s) there will be a reduction in peak discharge. This reduction in peak discharge is denoted decay by shock.

Simultaneous solution of Eqs. 4.2 and 4.3 for x_s yields:

$$x_s = \alpha h_o^{n-1} t_s \tag{4.4}$$

where h_o is the initial depth of the upstream boundary. The solution also yields t_s as three times t_c, if $n = 1.5$. Therefore,

$$x_s = 3 \alpha h_o^{1/2} t_c \tag{4.5}$$

is the solution for x_s. For points (t_1, x_1) beyond (t_s, x_s) the cumulative inflow can be equated to the total volume of storage (following a suggestion by D. A. Woolhiser):

$$\int_0^{t_1} Q(s)ds = b \int_0^{x_1} h(s)\, ds \tag{4.6}$$

where $Q(s)$ is the inflow hydrograph at the upstream boundary; $h(s)$ is the depth in the channel, and b

is the width of channel. The solution to Eq. 4.6 gives x_1 as a function of $t_1 > t_s$; h(x) is then a function of x_1, and t_1, and finally the peak discharge is Q_p as a function of h(x). The procedure is to select a value of t_1, then solve for x_1, h(x), and Q_p. This procedure is followed for the example discussed above. The results are shown as the solid line in Fig. 4.1. The channel properties for this example are summarized as the first row of Table 4.2. Numerical solution for the same example (Channel Configuration No. 1) is shown as the dashed line in Fig. 4.1. At $x = x_s = 853$ ft, the numerical solution seems to be about 9 percent in error. For distances less than x_s, the errors are somewhat less, but for $x > x_s$ the errors can be about 10 percent. Therefore, for all values of x, numerical errors are present. However, the numerical results agree with analytic results in predicting the magnitude of the decay by shock.

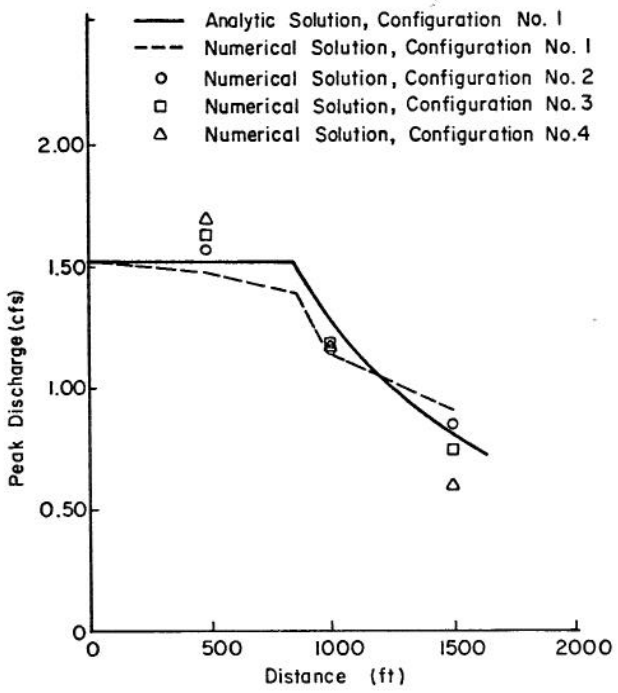

Fig. 4.1. Routed peak discharge as a function of distance for various channel configurations (as described in Table 4.2).

The effects of concavity in channel slopes are examined by simulation. The simulation results are for three channel segments in cascade as described in Table 4.2. These results are also shown in Fig. 4.1. Rows 2, 3, and 4 of Table 4.2 describe the channel configurations with time to peak and peak discharge at the downstream boundary shown in the last two columns. Time to peak increases and peak discharge decreases as concavity increases. These peak discharge values are shown as the circled points in Fig. 4.2. The last three rows of Table 4.2 correspond with uniform slope channels with equivalent slope by Gray's method. Peak discharge values at the downstream boundary for these equivalent slope channels are shown as the square points in Fig. 4.2.

If the downstream channel profile is concave (as described by a parabola with the same relief and thus the same average slope) and other factors are similar, then the distance to the beginning of decay by shock is less than in the uniform slope channel. For example, for a parabolic slope with the initial slope 1.5 times the uniform slope and the final slope 0.5 times the uniform slope, the distance x_s is 690 ft or about 80 percent of the value for a uniform slope channel. This value is consistent with the numerical results.

Assessing the effects of distortions in downstream channel concavity is possible when using

Table 4.2. Channel Characteristics and Corresponding Peak Discharge Values for the Routed Impulse Response* in the Assumed Channels.

Channel Configuration Number	Total Length of Channel (ft)	Equivalent Channel Slope S_c	Slopes for Channel Segments S_1	S_2	S_3**	Index of Concavity for Entire Channel I_c	Routed Impulse Response at Downstream Boundary: Time to Peak (min)	Peak Discharge (cfs)
1	1500.	.020	.020	.020	.020	1.000	24.	.91
2	1500.	.0178	.025	.020	.015	.889	25.	.84
3	1500.	.0156	.030	.020	.010	.778	26.	.74
4	1500.	.0133	.035	.020	.005	.667	30.	.59
2A	1500.	.0178	.0178	.0178	.0178	1.000	26.	.88
3A	1500.	.0156	.0156	.0156	.0156	1.000	27.	.85
4A	1500.	.0133	.0133	.0133	.0133	1.000	29.	.81

*Input to upstream end of channel reach is the impulse response of a plane, Test Case No. 5 as described in Table 3.1 and Fig. 3.8, with no lateral inflow.

**S_3 is the slope of the channel at the downstream boundary.

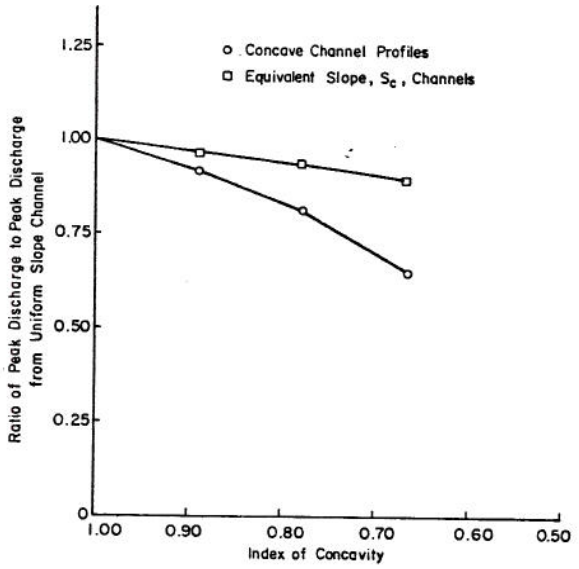

Fig. 4.2. Ratios of peak discharge of routed hydrographs to corresponding peak discharge for a uniform slope channel versus index of concavity.

kinematic flood routing. The distances involved may be large, but peak discharge of the routed hydrographs can decay by shock in the absence of lateral inflow. Concave channel profiles can result in increased time to peak and decreased peak discharge with respect to corresponding uniform slope channels. The magnitude of the changes in routed peak discharge is related to the index of concavity as shown in Fig. 4.2. Moreover, the differences between the two curves in Fig. 4.2 represent the errors in using an equivalent or weighted slope.

Effects of Distortions in Drainage Density. The previous example of flood routing in the absence of lateral inflow is not suited for inference in complex channel networks with lateral inflow as overland flow and tributary flow. As such channel networks fast become unmanageable in terms of detailed simulation and sensitivity analyses, drainage density is used as a single number representing many complex interactions of the varying factors. The veracity of this assumption is tested using simulation results and observed data.

Simulation Results. As an example of how distortions in drainage density affect the surface response, runoff from a simplified watershed is simulated using the finite difference program. The procedure is to simulate runoff from a given watershed with fixed area, roughness, slope, etc., but with changing drainage density. Since nearly all other watershed characteristics do not change, differences in surface response can be related to differences in drainage density. The three test configurations are shown schematically in Fig. 4.3. With respect to these configurations, the first is a single plane with zero drainage density, the second has two planes and one channel (Wooding model) with a drainage density of 0.005 ft/ft^2, and the third configuration has three channels and six lateral inflow-planes with a drainage density of 0.007 ft/ft^2. The third configuration is assumed as the true watershed with the other two as simple approximations. Impulse responses for the three configurations are shown in Fig. 4.4, where the number 1 refers to configuration number 1 as in

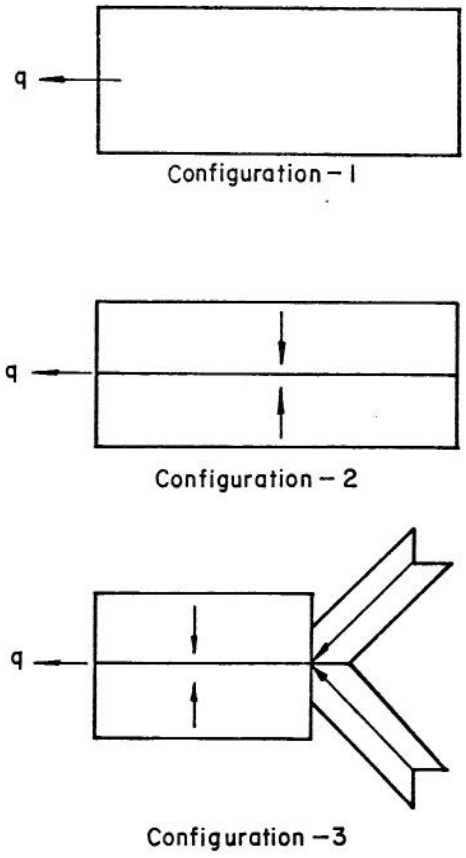

Fig. 4.3. Example configurations for simulation study of the effects of distortions in drainage density.

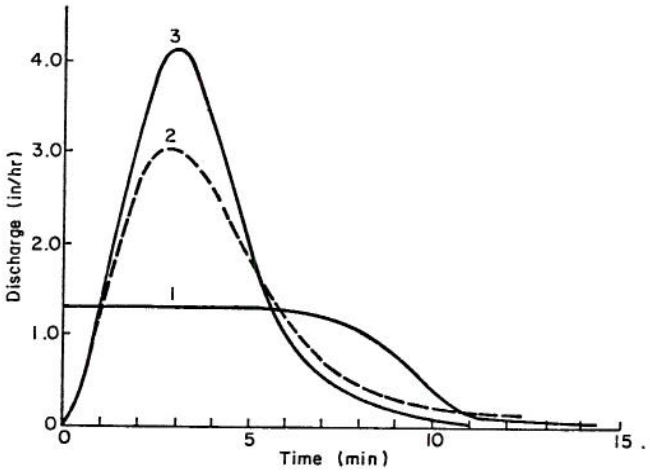

Fig. 4.4. Impulse responses for the three test configurations as shown in Fig. 4.3.

Fig. 4.3, 2 refers to configuration 2, and 3 refers to the impulse response from configuration number 3. There is a large difference in these hydrographs, particularly the difference in hydrographs labeled 2 and 3. A decrease of approximately 29 percent in drainage density resulted in a 26 percent decrease in peak discharge. Peak discharge values for this example are plotted against drainage density as the circled points in Fig. 4.5. Although this is a simple example (the next section deals with data from natural watersheds),

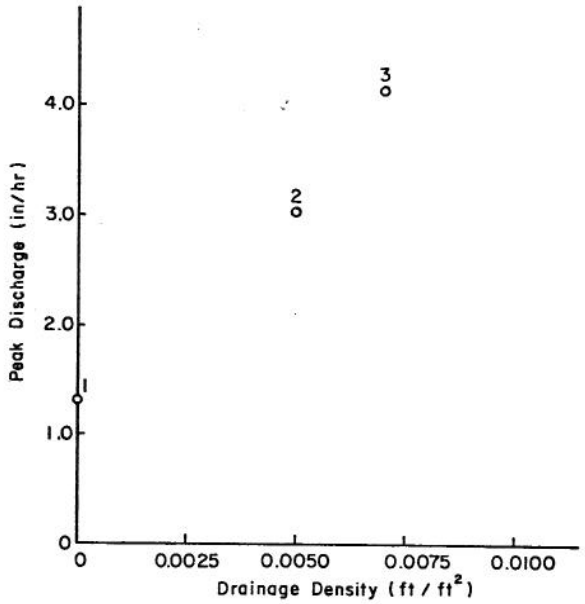

Fig. 4.5. Peak discharge values versus drainage density for the test configurations, identical inputs.

considering its implications can aid in determining the likely effects of distortions in drainage density.

If the relative porportion of overland flow to open channel flow influences the characteristics of surface runoff, then it should be apparent in the impulse responses of systems with different proportions. Moreover, drainage density is an index of this proportion. As seen in the above example, likely there is a strong relation between hydrograph characteristics (peak discharge, time to peak, etc.) and drainage density. The configuration with the highest drainage density had the shortest time characteristics and the highest peak discharge. Since open channel flow is relatively faster than overland flow, the results are as expected. As shown in the next section, other effects of changes in drainage density suggested by the existence of laminar and turbulent overland flow are in fact supported by data from natural watersheds.

Analysis of Observed Data. The effects of varying drainage density from watershed to watershed are studied using observed data from natural watersheds in conjunction with unit hydrograph theory. Nash (1957) published a paper proposing a functional form for the instantaneous unit hydrograph (IUH) as

$$h(t) = \frac{1}{K\Gamma(N)} \left(\frac{t}{K}\right)^{N-1} e^{-(t/K)} \qquad (4.7)$$

where $h(t)$ is an ordinate of the IUH at time t, K is a linear reservoir constant, and N is a parameter. Nash also proposed a conceptual model as a cascade of N linear reservoirs of time constant K. What is special about Nash's paper and the resulting model (Eq. 4.7), (hereafter called the "Nash model") is that it presented an equation and a conceptual model. Although the analogy has undoubtedly been overworked, e.g. to require that N be an integer, the model remains one of the foremost in unit hydrograph applications. The lag time or first moment of the IUH is

$$T_L = NK \qquad (4.8)$$

and the time to peak of the IUH is

$$T_p = (N-1)K \qquad (4.9)$$

where N and K are as described above.

Importance of the lag time in unit hydrograph theory was explained by Dooge (1973, p. 202): "One of the most important factors in surface water hydrology is the delay imposed on the precipitation excess by the action of the catchment. If the parameter representing this delay is to be useful for correlation studies, it should, if possible, be independent of the intensity and duration of rainfall. In the case of a linear system--and unit hydrograph theory assumes that the system under study is linear--the time parameters are independent of the intensity of precipitation excess, but only the lag time (t_L) has the property of being independent of both the intensity and duration. Accordingly, with the hindsight given by the systems approach, we can say that only the lag time should be used as a duration parameter in unit hydrograph studies." In extending the above concepts, these writers and R. S. Parker used the lag time, particularly its variation with rainfall-excess intensity, as a measure of nonlinearity. This study in nonlinearity was a concurrent and complimentary study (see Parker, 1975) to the work reported here. The experimental data were taken before this study so that the studies were concurrent only in the last phase of the analysis as described here.

Numerous investigators have examined the influence of drainage density upon surface runoff. For example, Hickok et al., (1959) related lag time (defined as the time from the center of mass of the rainfall to the hydrograph peak) to area, slope, and drainage density. The lag time and drainage density were found to be related with lag time proportional to drainage density to the approximately -0.3 power (see their Eqs. 1 and 2, p. 610). Therefore, a variation in lag time with varying drainage density suggests a direct effect of distorting drainage density in modeling surface runoff. However, there have also been numerous studies (e.g. Minshall, 1960, and discussions of his paper) indicating a variation in lag time with variations in intensity because hydrologic systems are in fact nonlinear. Thus, variations in lag time with drainage density and intensity of rainfall excess must be examined.

The principal source for data used in the following analyses is the Drainage Evolution Research Facility (DERF) at Colorado State University. This unique facility is described in detail by Parker (1975) so that only a brief description is given here. The DERF is essentially a laboratory facility (30 ft by 50 ft by 6 ft) filled with a soil which can be sprinkled at four intensities from 0.5 and 2.5 in./hr. The area of this experimental watershed is approximately 1240 ft^2 or 0.0285 acre. During 1971 rainfall, runoff, and geomorphic or network data were taken. As explained in detail by Parker (1975), the facility was open and exposed to wind during that year and the data taken contained errors. In 1972 the facility was enclosed in a building which eliminated the effects of wind and thus many of the errors in estimating the rainfall input. For this reason the 1972 data form the basis of the analyses but 1971 data are also used with the understanding that errors are likely. Therefore, except where noted, the following discussion refers to the 1972 data.

The basic data of interest here are rainfall-runoff data from the DERF along with the corresponding geomorphic parameters. The procedure was to sprinkle the facility for long periods until a particular drainage density was obtained and then to record a series of hydrographs. Rainfall was applied in a series of 1-min pulses for each of four intensities. Geomorphic data were then taken and the surface was again sprinkled for several hours to change the channel network before a new series of hydrographs were recorded. The 1972 data are from four networks with increasing, then decreasing, drainage density. A fifth network was the fourth network which was covered with a plastic sheet. The primary purpose was for calibration, but the plastic covered surface provided data from a different surface with the same overall configuration but drastically reduced drainage density. Throughout the 1972 experiments drainage density changed but total relief remained constant. In contrast, the 1971 DERF data were taken on networks with changing relief and drainage density.

As discussed above, all hydrographs from the DERF were the result of 1-min duration rainfall pulses. The changes in lag time with changes in rainfall (input) intensity provide a way of analyzing the degree of nonlinearity of the system. Systematic departures from independence of the lag time with changing intensity reflect the nonlinearity.

As lag time is a characteristic time, it can be related to input intensity in the following form

$$T_L = ai^{-b} \tag{4.10}$$

where T_L is the lag time; a is a coefficient, b is an exponent, and i is intensity of the rainfall excess. If the system were linear then b would be zero producing a constant lag time. Since in laminar flow the depth and local mean velocity are related with an exponent of 2.0 and in turbulent (Chezy) flow the exponent is 0.5, similar values might be expected in Eq. 4.10. Therefore, if the rainfall excess-surface runoff process is nonlinear, b should be greater than zero. Moreover, its magnitude is a measure of the degree of nonlinearity in the process. Values of i in Eq. 4.10 were estimated once using the ϕ-index (an average) for infiltration and once again using the Philip (1957) infiltration equation.

Values of a and b for the DERF data are shown in Table 4.3 and Fig. 4.6. The other data shown will be discussed later. The first three columns of Table 4.3 identify the data and describe the watershed. The next four columns give values of a and b from Eq. 4.10 for both methods of estimating rainfall excess. Lag time versus intensity is plotted in the lower portion of Fig. 4.6 for the 1972 data.

The coefficient, a, tends to increase as drainage density decreases. For the 1972 DERF data the regression equation relating the coefficient, a, and drainage density for the "average" rainfall excess is:

$$a = 3.97 - 5.83\, D_d \tag{4.11}$$

with a coefficient of determination $R^2 = 0.98$, while for all of the DERF data (1971 and 1972 combined) the corresponding equation is

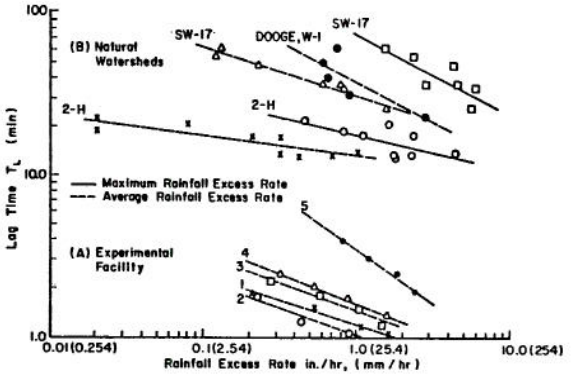

Fig. 4.6. Lag time, T_L, of Nash model as a function of intensity of rainfall excess.

$$a = 3.01 - 3.38\, D_d \tag{4.12}$$

with $R^2 = 0.65$.

For the 1972 data, the exponent b seems constant, except for the DERF-5, the plastic-covered surface which has a higher exponent. The high value of b = 0.66 for the plastic surface may indicate a change in the relative proportion of laminar-overland flow with respect to turbulent flow. The values of a and b are uniformly smaller for the cases where "average" rather than "maximum" rainfall excess data are used (Table 4.3). This suggests that using an average rainfall excess rate may result in underestimating the degree of nonlinearity.

Two natural watersheds were chosen to test the results indicated by analysis of the DERF experimental data. The two watersheds are similar with respect to drainage area and relief (see rows labeled SW-17 and 2-H in Table 4.3) but no well-defined channel system exists on the Riesel, Texas watershed (SW-17) while there is a definite channel system on the Hastings, Nebraska watershed (2-H) (see U.S.D.A., 1963, pp. 42.28-5 and 44.6-3). Values of a and b in Eq. 4.10 are also shown in Table 4.3 for these two watersheds. The solid lines in the upper portion of Fig. 4.6 are for these watersheds and rainfall excess estimated using Philip's equation. The corresponding dashed lines are for rainfall excess estimated using the ϕ-index. As in the data from the experimental facility, lag time decreases as rainfall excess-intensity increases, and the exponent and coefficient in the equation relating intensity and lag time are smaller when the ϕ-index is used.

Finally, some previous results are examined with the intention of seeking empirical support or refutation. A well-known example of nonlinearity in runoff from small agricultural watersheds was presented by Minshall (1960). In his Table 2 on page 29, he presented data used to derive unit hydrographs for W-1, Edwardsville, Illinois. Time to peak and peak discharge of the derived unit hydrographs were shown in Fig. 5 of his paper, and of these data he plotted five selected unit hydrographs in his Fig. 6. These five storms were chosen to represent a wide range of intensity. The intensity values presented were for total

Table 4.3. Summary of Relation Between Rainfall Excess Rate and Lag Time.

Data Set	Drainage Area (ft^2)[1]	Drainage Density (ft/ft^2)[2]	Rainfall Excess as the: Maximum Rate (in./hr) (from Philip Eq.) Coefficient a	Exponent b	Average Rate (in./hr) (from ϕ-index) Coefficient a	Exponent b	Source of Data
1972 DERF-1	1.24×10^3	.48	1.32	.37	1.19	.29	Parker, (1975)
" " -2	"	.50	1.17	.41	1.03	.33	"
" " -3	"	.46	1.62	.42	1.44	.34	"
" " -4	"	.37	1.81	.42	1.60	.36	"
" " -5	"	.099	___[3]		3.44	.66	"
1971 DERF-1	1.24×10^3	.35	1.19	.22	1.13	.19	Parker, (1975)
" " -2	"	.54	1.06	.21	.99	.17	"
" " -3	"	.63	1.12	.36	1.03	.32	"
" " -4	"	.75	1.20	.35	1.13	.34	"
SW-17	1.302×10^5	___[4]	71.7	.47	30.9	.29	USDA, (1963)
2-H	1.481×10^5	.0022	17.6	.21	13.1	.12	"
W-1	1.185×10^6	.0014	29.3[5]	.25	23.2	.10	Minshall, (1960) Table 2
W-1	1.185×10^6	.0014	28.9[5]	.55	19.2	.45	Minshall, (1960) Fig. 6 Amorocho, (1961) Eq. 14
W-1	1.185×10^6	.0014	58.3[5]	.60	37.2	.49	Dooge, (1967) Eq. 38

[1] $1\ ft^2 = 0.0929\ m^2$.

[2] $1\ ft/ft^2 = 3.281\ m/m^2$.

[3] Maximum and average rates are the same for plastic surface.

[4] No well-defined channels.

[5] Values are for rainfall, not rainfall excess. The equation gives time to peak, not lag time, except for Dooge (1967), who uses lag time.

rainfall, not rainfall excess as he stated on p. 31. Minshall's conclusion that using rainfall excess did not improve the correlation for his data was confirmed by using rainfall excess estimated by means of the data he presented and the ϕ-index. Values of a and b as in Eq. 4.10 but with time to peak are given in Table 4.3 in the last three rows labeled W-1. For total rainfall $b = 0.25$ while for average rainfall excess rate $b = 0.10$ using all 28 storms presented by Minshall.

Amorocho (1961) discussed Minshall's paper and by selecting the five storms (shown in Minshall's Fig. 6) demonstrated nonlinearity. The value of b in his equation relating time to peak and intensity was 0.547. If he had used average rainfall excess, the exponent would have been 0.45, while if he had used all of Minshall's data, instead of the five selected storms, the exponent would have been 0.25 for total rainfall and 0.10 for rainfall excess. These results are given in Table 4.3 in the rows labeled W-1.

Minshall and Amorocho were discussing time to peak and not lag time. A later analysis by Dooge (1967) examined lag time, but again he used rainfall rather than rainfall excess. Dooge used the same five storms as Amorocho and derived lag times for each unit hydrograph. His equation relating lag time (Eq. 38, p. 33) to intensity had an exponent of 0.605. If rainfall excess had been used, the exponent would have been 0.49. The line labeled "Dooge, W-1" (Fig. 4.6) is a plot of this relation.

Using all of the data, except for SW-17, resulted in an equation

$$a = 18.8 - 33.3\ D_d \qquad (4.13)$$

relating the coefficient a and drainage density. The value of R^2 for this equation is 0.59, but is consistent with Eq. 4.11.

The results of the analysis reported above and the reinterpretation of Minshall's data are summarized in Table 4.3. Misinterpretations of Minshall's data resulted in an overestimation of the degree of nonlinearity in the rainfall excess-surface runoff relation. The degree of nonlinearity in this relation is seen as a function of rainfall estimation procedure as well as the basin characteristics. Increasing drainage density tends to lower the lag time, while a drastic change in drainage density affected the rate of change of lag with changing intensity.

Returning to the question of the effects of distorting the observed drainage density in modeling a watershed, evidently a gross underestimation in drainage density could result in overestimating the lag time and the degree of nonlinearity. Suppose that lag time is fitted in an optimization procedure but that drainage density is underestimated. A likely result is underestimation of hydraulic roughness or a similar compensating error in another factor.

The effects of distorting main channel characteristics and drainage density upon surface runoff are seen as significant modificiations in the surface runoff hydrograph. Quantifying the hydrologic effects of each distortion resulting from simplifications assumed in the mathematical modeling is difficult due to the complexity of the problem. However, several goodness-of-fit statistics have been proposed and illustrated by simulation results.

4.2 Goodness-of-Fit Statistics for the Simplified Geometry

Several goodness-of-fit statistics are proposed in this study for modeling complex natural watersheds and their components by simplified geometrical representations. The obvious question resulting from such modeling is how well does the simplified model represent the complex natural system. This question can be considered in two parts: First is the goodness-of-fit of the simplified geometrical representation to its complex prototype, its topographic features, and second is the goodness-of-fit of the hydrologic response of the simplified geometry to the hydrologic response of the complex prototype hydrographs. The first part is the subject of this section and the second is covered in the next section.

Three dimensional coordinate data (x_i, y_i, z_i) for $i = 1, 2, \ldots, N$ are taken from a topographic map. The normal procedure is to take x_1, y_1, and z_1 equal to zero at the watershed outlet so that all elevation values are positive. A function measuring departures of fitted elevation values, e_i, from given or observed elevation values, z_i, is G such that

$$G = \sum_{i=1}^{N} (z_i - e_i)^2 \tag{4.14}$$

where N is the number of selected data points. If a plane is fit to N data points by least squares, the result is a minimum G as defined by Eq. 4.14. The mean or average elevation is

$$\bar{h} = \sum_{i=1}^{N} z_i/N \tag{4.15}$$

so that the sample variance of the observed elevation data about their mean is

$$S_1^2 = \sum_{i=1}^{N} (z_i - \bar{h})^2/(N-1). \tag{4.16}$$

The sample variance of the observed data about the best fit plane is

$$S_2^2 = \sum_{i=1}^{N} (z_i - e_i)^2/(N-1) = G/(N-1) \tag{4.17}$$

since the mean deviation is zero. The proposed goodness-of-fit statistic is

$$R_p^2 = \frac{S_1^2 - S_2^2}{S_1^2} \tag{4.18}$$

as a measure of the residual variance. If the average elevation were the best fit plane, then $R_p^2 = 0$, and if the least squares plane had a perfect fit to the observed coordinates then $R_p^2 = 1$. Therefore, $R_p^2 \times 100$ is the percent of the total variance explained by the least squares fit plane. The statistic, R_p^2, is called the "geometric goodness-of-fit statistic." It can be used for a single plane fit to hillslope data or for an entire cascade of planes fit to watershed coordinate data. For a cascade of planes, S_1^2 and S_2^2 are calculated for all planes as is R_p^2.

In a manner similar to that described above, coordinate data are taken for points along the main channel. Distances along the main channel are calculated by

$$d_i = \sqrt{(x_{i+1} - x_i)^2 + (y_{i+1} - y_i)^2} \tag{4.19}$$

for all points along the channel reach.

The length of the main channel is then

$$L_c = \sum_{i=1}^{N-1} d_i \tag{4.20}$$

where N is the number of data points. Also the total relief of the main channel is

$$H_c = z_N - z_1 \tag{4.21}$$

where z_i are the observed elevation data. If the area under the stream profile formed by (d_i, z_i) is calculated and a right triangle with base length L_c and the same area as under the profile is constructed, then for h as the altitude of this triangle the slope of the hypotenuse is

$$S_c = h/L_c \tag{4.22}$$

as Gray's slope or the equivalent channel slope. The index of concavity described earlier is

$$I_c = h/H_c \tag{4.23}$$

with values less than one for a concave profile and values greater than one for convex profiles.

"Drainage density" is defined as the ratio of the total length of all streams to the drainage area. If drainage density for the watershed is D_d and drainage density of the simplified geometry is d_d, then

$$I_d = d_d/D_d \tag{4.24}$$

is the proposed statistic measuring the goodness-of-fit with respect to the drainage density. I_d will vary between zero and one, since d_d will always be less than D_d.

The above three goodness-of-fit statistics--R_p^2, the geometric goodness-of-fit statistic; I_c, the index of concavity; and I_d, the drainage density ratio--form the set of goodness-of-fit statistics used here. In the most simplified terms, R_p^2 is a measure of the goodness-of-fit for the overland flow portion of the model; I_c is a measure of the goodness-of-fit of the main channel slope, and I_d is an overall goodness-of-fit measure. That is, there is a watershed-slope statistic, a channel-slope statistic, and an overall statistic. These statistics are summarized in Table 4.4. The first two columns describe the element modeled. The first column labeled "watershed" refers to the quantity being modeled as a component of the natural system, and the column labeled "model" refers to the corresponding component in the simplified geometrical representation. The third column lists the symbols used with explanatory comments listed in the last column.

Table 4.4. Summary of Proposed Goodness-of-Fit Statistics for the Simplified Geometrical Representation.

Element or Component of System		Goodness-of-fit Statistic for the Simplified Geometry	Comments
Watershed	Model		
Hillslope or Watershed	Cascade of Planes	R_p^2	Ratio of residual variance about fitted planes to original variance of elevation coordinate data. Also used for entire watershed.
Main Channel	Cascade of Channels	I_c	Index of concavity, ratio of height of equal area, equivalent slope triangle to total relief of main channel.
Watershed	Cascade of Planes and Channels	I_d	Ratio of drainage density in model to observed drainage density in the watershed.

Watershed characteristics and some goodness-of-fit statistics are shown in Table 4.5. The first column gives the watershed identification (see U.S.D.A., 1963 and earlier publications). "Riesel" refers to selected watersheds at Riesel, Texas; "Hastings" refers to the watershed at Hastings, Nebraska; "Tombstone" refers to watersheds on Walnut Gulch Experimental Watershed near Tombstone, Arizona; and "Pawnee" refers to watersheds at the Pawnee Site, Grasslands BIOME in Colorado. The second column of Table 4.5 lists the watershed area. The next column gives N, the number of coordinate data points read from topographic maps and used in least squares fitting. The fourth column gives the slope of the plane fit to the N points, and column 5 gives the geometric goodness-of-fit statistic R_p^2 for each watershed. The next three columns give the length, slope, and index of concavity for the main channel on each watershed. The final column gives the source of data for each watershed which are presented to show the range of the proposed statistics and for reference in subsequent analyses. Some of the watersheds do not have well-defined channel systems and since only a single plane was fit to data from each watershed, the ratio of drainage densities was not calculated.

Of the 27 watersheds represented in Table 4.5, four of the Riesel watersheds were selected for additional analysis--W-C, W-D, SW-12, and SW-17(Fig. 4.7). Values of R_p^2, for increasing numbers of planes in cascade, were calculated for these four watersheds. These values of R_p^2 versus the number of planes in the simplified geometry are shown in Fig. 4.8. Watersheds C and D require two or more planes to produce a high value of R_p^2 while one plane produces a high value for watersheds SW-12 and SW-17. Moreover, the necessity of interpolating for boundary points, as the number of planes increases, can slightly reduce R_p^2 by adding additional errors without improving the fit. This is what happened for SW-12.

4.3 Goodness-of-Fit Statistics for Hydrograph Fitting

Of the four auxiliary objectives listed in the Introduction, the two dealing with watershed characteristics were discussed in the previous sections. This section examines hydrograph characteristics and their associated goodness-of-fit statistics. Before the analysis, some basic notions need to be defined.

There is often a great deal of confusion concerning the terms "fitted" and "predicted." For this reason the two terms are given rather restricted meanings here. A "fitted hydrograph" is one produced with a knowledge of and by using the observed hydrograph; i.e., a hydrograph is fitted or calibrated to a known hydrograph and then the goodness-of-fit is judged with respect to the given observed hydrograph. For the predicted hydrograph, the observed hydrograph can be used to judge the goodness-of-fit, but it is not used in making the prediction. The emphasis in this chapter is upon fitting rather than predicting.

Table 4.5. Summary of Some Goodness-of-Fit Statistics for Selected Experimental Watersheds.

Watershed ID.	Drainage Area (acres)	Single Plane Fit to Coordinate Data: Number of Data Points N	Slope of Best Fit Plane S	Goodness-of-Fit Statistic R_p^2	Main Channel: Length L_c ($ftx10^3$)	Equivalent Slope S_c	Index of Concavity I_c	Source of Data
RIESEL								
W-C	579.	47	.005	.38	7.05	.0056	.79	USDA Misc. Publication
W-D	1110.	75	.004	.41	10.74	.0041	.72	
W-G	4380.	185	.003	.38	22.77	.0034	.78	"
W-1	176.	81	.009	.66	4.65	.0101	1.07	"
W-2	130.	75	.015	.56	2.68	.0161	1.03	"
W-6	42.3	30	.017	.76	1.38	.0139	.96	"
W-10	19.7	22	.022	.72	.58	.0299	.92	"
W-Y	309.	125	.010	.64	3.86	.0099	.81	"
W-Y2	132.5	62	.012	.53	2.78	.0113	.82	"
W-Y4	79.9	42	.011	.39	2.18	.0121	.82	"
W-Y6	16.3	22	.020	.87	1.00	.0285	1.18	"
W-Y7	37.9	28	.012	.62	.93	.0195	.87	"
W-Y8	20.8	22	.021	.95	.94	.0284	1.03	"
W-Y10	18.1	21	.009	.17	.66	.0177	.78	"
SW-12	2.97	120	.030	.87	*			"
SW-17	2.99	56	.020	.92	*			"
HASTINGS								
2-H	3.40	74	.035	.72	.28	.0388	.82	"
TOMBSTONE								
LH-5	.56	21	.067	.46	.29	.0543	.98	SW Watershed Research Center Tucson, Arizona
LH-6	1.07	30	.078	.89	.21	.0542	.77	
PAWNEE								
P-1	1.24	87	.031	.95	*			Smith & Strifler (1969)
P-2	1.24	62	.018	.98				
P-3	1.23	81	.025	.97				"
P-4	1.23	137	.050	.98				"
P-5	1.24	160	.053	.98				"
P-6	1.23	126	.042	.97				"
P-7	1.23	92	.030	.98				"
P-8	1.24	97	.036	.94				"

*No well-defined channels on these watersheds.

The concept of an observed hydrograph and the associated fitted hydrograph is illustrated in Fig. 4.9. The solid line represents the observed or measured hydrograph and the dashed line represents the fitted hydrograph. The regular symbols represent variables associated with the measured hydrograph, while those with hats correspond to the fitted hydrograph. Therefore, funtions involving the differences between observed and fitted variables can be used as goodness-of-fit measures.

Unit hydrograph procedure, especially the Nash model, is used in analyses of goodness-of-fit statistics for hydrograph fitting. Observed data for the analyses are from the sixteen ARS watersheds at Riesel, Texas, (see Table 4.5, watersheds at Riesel).

4.3.1 Sum of Squared Errors

Each of a set of n hydrographs has $m_i (i = 1, 2, \ldots, n)$ ordinates or discharge values at corresponding times. For example, see the point labeled (t_i, q_i) in Fig. 4.9.

An objective function, G_1, is defined as

$$G_1 = \sum_{i=1}^{n} \sum_{j=1}^{m_i} (q_j - \hat{q}_j)^2 \qquad (4.25)$$

where m_i is the number of ordinates for the i^{th} event, n is the number of events, q is observed

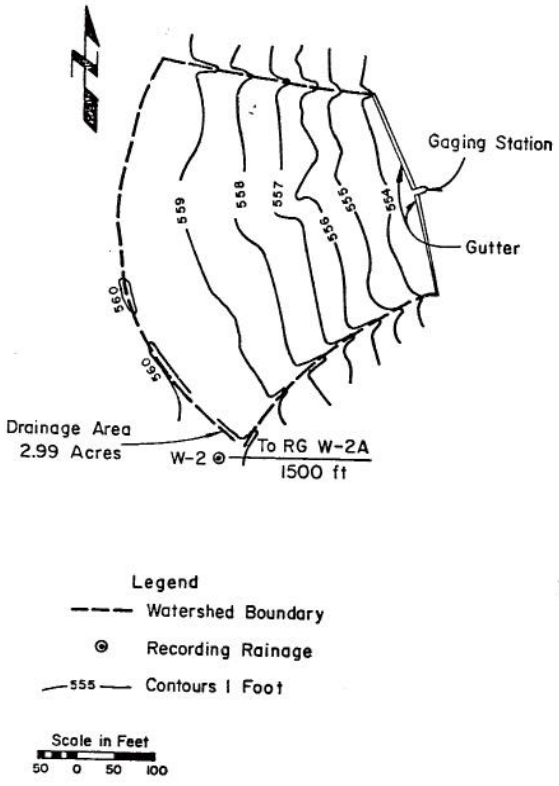

Fig. 4.7. Topographic map of watershed SW-17 at Riesel, Texas (from USDA Misc. Pub.).

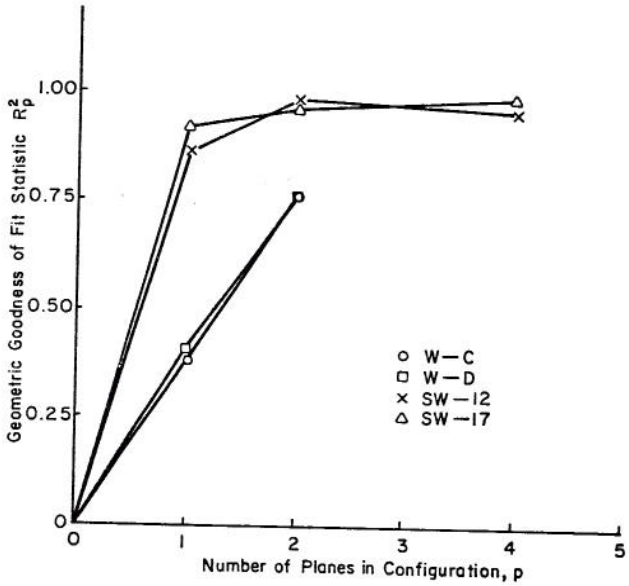

Fig. 4.8. Relation between geometric goodness-of-fit statistic, R_p^2, and the number of planes, p, in the geometry for selected Riesel, Texas watersheds.

discharge, and $\hat{q}$ is the fitted discharge. Parameters of the Nash IUH, Eq. 4.7, are estimated minimizing G_1 subject to

$$N > 0, \text{ and } K > 0. \tag{4.26}$$

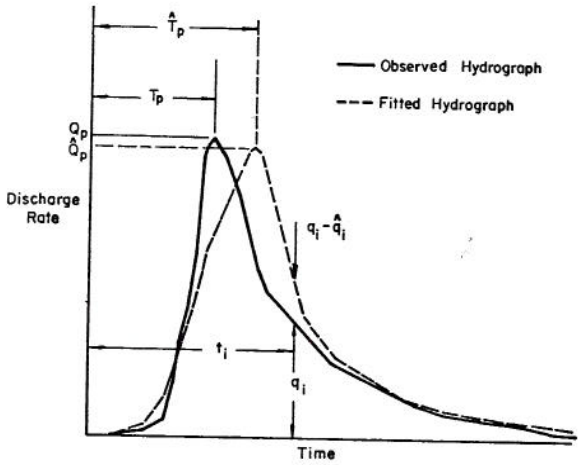

Fig. 4.9. Definition sketch for observed and fitted hydrographs and associated variables.

Values of N and K satisfying Eqs. 4.25 and 4.26 are called the "optimal values" of the parameters and G_1 is called the "sums-of-squares" objective function. The optimization procedure used is Rosenbrock's (Rosenbrock, 1960 and Palmer, 1969) as programmed by Singh (1974). In summary, each hydrograph is fitted and produces a sum of squared errors, and then these sums are in turn summed over a set of n hydrographs. Predicted values of $\hat{q}_j$ result from convolution of rainfall excess (via the Philip equation) and the IUH (Eq. 4.7).

4.3.2 Deviation of Peaks

For each of the n hydrographs there is a maximum or peak value, Q_p in Fig. 4.9, at a time t_p. An objective function G_2 is defined as (Singh, 1974):

$$G_2 = \sum_{i=1}^{n} (Q_{pi} - \hat{Q}_{pi})^2 \tag{4.27}$$

where n is the number of hydrographs; Q_p is observed peak discharge and $\hat{Q}_p$ is fitted peak discharge. Optimal parameters of the Nash model are obtained as before by minimizing G_2 subject to Eq. 4.26. The function G_2 is called the "optimization on peaks objective function." In summary, each hydrograph is fitted and produces an error in peak discharge and then these errors are squared and summed over a set of n hydrographs.

4.3.3 Comparison of Characteristics of the Fitted Hydrographs

There are many characteristics or associated variables (Fig. 4.9) of the hydrographs which can be compared to aid in the choice of objective functions. In general, and as is confirmed by plotting observed and fitted hydrographs, the peaks objective function should result in better reproduction of peak discharge but perhaps not hydrograph shape when compared with the total sums-of-squares optimization method.

Fitted peak discharge can be compared with the corresponding observed peak discharge by a linear regression equation

$$\hat{Q}_p = a + b\,Q_p \qquad (4.28)$$

where Q_p is observed peak discharge and $\hat{Q}_p$ is fitted peak discharge.

A perfect fit would result in a zero value for the intercept, a, and a 1.0 value for the slope, b, in Eq. 4.28. The coefficient of determination, R^2, for this regression equation is the proportion of the variance of fitted peak discharge about the mean which is explained by the equation. The standard error of estimate, S_e, is the standard deviation of the residuals or the errors about the regression line. The term R^2 can be considered a goodness-of-fit statistic for the fitted peak discharge. Results of fitting hydrographs for the 16 Riesel, Texas watersheds are summarized in Table 4.6. The intercept, a, is near zero for both optimization methods, but the slope term for the optimization on total sums-of-squares is significantly different from 1.0 at the 10 percent level. However, the coefficients of determination and standard errors are comparable for both methods.

Table 4.6. Summary of Fitted Peak Discharge and Optimal Nash IUH Parameters for the Two Optimization Methods.

Objective Function	Regression Equation Relating Observed and Fitted Peak Discharge*				Optimal IUH Parameters for Nash Model			
	$\hat{Q}_p = a + bQ_p$						Lag Time T_L	
	Intercept a	Slope b	Coefficient of Determination R^2	Standard Error of Estimate S_e (in./hr)	Mean** N	Mean K (min)	Mean (min)	Standard Deviation (min)
Optimization on sums-of-squares	-0.006	0.70	0.76	0.31	3.42	24.4	75.1	61.8
Optimization on peaks	0.016	0.92	0.81	0.35	2.84	20.3	54.8	66.5

*Data base is for 122 hydrographs from 16 watersheds at Riesel, Texas.

**Means and standard deviations computed from 16 optimal values.

Values of N and K are shown in Table 4.6 for both procedures. The last two columns of Table 4.6 give means and standard deviations for lag time on the Texas watersheds. As discussed earlier, the lag time is an important time characteristic in unit hydrograph theory and is an overall measure of watershed performance. Mean lag times are statistically different at approximately the 10 percent level, i.e., apparently the sums-of-squares optimization method produces larger values of lag time than does the optimization on peaks method. The standard deviations of lag time are nearly the same so that the coefficients of variation are 0.82 for the sums-of-squares method and 1.21 for the peaks method. Thus, the sums-of-squares optimization procedure may produce a relatively lower variability in lag time estimates.

Results of the analyses indicate significant differences in parameter estimates depending upon the objective function used. However, the choice of objective function remains a subjective decision. Evaluation of the above results using criteria emphasizing peak discharge would result in choosing the optimization on peaks objective function. Conversely, evaluation of the results using criteria emphasizing overall hydrograph shape and relative variability of estimated lag time would result in choosing the total sums-of-squares objective function.

Finally, it is possible to construct goodness-of-fit statistics based upon the objective function. As before, the intent is to derive a measure of the degree of improvement over using the mean discharge. Define the "mean discharge" as

$$\bar{q} = \sum_{j=1}^{m_i} q_j / m_i \qquad (4.29)$$

for the observed data. The sum-of-squares about the mean is then

$$S_Q^2 = \sum_{j=1}^{m_i} (q_j - \bar{q})^2 \qquad (4.30)$$

where q_j are the observed hydrograph ordinates. The proposed goodness-of-fit statistic is

$$R_Q^2 = \frac{\sum_{j=1}^{m_i} (q_j - \bar{q})^2 - \sum_{j=1}^{m_i} (q_j - \hat{q}_j)^2}{\sum_{j=1}^{m_i} (q_j - \bar{q})^2} \qquad (4.31)$$

which is equal to

$$R_Q^2 = \frac{S_Q^2 - G_1}{S_Q^2} \qquad (4.32)$$

as the degree of improvement over using the mean discharge. Thus, there is a hydrograph goodness-of-fit statistic for each hydrograph.

4.4 Relating Statistics of the Simplified Geometry to Statistics of the Fitted Hydrographs

Recall the objective as given in the Introduction: "To relate statistics of the simplified geometry to watershed characteristics and to hydrograph characteristics in order to define the simplest geometry which when used in simulation will preserve the selected hydrograph characteristics to a given degree of accuracy." This section deals with relating statistics of the simplified geometry to statistics of the fitted hydrographs. If this objective is met for watersheds with topographic, rainfall, and runoff data given, the means will be available to objectively choose adequate geometric representations as simplified models of these watersheds.

The procedure adopted here is graphically represented in Fig. 4.10. A given natural watershed produces an observed hydrograph as illustrated in the left portion of this figure. A single plane is fit to topographic data (x, y, z coordinates) producing R_1^2 as a geometric goodness-of-fit statistic. The equations of overland flow are solved for the given rainfall input producing the fitted hydrograph as the dashed line in the central portion of Fig. 4.10. From the fitted and observed hydrographs, a goodness-of-fit statistic, R_Q^2, is computed using Eq. 4.32. The procedure is repeated for two planes and one channel

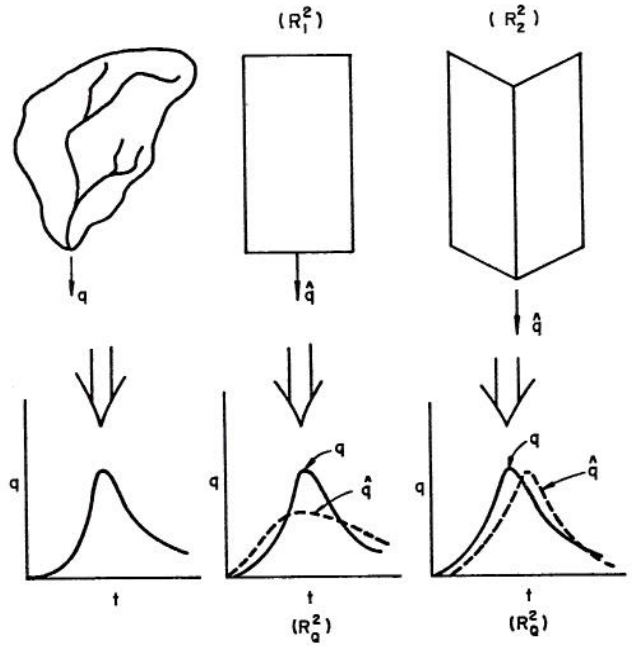

Fig. 4.10. Schematic representation of a watershed, simplified models, and associated goodness-of-fit statistics.

(Wooding model) as shown in the right portion of Fig. 4.10. The procedure could then be repeated to any degree of complexity.

Hypothetical relationships between R_p^2 and R_Q^2 for various geometries are shown in Fig. 4.11. The upper curve (A) might result from a small watershed where one or two planes provide a relatively good fit geometrically and hydrologically. The lower curve (B) might result from a larger watershed with a more developed channel system. Here a more complex configuration might be necessary. The goodness-of-fit statistics can be related for real watersheds using plots such as in Fig. 4.11.

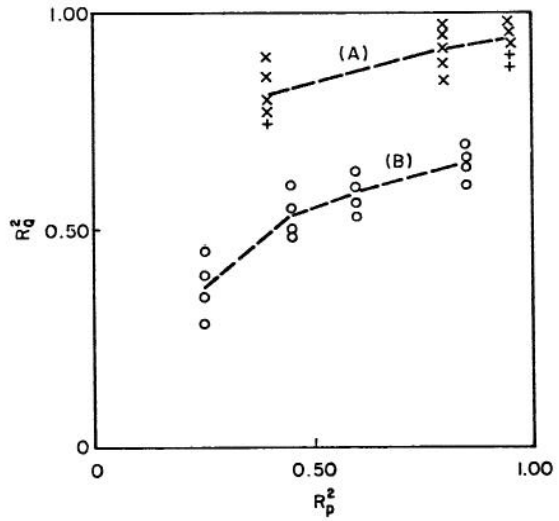

Fig. 4.11. Hypothetical relation between geometric and hydrograph goodness-of-fit statistics. Curve A represents small watersheds and Curve B represents larger watersheds with a more developed channel system.

To represent a range of watershed characteristics, watersheds W-C and SW-17 at Riesel, Texas are chosen. Geometric goodness-of-fit statistics for these two watersheds are shown in Table 4.5 and Fig. 4.8. The curves in Fig. 4.8 are quite different from W-C and SW-17.

The finite difference program for a kinematic cascade of planes and channels was modified to determine optimal roughness values for the planes and channels separately. The procedure is to find optimal roughness values for K on planes given a Chezy C in the channels. The procedure is repeated over a range of channel parameters to find the best of a set of optimal roughness coefficients for the planes. Values of the objective function, G_1, are shown in Fig. 4.12. The event is for the storm of 6/10/41 on watershed W-C at Riesel, Texas. The upper portion of Fig. 4.12 shows the objective function G_1 and associated optimal values of K for each of four values of C in the channel. Optimal values of C = 42 and K = 1870 are indicated for the point at the minimum of the objective function. The lower graph of Fig. 4.12 shows a plot of channel C versus plane K for this example.

Observed and fitted hydrographs for the event of 6/10/41 on watershed W-C at Riesel, Texas are shown in Fig. 4.13. The hydrograph labeled (0) is the observed surface runoff resulting from the rainfall

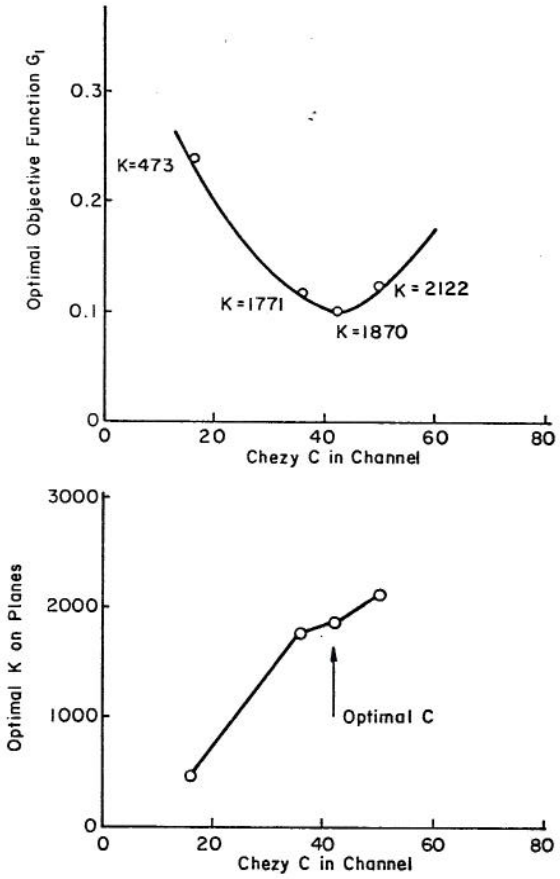

Fig. 4.12. Illustration of procedure for selection of optimal Chezy C in the Wooding model, W-C, Riesel, Texas. Event of 6/10/41.

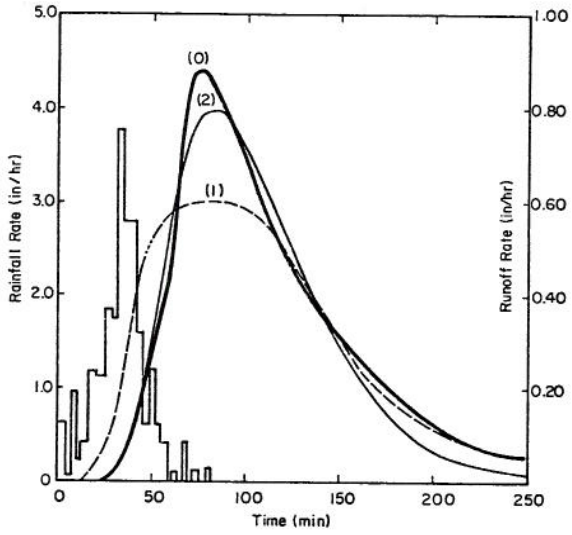

Fig. 4.13. Observed and fitted hydrographs (for a kinematic cascade model) for watershed W-C, Riesel, Texas. Event of 6/10/41.

pattern shown. That labeled (1) is the best fit hydrograph for a single plane with $R_Q^2 = 0.78$. The curve labeled (2) is the best fit hydrograph for the Wooding model--two planes and one channel with $R_Q^2 = 0.95$. The above example illustrates the procedure followed in examining data from the two watersheds as discussed below.

4.4.1 Single Plane--The Simplest Geometry

Watershed SW-17 when modeled as a single plane has a mean 0.020 slope, a 392 ft length, and a 332 ft width. As discussed earlier, the geometric goodness-of-fit statistic is $R_1^2 = 0.92$. Corresponding values for watershed W-C at Riesel, Texas are $S = 0.005$ and $R_1^2 = 0.38$. For watershed 2-H at Hastings, Nebraska the values are $S = 0.035$ and $R_1^2 = 0.72$. Values of observed peak discharge and time to peak (from beginning of rainfall) are shown in Table 4.7 along with the corresponding values for the fitted hydrographs. The last column in Table 4.7 shows the hydrograph goodness-of-fit statistic and its mean value for each watershed.

Originally, the intent was to examine the two Texas watersheds in detail but the third watershed at Hastings, Nebraska is included to extend the analysis beyond Texas and to include a watershed of nearly the same size as SW-17, but with a well-defined channel system.

For SW-17 the peak discharge was, as expected, underestimated using a single plane as was the time to peak. The most serious error is for the largest event. In Table 4.7 the range of R_Q^2 is 0.44 to 0.96 with a mean value of 0.69, i.e., approximately 70 percent of the variance about the mean discharge is explained (on the average) by the best-fit hydrograph derived from modeling the watershed as a single plane. This is a surprisingly good fit. Except for the large event discussed above, unlikely more complex geometries will result in much improvement in the hydrograph goodness-of-fit statistic R_Q^2. However, likely peak discharge and time to peak will be better represented by a more complex geometry.

For watershed W-C, the peak discharge values were also underestimated and as on SW-17, the most serious error was associated with the largest event. The range in R_Q^2 is 0.22 to 0.78 with a mean value of 0.53; i.e., on the average, approximately 50 percent of the variance in discharge about the mean discharge is explained by fitting a single plane to data from watershed W-C. As expected, this value is lower than for watershed SW-17 (Fig. 4.11). In contrast to SW-17 likely a better geometric fit would produce a better hydrograph goodness-of-fit statistic for watershed W-C. Better reproductions of peak discharge and time to peak values are also expected.

Data for watershed 2-H at Hastings, Nebraska are shown in the bottom of Table 4.7. In general, peak discharge is underestimated, but unlike before, the largest peak discharge is well fitted. Values of R_Q^2 vary from .0 to 0.92 with a mean value of 0.44. These results are more comparable with those for W-C than for SW-17. Recall that SW-17 has a drainage area of 2.99 acres, W-C has 579 acres, while 2-H has 3.40 acres (Table 4.5). Therefore, the reasons for the

Table 4.7. Summary of Goodness-of-Fit Statistics for a Single Plane as the Simplest Geometry.*

Watershed	Observed Data		Fitted Data		Hydrograph Goodness-of-Fit Statistic
	Peak Discharge (in./hr)	Time to Peak (min)	Peak Discharge (in./hr)	Time to Peak (min)	R_Q^2
SW-17	1.61	48.	1.10	47.	.66
	.44	17.	.20	10.	.56
R_p^2 = .92	1.74	28.	1.47	30.	.94
	2.17	51.	2.08	51.	.96
	.60	159.	.28	150.	.63
	.35	33.	.17	20.	.44
	3.79	40.	1.93	34.	.63
					Mean = 0.69
W-C	.88	77.	.60	80.	.78
	.87	71.	.58	50.	.73
R_p^2 = .38	.57	92.	.33	50.	.53
	.62	148.	.31	60.	.37
	.15	137.	.088	30.	.22
	.31	128.	.17	70.	.37
	1.38	183.	.75	150.	.68
					Mean = 0.53
2-H	.28	39.	.033	27.	.13
	3.47	23.	3.52	24.	.92
R_p^2 = .72	.85	16.	.96	13.	.55
	.81	9.	.62	12.	.86
	1.48	28.	.30	18.	.14
	.99	27.	.46	21.	.42
	1.39	17.	.56	14.	.53
	.90	150.	.41	148.	.58
	1.11	16.	.30	11.	.30
	.068	29.	.01	11.	.0
					Mean = 0.44

*Data taken as tabulated, no arbitrary time corrections.

apparent differences in R_Q^2 for the two 3-acre watersheds must be examined. The first comparisons are between the goodness-of-fit statistics for the simplified geometrical representations as summarized in Table 4.4.

Watershed characteristics for watersheds SW-17, W-C, and 2-H are listed in Table 4.5. Some associated geometric goodness-of-fit statistics are shown in Table 4.8. The first row in each of the three sections of Table 4.5 is for a single plane fit to the coordinate data. For example, the drainage density ratio, I_d, is zero whenever a watershed is modeled as a single plane. However, since there are no well-defined channels on SW-17, the drainage density ratio and the index of concavity are not defined for this watershed. The sole statistic for this watershed is the geometric goodness-of-fit statistic, R_p^2. Drainage density is highest on watershed 2-H.

The values of R_Q^2 seem to decrease as drainage density increases. To test this hypothesis, data from two of the artificial watersheds at Colorado State University DERF-4 and DERF-5 (see Table 4.3) were included in the analysis; i.e., a single plane was fit to coordinate data and used as a model for the two watersheds. The resulting mean hydrograph goodness-of-fit statistics, $\bar{R}_Q^2$, are then related to drainage density for the four watersheds: W-C, 2-H, DERF-4, and DERF-5. These data are shown as the circled points in Fig. 4.14. As hypothesized, the mean value of R_Q^2 decreases as drainage density increases. In fact, the least squares line shown in Fig. 4.14 and labeled single plane is

$$\bar{R}_Q^2 = 0.24\ D_d^{-0.11} \tag{4.33}$$

where $\bar{R}_Q^2$ is the mean hydrograph goodness-of-fit statistic and D_d is the drainage density.

If the relationship shown in Fig. 4.14 and described by Eq. 4.33 is representative of small watersheds as considered here, possibly some implications for watershed modeling can be discussed. Also recall the variation of lag time with intensity as a measure of nonlinearity (Fig. 4.6 and Table 4.3). Simple watersheds with a relatively low drainage density can be modeled with a small number of planes in a kinematic cascade (Fig. 4.14). However, more complex watersheds with high drainage density cannot be as adequately modeled with such simple geometrical representations. However, these very complex watersheds may be the ones which could be modeled as a

Table 4.8. Some Goodness-of-Fit Statistics for Selected Geometrical Representations of the Three Watersheds.

Watershed	Drainage Density (ft/ft^2)			Simplified Geometry		Comments
	Observed D_d	Modeled d_d	$I_d = d_d/D_d$	Number of Planes	Geometric Goodness-of-Fit Statistic R_p^2	
SW-17	-	-	-	1	.92	No well-defined channels
W-C	.00069	0.0	0.0	1	.38	Single plane
W-C	.00069	.00028	0.40	2	.76	Wooding Model
2-H	.0022	0.0	0.0	1	.72	Single plane
2-H	.0022	.0019	0.85	2	.91	Wooding Model

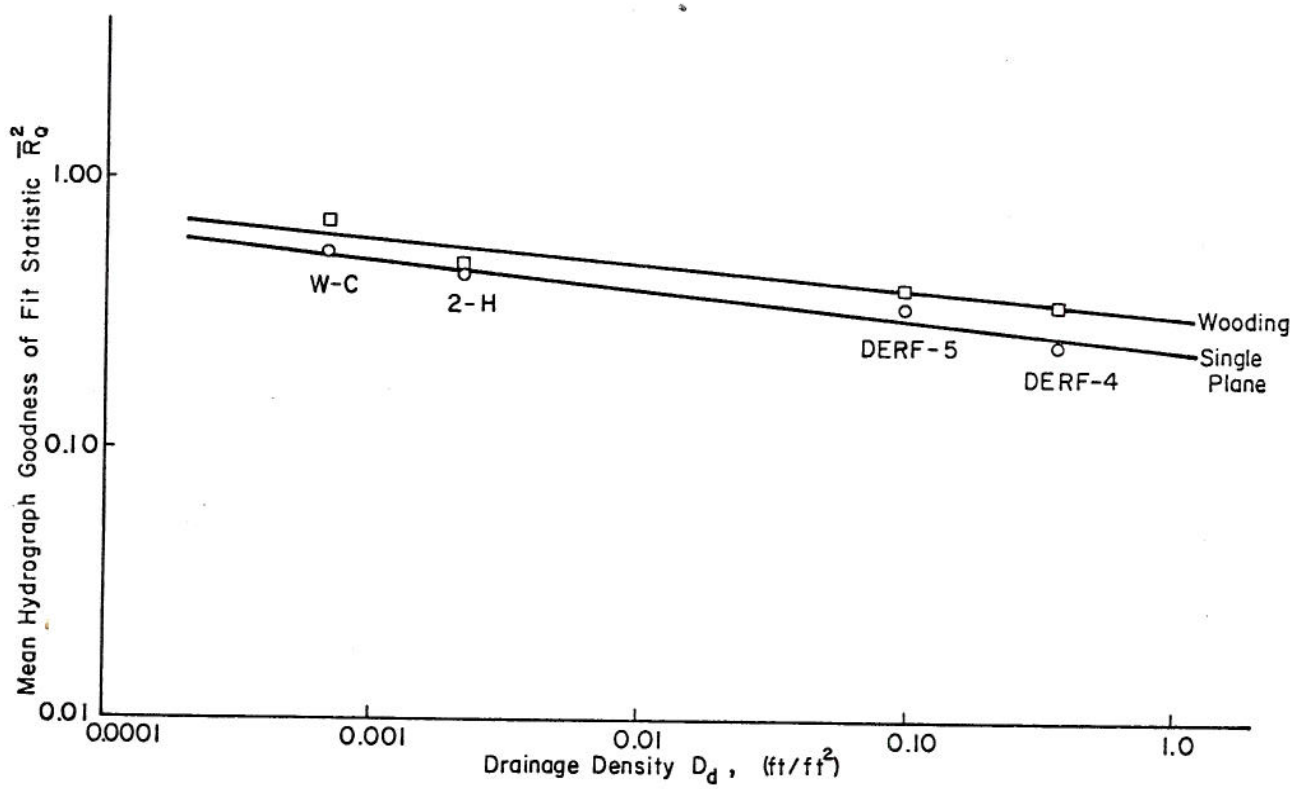

Fig. 4.14. Relation between drainage density and mean hydrograph goodness-of-fit statistic.

linear system (Fig. 4.6). Before elaborating upon this hypothetical situation, the hydrograph goodness-of-fit statistics for more complex geometrical representations must be examined.

4.4.2 More Complex Geometry--Wooding Model

Hydrographs were also fitted for these four watersheds using the Wooding model--two planes contributing to a channel. These data are shown as the square points in Fig. 4.14 and the line labeled Wooding. The least squares line is

$$\bar{R}_Q^2 = 0.32\ D_d^{-0.09} \qquad (4.34)$$

where $\bar{R}_Q^2$ is the mean hydrograph goodness-of-fit statistic for the Wooding model, and D_d is drainage density. Thus, the hypothesized relation, based on results from the previous section, seems to hold for the Wooding model; i.e., drainage density can be used as an index of the relative goodness-of-fit in hydrograph fitting.

The effects of drainage density can be seen if R_Q^2 is related to R_p^2, the geometric goodness-of-fit statistic. Values of R_Q^2 and R_p^2 are shown in Fig. 4.15 for each of the four watersheds. Again, the two points represent a single plane and the Wooding model, with the left point for the plane and the right point for the Wooding model. Values of drainage density are given below the watershed identification in Fig. 4.15. The points in Fig. 4.15 are connected by lines to associate each point with a watershed, not to represent values of the variables between or outside the points.

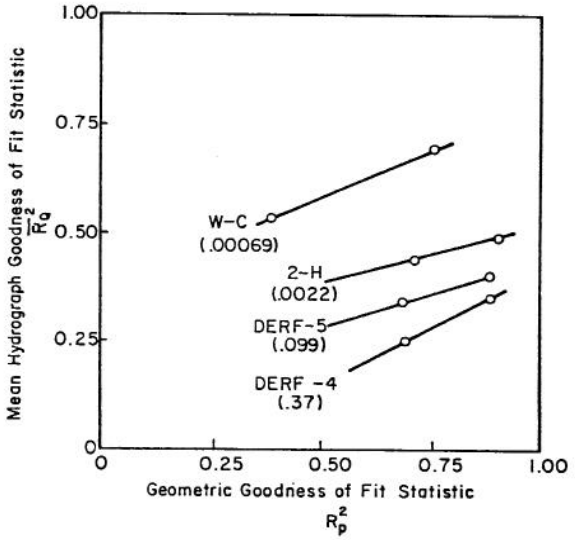

Fig. 4.15. Relation between geometric and hydrograph goodness-of-fit statistics for watersheds with different drainage densities.

Some implications of the results shown in Fig. 4.15 are relevant in evaluating the geometric goodness-of-fit statistic. A high R_p^2 value is not in itself sufficient to insure a correspondingly high value of R_Q^2. Drainage density is shown as an important index for the watersheds tested; i.e., a relatively high value of drainage density may indicate a correspondingly complex system. Therefore, the geometric goodness-of-fit statistic is a valuable measure of how well the watershed topography is represented in the model, but it must be interpreted with respect to drainage density. However, for a single watershed with a fixed drainage density, R_p^2 is a good indicator of how well the watershed is being represented geometrically (Fig. 4.15).

Distortions caused by underestimating the drainage density from Figs. 4.14 and 4.15, result if the model drainage density is less than the watershed drainage density and then the hydrograph goodness-of-fit statistic will probably be smaller; i.e., the value of R_Q^2 will be less than if the drainage density had been better represented.

4.5 Relation Between Combined Goodness-of-Fit Statistics and Hydraulic Roughness Parameters

Given rainfall-runoff data and an assumed model, optimal roughness parameters can be derived. Data errors as well as geometric distortions will be reflected in these estimated roughness parameters. Thus, it is reasonable to expect distortions in optimal roughness parameters when there are distortions in other watershed characteristics. Throughout the following discussion, a transition Reynolds number of 500 is assumed. By matching friction factors at this transition from laminar to turbulent flow, the problem reduces to determining a single roughness parameter, K. The next chapter gives details for a priori estimates of roughness parameters. For now, assume that empirically derived roughness coefficients can be obtained from graphs like that presented subsequently in Fig. 5.2. The mid or median value of such estimates is denoted K_o.

Examination of data in Table 4.7 suggests that low R_Q^2 values are associated with the events where the fitted and observed times to peak are very different. For this reason those events where the times to peak differed by 50 percent or more were excluded from the following analysis. Data from watershed W-C at Riesel, Texas; watershed 2-H at Hastings, Nebraska; network 4 (DERF-4), and network 5 (DERF-5) at Colorado State University were used to derive optimal roughness parameters for a plane and for the Wooding model. The mean values of the optimal K values are then related to $I_d R_p^2$ as a combined geometric goodness-of-fit statistic. Data from a more complex geometry for watershed W-C at Riesel, Texas and watershed LH-6 at Tombstone, Arizona are used to check the derived relation between optimal K values and the combined goodness-of-fit statistic.

The optimal roughness parameters can be normalized by K_o, the a priori estimates from Fig. 5.2. If the ratios of K/K_o are different from one, then this indicates a distortion in the optimal roughness coefficient. Moreover, if this ratio is related to goodness-of-fit statistics reflecting the degree of geometric distortion, then possibly a priori estimates of roughness parameters can be adjusted for use in simplified models. The circled points in Fig. 4.16 were used to derive the relation shown. The two plus signs in Fig. 4.16 are for more complex models for watersheds W-C and LH-6. These points agree with the least squares curve through the circled points. The two arrows at the right of Fig. 4.16 are for watersheds SW-17 at Riesel, Texas and P-1 and P-7 at the Pawnee site. Ratios of K/K_o were determined for these watersheds but there are no $I_d R_p^2$ values.

The major difficulty with data, as presented in Fig. 4.16, is the subjective nature of the a priori roughness parameters. For this reason and because K is determined from a sample, the equation relating K/K_o and $I_d R_p^2$ may be unique. However, optimal roughness parameters will likely increase as the geometric distortions in simplified models decrease.

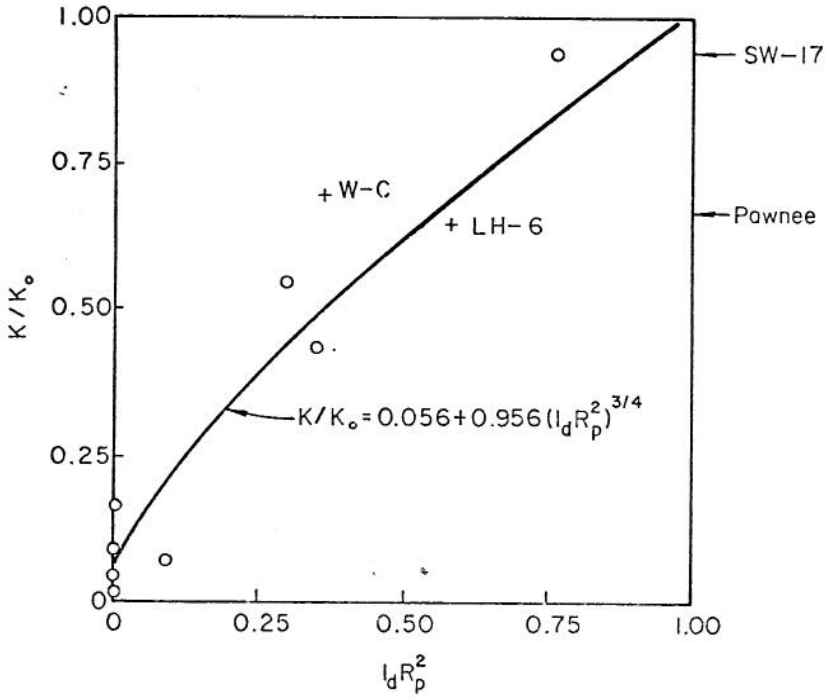

Fig. 4.16. Relation between combined goodness-of-fit statistic and normalized roughness coefficient.

Chapter V
PARAMETER ESTIMATION AND MODEL TESTING

This chapter describes parameter determination techniques from previous chapters, presents some new material on roughness parameter estimation and some example or test cases chosen so as to test hypotheses arising from analyses in previous chapters. As sensitivity analysis was implicit in previous chapters, the emphasis here is on empirical support or refutation via specific examples.

5.1 Selection Criteria for Simplified Geometry

Recall the definition of R_p^2 as the geometric goodness-of-fit statistic expressing the degree of improvement by fitting a set of planes to coordinate data over using the mean elevation. This statistic was seen to be associated with the overland flow portion of the kinematic cascade model. Moreover, the coefficient α in the depth-discharge equation for a plane is a function of the plane slope

$$\alpha = \frac{8gS}{K\nu} \tag{5.1}$$

for laminar flow and

$$\alpha = C\sqrt{S} \tag{5.2}$$

for turbulent flow. Therefore, since the slope S assumes a direct role in α and thus in determining the discharge, it must be estimated which is the result of least squares fitting.

The geometric goodness-of-fit statistic was related to the peak discharge of the overland flow impulse response. For more complex watersheds with overland and open channel flow, R_Q^2 was related to drainage density in an inverse manner. With drainage density variations allowed, R_p^2 was also related to R_Q^2, the hydrograph goodness-of-fit statistic. With respect to simulation of surface runoff, the degree of geometric complexity required can be determined by constructing a graph relating R_Q^2 and R_p^2. In such a procedure, a decision concerning the required level of R_Q^2 is necessary. As with the choice of objective function, this level will be based upon user requirements. However, given a required R_Q^2, such a plot will determine if it can be reached, and if so, the required geometric complexity. Obviously other criteria might require different degrees of geometric goodness-of-fit.

The procedure for determining the number of channel elements in cascade required to represent the main channel is analogous to the procedure described above; i.e., the index of concavity is related to the hydrologic characteristic of interest. The number of elements is increased until the index of concavity is sufficiently close to 1.0 to meet the required hydrograph criterion.

The above notions are graphically summarized in Fig. 5.1. The upper portion relates R_p^2 and R_Q^2 for fitting planes to coordinate data. Assume that

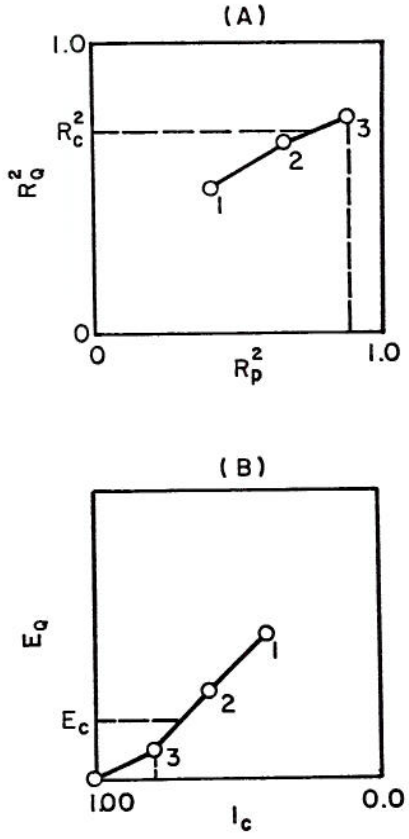

Fig. 5.1. Illustration of procedures for selecting the simplest kinematic cascade of planes and channels to meet given hydrograph criteria. (A) Geometric goodness-of-fit, determination of degree of geometric complexity. (B) Main channel concavity, determination of number of channel elements in cascade.

rainfall, runoff, and topographic data are available on a given watershed. A set of rainfall-runoff events is selected for analysis. Best fit hydrographs are produced for each of three proposed geometries--labeled 1, 2, and 3 in the upper portion of Fig. 5.1. Furthermore, assume that on the average, it is required to explain R_c^2 of the variance in discharge about the mean discharge. Configuration No. 3 would be chosen (see dashed lines) as the required model--the simplest configuration meeting the criterion $R_Q^2 \geq R_c^2$.

To determine the number of channel elements in cascade necessary to reproduce the hydrologic character, with respect to downstream concavity of the main channel, a graph must be constructed as in the lower portion of Fig. 5.1. Assume that hydrographs are routed down main channels consisting of one, two, etc. channel segments in cascade. Each added channel segment increases the concavity and thus increases the index of concavity. If the error in routed peak discharge, E_Q, is chosen as the required hydrograph criterion, and E_c is the required level or maximum error allowed, then it would be necessary to have

three channel elements in cascade. Thus, it is possible to construct graphs which then can be used to specify the simplest geometry (with respect to planes and channels) which when used in simulation will, usually, preserve the selected hydrograph characteristics to a given degree of accuracy. In the examples discussed here the selected hydrograph characteristics are R_Q^2, the hydrograph goodness-of-fit statistic and E_Q, the error in routed peak discharge due to underestimating the degree of concavity in the main stream.

5.2 Determination of Roughness Parameters

In overland flow there are two roughness parameters, K as in Eq. 5.1 and C as in Eq. 5.2 (see Chapter III for details). If the Reynolds number for transition from laminar to turbulent flow is specified, then given K or C, the parameter not given is determined. A transition number is assumed leaving K as the single overland flow-roughness parameter to be determined. Channel flow is assumed to always be turbulent so that only the Chezy C value needs to be determined. Two cases arise: (1) When initial estimates or a priori estimates of roughness parameters are needed; and (2) When data are available to derive optimal roughness parameters. Since for efficient optimization the initial values should be as close as possible to the optimal values, estimates (even if only initial values are needed) of roughness parameters must always be made.

5.2.1 A Priori Estimates of Roughness Parameters

As discussed in Chapter IV, the degree of complexity in the simplified model is related to the apparent roughness. A gross misrepresentation in geometry may result in a compensating error in estimated roughness coefficients. Therefore, it is assumed that the roughness parameter is for sufficiently complex geometrical configurations so that the geometry-roughness interaction is minimal.

For open channel flow any of several handbooks, (e.g. King and Brater, 1963), can be used to estimate Chezy coefficients directly or from tabular values of Manning's n. The equation relating n and C is

$$C = \frac{1.5}{n} R^{1/6} \tag{5.3}$$

where R is hydraulic radius. There is a broad class of references where estimates of roughness parameters for open channel flow may be obtained (e.g. Barnes, 1967). For this reason, the emphasis in this section is on roughness parameters (K, C, n) for overland flow.

Data presented in a table by Woolhiser (1974) are summarized in Fig. 5.2. The line in Fig. 5.2 relates K and C for a transition from laminar to turbulent flow at a Reynolds number of 500. Ranges of K values for several surfaces are shown by the arrows in Fig. 5.2. Values of n for the Manning formula are shown below each surface description. For example, with a bare sand surface, K varies from 30 to 120, C varies from 65 to 32, and n varies from 0.01 to 0.016. As can be seen from the wide ranges of roughness coefficients, there is a great deal of freedom in interpreting a specific value of a coefficient. In spite of this, Fig. 5.2 provides the best available basis for interpreting roughness-surface relations for natural watersheds.

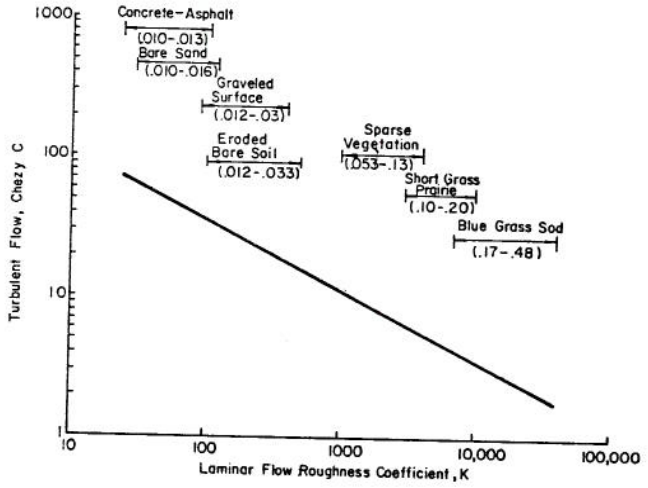

Fig. 5.2. Laminar and turbulent roughness coefficients for overland flow. Manning n values given below surface description.

5.2.2 Optimal Values of Roughness Parameters

Recall the sums-of-squares objective function given as

$$G_1 = \sum_{j=1}^{m} (q_j - \hat{q}_j)^2 \tag{5.4}$$

where q_j is an observed hydrograph ordinate and $\hat{q}_j$ is the fitted value. Optimal roughness parameters (K and C for a plane) are the values which minimize G_1. Again, for a specified transition number, the value of K determines the value of C. The optimization procedure used here is a two-stage method optimizing on planes and channels separately. The procedure is illustrated in Fig. 4.12. For a given value of C in the channels an optimal value of K on the planes is derived. The process is repeated over a range of channel C values until G_1 is a minimum. The resulting channel C and plane K values are the optimal values for that hydrograph.

5.3 Model Testing

Procedures outlined in the first two sections of this chapter are tested using data from experimental watersheds. The intent is to apply techniques presented in earlier chapters to watersheds not used in their development, thus testing their efficacy. In effect, the tests will be for the model selected and for its selection procedure.

5.3.1 Effects of Nonuniform Slopes Upon Overland Flow

To test the effects of slope shape upon overland flow hydrographs, two simple experiments were conducted on the erosion (DERF) facility at Colorado State University. The first involved recording runoff hydrographs for three durations and four intensities on an impervious plastic surface graded to uniform slope. The surface was a V-configuration (see Wooding, 1965, p. 258), symmetric about a channel 24 ft long with a 0.03 slope. The lateral slope of the two 14-ft planes was 0.04.

three channel elements in cascade. Thus, it is possible to construct graphs which then can be used to specify the simplest geometry (with respect to planes and channels) which when used in simulation will, usually, preserve the selected hydrograph characteristics to a given degree of accuracy. In the examples discussed here the selected hydrograph characteristics are R_Q^2, the hydrograph goodness-of-fit statistic and E_Q, the error in routed peak discharge due to underestimating the degree of concavity in the main stream.

5.2 Determination of Roughness Parameters

In overland flow there are two roughness parameters, K as in Eq. 5.1 and C as in Eq. 5.2 (see Chapter III for details). If the Reynolds number for transition from laminar to turbulent flow is specified, then given K or C, the parameter not given is determined. A transition number is assumed leaving K as the single overland flow-roughness parameter to be determined. Channel flow is assumed to always be turbulent so that only the Chezy C value needs to be determined. Two cases arise: (1) When initial estimates or a priori estimates of roughness parameters are needed; and (2) When data are available to derive optimal roughness parameters. Since for efficient optimization the initial values should be as close as possible to the optimal values, estimates (even if only initial values are needed) of roughness parameters must always be made.

5.2.1 A Priori Estimates of Roughness Parameters

As discussed in Chapter IV, the degree of complexity in the simplified model is related to the apparent roughness. A gross misrepresentation in geometry may result in a compensating error in estimated roughness coefficients. Therefore, it is assumed that the roughness parameter is for sufficiently complex geometrical configurations so that the geometry-roughness interaction is minimal.

For open channel flow any of several handbooks, (e.g. King and Brater, 1963), can be used to estimate Chezy coefficients directly or from tabular values of Manning's n. The equation relating n and C is

$$C = \frac{1.5}{n} R^{1/6} \tag{5.3}$$

where R is hydraulic radius. There is a broad class of references where estimates of roughness parameters for open channel flow may be obtained (e.g. Barnes, 1967). For this reason, the emphasis in this section is on roughness parameters (K, C, n) for overland flow.

Data presented in a table by Woolhiser (1974) are summarized in Fig. 5.2. The line in Fig. 5.2 relates K and C for a transition from laminar to turbulent flow at a Reynolds number of 500. Ranges of K values for several surfaces are shown by the arrows in Fig. 5.2. Values of n for the Manning formula are shown below each surface description. For example, with a bare sand surface, K varies from 30 to 120, C varies from 65 to 32, and n varies from 0.01 to 0.016. As can be seen from the wide ranges of roughness coefficients, there is a great deal of freedom in interpreting a specific value of a coefficient. In spite of this, Fig. 5.2 provides the best available basis for interpreting roughness-surface relations for natural watersheds.

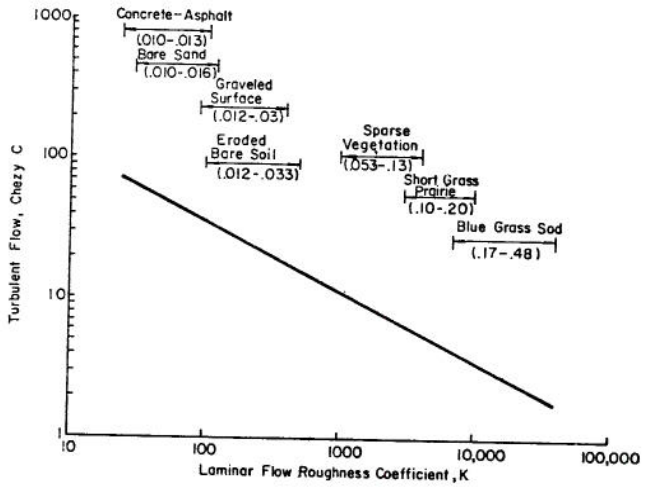

Fig. 5.2. Laminar and turbulent roughness coefficients for overland flow. Manning n values given below surface description.

5.2.2 Optimal Values of Roughness Parameters

Recall the sums-of-squares objective function given as

$$G_1 = \sum_{j=1}^{m} (q_j - \hat{q}_j)^2 \tag{5.4}$$

where q_j is an observed hydrograph ordinate and $\hat{q}_j$ is the fitted value. Optimal roughness parameters (K and C for a plane) are the values which minimize G_1. Again, for a specified transition number, the value of K determines the value of C. The optimization procedure used here is a two-stage method optimizing on planes and channels separately. The procedure is illustrated in Fig. 4.12. For a given value of C in the channels an optimal value of K on the planes is derived. The process is repeated over a range of channel C values until G_1 is a minimum. The resulting channel C and plane K values are the optimal values for that hydrograph.

5.3 Model Testing

Procedures outlined in the first two sections of this chapter are tested using data from experimental watersheds. The intent is to apply techniques presented in earlier chapters to watersheds not used in their development, thus testing their efficacy. In effect, the tests will be for the model selected and for its selection procedure.

5.3.1 Effects of Nonuniform Slopes Upon Overland Flow

To test the effects of slope shape upon overland flow hydrographs, two simple experiments were conducted on the erosion (DERF) facility at Colorado State University. The first involved recording runoff hydrographs for three durations and four intensities on an impervious plastic surface graded to uniform slope. The surface was a V-configuration (see Wooding, 1965, p. 258), symmetric about a channel 24 ft long with a 0.03 slope. The lateral slope of the two 14-ft planes was 0.04.

The second experiment was similar, except the two side slopes were regraded to each form cascades of three 4.67-ft planes with lateral slopes of 0.07, 0.04, and 0.01, respectively. The lowest (0.01) slope was at the bottom of the cascade. The second channel was inadvertently modified to a slightly concave profile with an equivalent slope of 0.028, with an index of concavity of approximately 0.90. Compounding this error, the channel cross-section was changed from a triangular section with side slopes of 0.04 to a triangular section with side slopes of 0.01. Together these inadvertent modifications in the main channel significantly changed its character. A second inadvertent modification was in the length of overland flow. While drainage density remained the same in both experiments, the maximum length of overland flow was approximately 17 ft in the first experiment and approximately 31 ft in the second experiment.

As a measure of the influence of concavity on overland flow, peak runoff rates were compared from the uniform and concave configurations. Experimental results indicated an approximately 40 percent reduction in peak rate for the concave configuration. To determine the cause of this difference in peak discharge, optimal roughness parameters were obtained using data from both configurations. Simulation analyses were then conducted using the previously determined parameters. From the simulation results, the relative effects of several factors can be estimated which might have influenced the magnitude of 40 percent reduction in peak discharge in the second experiment. Changes in the channel (as described above) should result in a decrease of 6 to 10 percent in the routed hydrograph. In contrast, the concave overland flow should produce about 7 to 10 percent increase in peak discharge. Nonuniform input might have resulted in a decrease due to its greater influence on the flatter-sloped planes of the concave configuration. Changes in the length of overland flow may have affected peak discharge by increasing the time to equilibrium in the second experiment. However, this is difficult to simulate due to other distortions in model geometry required to account for the difference in length of flow. The main conclusion from these simulation studies was that the effect being sought was likely to be completely masked by larger effects from uncontrolled changes from the first to the second experiment.

The experiments described above were valuable in emphasizing the need for complete experimental design and devotion to detail in experimental work. In terms of testing the effects of slope shape upon overland flow, variability in the data due to uncontrolled factors masked the anticipated effects of concavity.

In an additional attempt to test the hypothesized influence of slope shape upon overland flow, data from two of the Pawnee watersheds (see Table 4.5) were chosen for analysis. Watershed P-1 has a mean slope of 0.031, while watershed P-7 has a mean slope of 0.036. Watershed P-1 has a concave shape with an index of concavity from a midwatershed slope profile of $I_c = 0.76$. Watershed P-7 has a convex shape with an index of concavity for the midwatershed profile of $I_c = 1.09$. Four planes were fit to each watershed to adequately account for the concavity and convexity. Optimal roughness parameters were then derived for each watershed from the rainfall-runoff event of September 11, 1973. As an example, rainfall excess, observed runoff, and fitted runoff are shown in Fig. 5.3 for watershed P-1. Optimal roughness parameters are K = 1690 for watershed P-1, and K = 1670 for

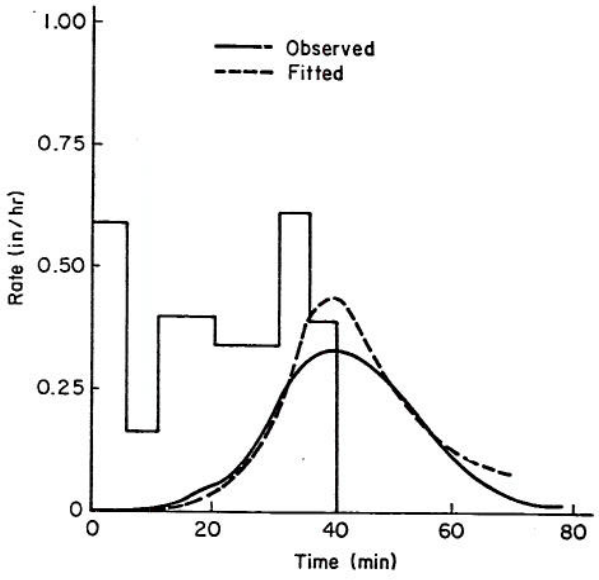

Fig. 5.3. Observed and fitted hydrographs for Pawnee Watershed P-1, September 11, 1973.

watershed P-7. These values are very close so that any differences in simulated runoff would not be due to different values of estimated roughness coefficients. As shown in Fig. 5.3, the rainfall input pattern for the observed data is quite complex. For this reason, optimal roughness parameters were used to simulate responses to a partial equilibrium-pulse input on both watersheds. This procedure--calibrate, simulate to insure similar input, and then compare results--is implicit throughout this study. Any differences in the responses should be due to geometrical differences--concavity versus convexity. The responses are shown in Fig. 5.4 wherein (1) refers to the hydrograph from watershed P-1 (concave) while (7) refers to the hydrograph from watershed P-7 (convex). The differences in the hydrographs are as hypothesized. The concave watershed produces a more delayed response when compared with the convex watershed. Peak discharge values are comparable for the two

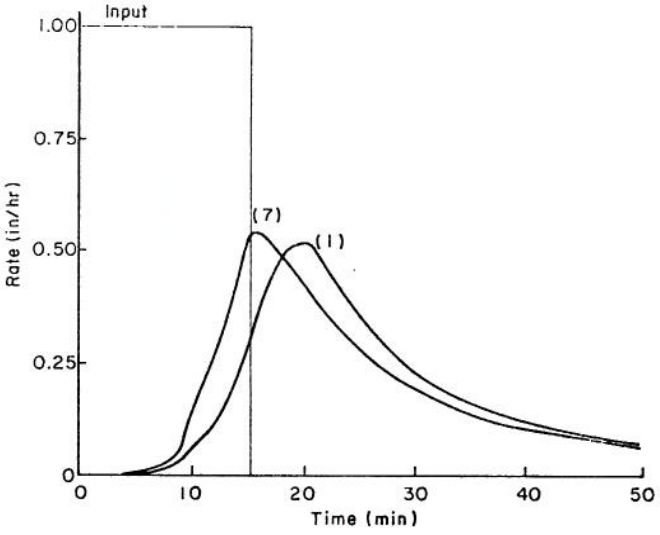

Fig. 5.4. Partial equilibrium-pulse responses for Pawnee Watersheds, complex geometry, optimal roughness.

watersheds. However, the differences in the hydrographs shown in Fig. 5.4 are small, about 20 percent in time to peak and about 5 percent in peak discharge, leading to the conclusion of no significant difference in peak discharge. That is, under conditions as observed on the Pawnee watersheds, the effects of slope shape upon overland flow may be significant with respect to time to peak but may not be significant with respect to peak discharge.

As a final comparison for these watersheds, impulse responses were computed as shown in Fig. 5.5. As expected, impulse response analysis is most powerful in detecting the influence of slope shape. The impulse response of the concave watershed is delayed in comparison with the response from the convex watershed. There are no significant differences in the recessions of the impulse responses.

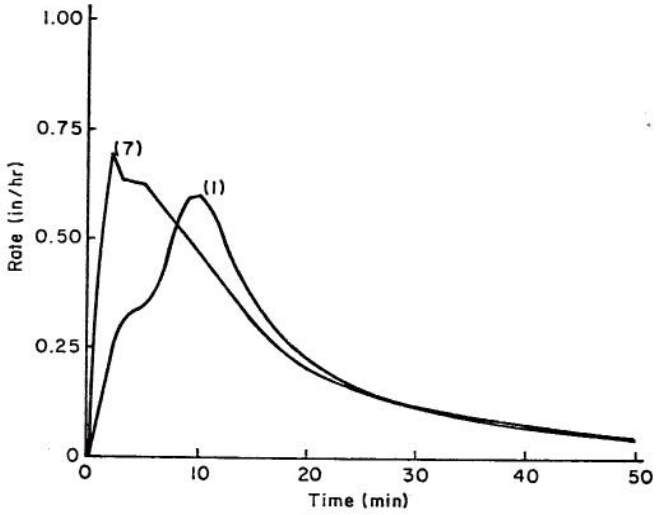

Fig. 5.5. Impulse responses for Pawnee Watersheds, complex geometry, optimal roughness.

Overton (1971) made an independent analysis of the influence of slope shape upon overland flow. Unfortunately, Overton considered steady-state conditions so that peak discharge was not a part of his analysis. His conclusions were for a particular definition of lag time (related by a constant factor to equilibrium time). As shown in Fig. 3.4 herein, minimum time differences will be at equilibrium. This is in agreement with Overton's (1971) conclusion that slope shape has little effect upon his lag or hydrologic response time. Therefore, to the extent that they are comparable, the results reported here are consistent with Overton's.

5.3.2 Complex Watersheds

To test the proposed procedure for modeling complex watersheds, watershed LH-6 on the Walnut Gulch Experimental Watershed near Tombstone, Arizona was selected as an example. As shown in Table 4.5, LH-6 is a 1.07 acre watershed with a concave main channel profile. A detailed description of Walnut Gulch is given by Renard (1970). While LH-6 is slightly smaller than the Pawnee watersheds, the sizes are comparable. Moreover, LH-6 has a rather high drainage density of 0.012 ft/ft^2 in contrast with the absence of channels on the Pawnee watershed.

A complex geometrical representation of watershed LH-6 consists of nine planes and three channels. Model drainage density is 0.007 ft/ft^2 so that the drainage density ratio is $I_d = 0.6$, which means that the total length of channels in the kinematic cascade model is 60 percent of the total length of channels in the watershed. The geometric goodness-of-fit statistic for the complex configuration is $R_p^2 = 0.96$.

Fitted and observed hydrographs for the event of August 18, 1971, are shown in Fig. 5.6. The optimal

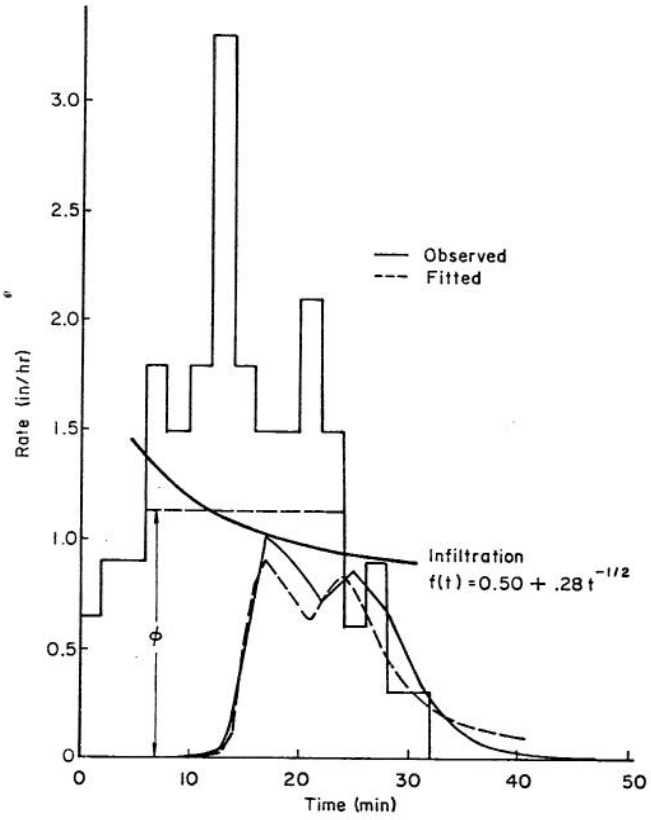

Fig. 5.6. Fitted and observed hydrographs for the event of August 18, 1971, on watershed LH-6.

K value is 1630, and the hydrograph goodness-of-fit statistic is $R_Q^2 = 0.89$. The most serious errors for this event are in peak discharge and later recession values. In this example rainfall excess-volume is known since runoff volume is known and observed runoff data are used in determining the optimal roughness parameter. In the next example (Fig. 5.7) rainfall excess-volume is known but the roughness parameter is assumed. Thus the term simulation is used. In the third example rainfall excess-volume is not known and the roughness parameter is assumed. This situation is termed predicting. Infiltration parameters from the event of August 10, 1971 (Fig. 5.7) were assumed for the event of August 12, 1971, as shown in Fig. 5.8. Also, a roughness parameter of K = 2000, which roughly corresponds with the optimal value from the event of August 18, 1971, was assumed for this example.

The simulated hydrograph as shown in Fig. 5.7 represents an example of a good reproduction of hydrograph shape and peak rate but a poor time correspondence. Parameters determined from optimization on data such as these would be quite different from those

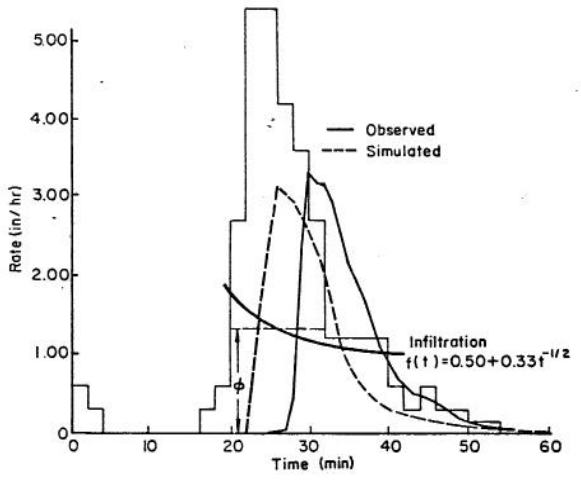

Fig. 5.7. Simulated and observed hydrographs for the event of August 10, 1971, on watershed LH-6.

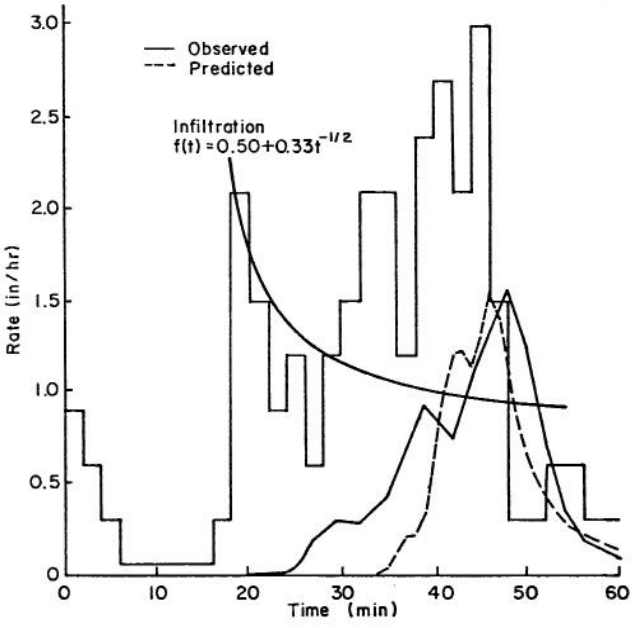

Fig. 5.8. Predicted and observed hydrographs for the event of August 12, 1971, on watershed LH-6.

obtained if there had been better timing correspondence. As expected, the predicted hydrograph (Fig. 5.8) is a poorer reproduction of the observed hydrograph than in the fitted and simulated cases. Even so, this example is probably a better-than-average case, especially with respect to peak discharge. There are timing, volume, and hydrograph shape errors in this test case.

Some watershed characteristics for W-C at Riesel, Texas are shown in Tables 4.5 and 4.8. A third model for this watershed consists of two channels in cascade each with two lateral planes. Thus, the model is composed of four planes and two channels as discussed in Section 4.5. Selected runoff events were used to obtain optimal roughness parameters for the watershed modeled as a single plane, the Wooding model, and the four plane configuration. Mean hydrograph goodness-of-fit statistics and the corresponding geometric goodness-of-fit statistics for these data are shown in Fig. 5.9. The following observations can be drawn from this graph. A twofold increase in

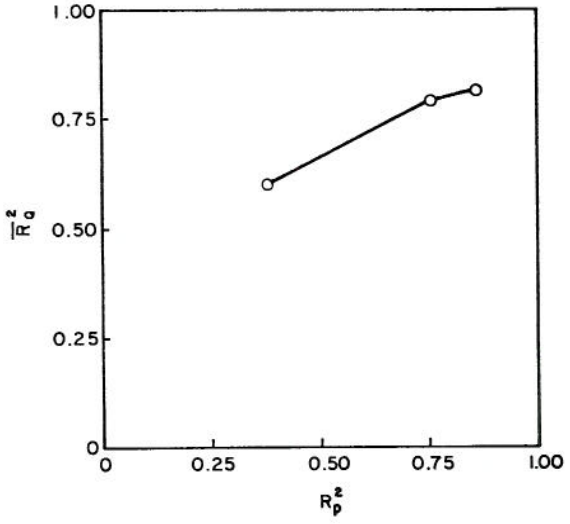

Fig. 5.9. Relation between goodness-of-fit statistics for watershed W-C.

R^2_p results in an increase of about one-third in $\bar{R}^2_Q$. The rate of increase in $\bar{R}^2_Q$ with increasing R^2_p decreases in going from the second to the third model. Expanding upon these observations, the upper portion of Fig. 5.10 shows the relation between $\bar{R}^2_Q$ and the

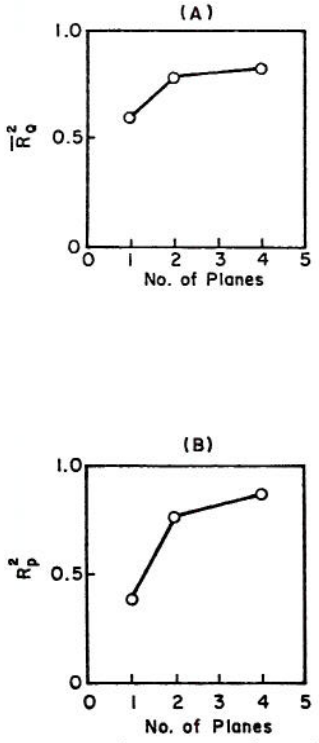

Fig. 5.10. Relation between number of planes in kinematic cascade model and: (A) Hydrograph goodness-of-fit statistic, (B) Geometric goodness-of-fit statistic, for watershed W-C.

number of planes in each model. The lower portion of Fig. 5.10 is a plot of the geometric goodness-of-fit versus the number of planes in the models. Goodness-of-fit statistics increase as geometric complexity increases but at a decreasing rate.

Therefore, for watersheds, as examined here, it seems reasonable to assume that there will be diminishing return in hydrograph goodness-of-fit for increasing geometric complexity. This is not to suggest that there will not be additional benefits associated with the increasing distribution in space of other watershed characteristics. For the simplest geometry, the kinematic cascade model is a lumped parameter model. As the geometric complexity increases, so does the potential for distributing associated model parameters in space.

A second cautionary note is with respect to optimal roughness parameters. An increase in geometric complexity yields a diminishing return in hydrograph goodness-of-fit but not in terms of roughness parameter estimation. The data in Fig. 4.16 suggest a nearly linear relation between a combined goodness-of-fit statistic for watershed geometry and normalized roughness coefficients. This concept is illustrated in Fig. 5.11, where relatively small increases in $\overline{R}_Q^2$ are associated with larger increases in the normalized roughness parameter.

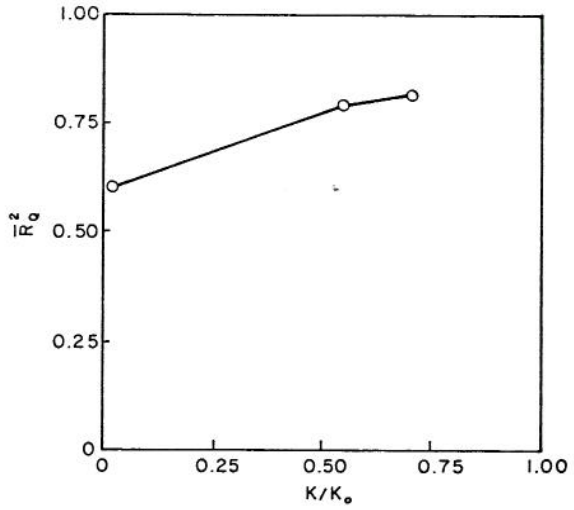

Fig. 5.11. Relation between distortion in roughness parameter and hydrograph goodness-of-fit statistic for watershed W-C.

Chapter VI
CONCLUSIONS AND RECOMMENDATIONS

Surface runoff, conceptualized here as overland and open channel flow, is a complex process which is invariably simplified in the formulation of mathematical models. This thesis is an endeavor to develop objective procedures for geometric simplification of complex watersheds modeled as kinematic cascades of planes and channels. The development of goodness-of-fit statistics for geometric and hydrograph fitting represents a theoretical basis for empirical development of inferential relationships between geometric and hydrograph goodness-of-fit statistics.

6.1 Conclusions

Throughout this research, the writers were often led to conclusions concerning the mechanism whereby rainfall becomes runoff on small watersheds. Many of these conclusions are of a subtle nature and, as yet, not succinctly formulated to allow expression. The conclusions presented do reflect areas where sufficient theory, data, and experience were brought together to justify specific conclusions.

Conclusions resulting from this study are:

1. A simple concept of the surface of a watershed is that it consists of the channel network and the interchannel areas of overland flow within the watershed perimeter. This study verifies that this simple concept is useful in modeling surface runoff.

2. Kinematic impulse response analysis was demonstrated to emphasize the influence of surface configuration upon overland flow.

3. Peak discharge of the kinematic impulse response is greater for parabolic than for uniform slope overland flow surfaces, and the differences are greater for laminar flow than for turbulent flow.

4. Analyses of partial equilibrium-overland flow hydrographs from uniform and parabolic slopes indicate that concave slopes produce higher peak discharge for laminar flow and higher or lower peak discharge for mixed laminar and turbulent flow depending on the duration of the input pulse.

5. Simulation results for complex watersheds suggest that underestimating the drainage density would result in overestimated time characteristics and underestimated peak discharge, unless there were compensating errors in other parameters. In the absence of such errors, underestimating drainage density would probably result in overestimated lag time and increased nonlinearity in the rainfall excess-surface runoff relation.

6. The hydrograph goodness-of-fit statistic, R_Q^2, is related to the geometric goodness-of-fit statistic, R_p^2, and to drainage density.

7. The ratio of optimal roughness parameters to experimentally derived roughness parameters is related to a combined goodness-of-fit statistic as the product of the drainage density ratio and the geometric goodness-of-fit statistic.

8. Under real conditions, as observed on the Pawnee watersheds, the effects of slope shape upon overland flow are significant with respect to time to peak but may not be significant with respect to equilibrium time or peak discharge.

9. Successive increases in complexity of kinematic cascade models may yield diminishing returns in hydrograph goodness-of-fit but not in terms of roughness parameter estimates.

6.2 Recommendations for Further Research

Four main areas of study, where additional research may yield answers to questions raised by this study, are: (1) To obtain better timing relationships between rainfall, rainfall excess, and runoff; (2) To obtain more accurate rainfall excess estimates particularly with respect to initial abstractions and temporal variation caused by the action of different processes varying in space; (3) To develop a nonlinear identification and linear prediction procedure (as suggested by the research of Singh (1974) and that reported here); and (4) To conduct an empirical study relating geometric with hydrograph goodness-of-fit statistics.

6.2.1 Timing Relationships

Synchronous measurements of rainfall and runoff on small watersheds, such as the Pawnee and Lucky Hills watersheds, are needed. It is suggested that a simple electrical link between the rain gage and water stage recorders be established. For example, two solenoids could make simultaneous marks upon the rain gage and runoff charts at the beginning of a rainfall event which would not only reduce the variability of future data but also aid in interpreting existing data. With the mechanical timing errors eliminated, it would then be possible to investigate the true nature of the timing relationships.

6.2.2 More Accurate Rainfall Excess Estimates

Although an oversimplification, the assumption of a simple infiltration function as used here is common. That a block of rainfall divided into infiltration and rainfall-excess providing input to a routing model is an oversimplification is well-known (see e.g. Foster (1968), Smith (1970), or Smith and Woolhiser (1971)). One infiltration equation may be necessary during rainfall when the entire area is active and another after rainfall when the rills and microrills are still active but the interrill areas of overland flow are not. The procedure (as discussed by Foster (1971), p. 174) may be a logical starting point. If the timing errors can be eliminated, possibly only the inclusion of an initial abstraction term may satisfy observed time lag phenomena. The procedure (described by Langford and Turner (1971) or the threshold procedure discussed by Lane (1972)) may be logical starting points. In any event, if the errors due to distortions in geometric simplification can be quantified then it may be fruitful to begin quantifying the errors due to oversimplification in estimated rainfall excess. A second step in attacking the problem might be via a calibrated simulation model, as suggested by the example of the effects of variability of rainfall excess upon overland flow hydrographs. Finally, since drainage density is a measure of all channels in an area, it may prove to be an important parameter in studying rill infiltration, as suggested

by Foster and others. This would seem to be another potential area for additional research.

6.2.3 Toward an Optimal Nonlinear Identification--Linear Prediction Scheme

As stated earlier, the work of Singh (1974) in analyzing prediction results with linear and nonlinear models and this work analyzing effects of watershed characteristics upon overland flow may provide a starting point for further research. These studies provide a reason for asking the questions: Is there an optimal procedure, with respect to power of identification and accuracy of prediction, for nonlinear system identification and linear system prediction in surface runoff and when can one say that with specified degree of accuracy a given hydrologic system can be assumed linear?

6.2.4 Empirical Development of Inferential Relationships Between Geometric and Hydrograph Goodness-of-Fit Statistics

Assuming that timing errors can be overcome and that rainfall excess-estimates of sufficient accuracy can be made, then if R_Q^2 and R_p^2 can be related there is a basis for inference in modeling rainfall excess-surface runoff on small watersheds. Moreover, this inferential procedure (geometric to hydrologic goodness-of-fit) may provide a method for extending more meaningful rainfall-runoff relationships to ungaged basins. Therefore, there is need for an empirical study relating R_Q^2 to R_p^2 and other watershed characteristics for a variety of small watersheds.

As discussed earlier, the process of surface runoff is complex with a large number of variables involved. An alternative approach to the problem of analysis of the significance of selected geomorphic parameters in determining hydrograph goodness-of-fit statistics may be through multivariate analysis. For example, Overton (1969) used principal component analysis to investigate the interrelation of geomorphic parameters. Yevjevich, et al., (1972) showed the possibility of selecting a smaller number of parameters from an extensive list of geomorphic parameters related to flood characteristics on small watersheds. Similar analyses might prove fruitful in relating R_Q^2 to R_p^2 and to other watershed characteristics.

REFERENCES

Amorocho, J. Discussion of "Predicting Storm Runoff on Small Experimental Watersheds." Proc. ASCE Jour. Hyd. Div., Vol. 87, No. HY2, pp. 185-191. 1961.

Barnes, H. H. Roughness Characteristics of Natural Channels. USGS Water Supply Paper 1849, 213 p. 1967.

Brakensiek, D. L. A Simulated Watershed Flow System for Hydrograph Prediction: A Kinematic Application. Paper No. 3, Proc. Int. Hyd. Symposium, Fort Collins, Colorado. 1967.

Chitale, S. V. Theories and Relationships of River Channel Patterns. Jour. of Hyd., Vol. 19, No. 4, pp. 285-308. 1973.

Conte, S. D. Elementary Numerical Analysis. McGraw-Hill Book Co., New York, 278 p. 1965.

Dooge, J. C. I. Hydrologic Systems with Uniform Non-Linearity. Memo. Univ. College, Cork, Civil Engr. Dept., 48 p. 1967.

Dooge, J. C. I. Linear Theory of Hydrologic Systems. U.S. Dept. of Agric. Tech. Bull. No. 1468. Washington, D.C., 327 p. 1973.

Eagleson, P. S. A Distributed Linear Model for Peak Catchment Discharge. Proc. Int. Hyd. Symposium, Fort Collins, Colorado, pp. 1-8. 1967.

Eagleson, P. S. Dynamic Hydrology. McGraw-Hill Book Co., New York, 462 p. 1970.

Foster, G. R. Analysis of Overland Flow on Short Erosion Plots. Unpub. M.S. Thesis, Purdue Univ., Lafayette, Indiana. 1968.

Foster, G. R. The Overland Flow Process Under Natural Conditions. Proc. Third Int. Seminar for Hyd. Prof., "Biological Effects in the Hydrological Cycle," pp. 173-185. Dept. of Agric. Engr., Agric. Exp. Sta., Purdue Univ., West Lafayette, Indiana. 1971.

Golany, P. and Larson, C. L. Effects of Channel Characteristics on Time Parameters for Small Watershed Runoff Hydrographs. Bull. 31, Water Resources Research Center, Univ. of Minnesota, Minneapolis, 130 p. 1971.

Gray, D. M. Synthetic Unit Hydrographs for Small Watersheds. Proc. ASCE, Jour. of Hyd. Div., Vol. 87, No. HY4, pp. 33-54. 1961.

Gupta, S. C. Transform and State Variable Methods in Linear Systems. John Wiley & Sons, Inc., New York, 426 p. 1966.

Harley, B. M. et al. A Modular Distributed Model of Catchment Dynamics. Report No. 133, Ralph M. Parson's Lab., Dept. of Civil Engr., Massachusetts Inst. of Tech., Cambridge, Massachusetts, 537 p. 1970.

Henderson, F. M. and Wooding, R. A. Overland Flow and Groundwater Flow from a Steady Rainfall of Finite Duration. Jour. of Geophys. Res., Vol. 69, No. 8, pp. 1531-1540. 1964.

Hickok, R. B. et al. Hydrograph Synthesis for Small Arid Land Watersheds. Trans. ASAE, Vol. 40, pp. 608-611, 615. 1959.

Hobson, R. D. FORTRAN IV Programs to Determine Surface Roughness in Topography for the CDC 3400 Computer. Kansas Computer Contribution No. 14, 28 p. 1967.

Horton, R. E. Drainage-Basin Characteristics. Trans. AGU, No. 13, pp. 350-361. 1932.

Horton, R. E. Erosional Development of Streams and Their Drainage Basins; Hydrophysical Approach to Quantitative Morphology. Bull. Geol. Soc. of Amer., Vol. 56, pp. 275-370. 1945.

Houghton, D. D. and Kasahara, A. Nonlinear Shallow Fluid Flow Over an Isolated Ridge. Comm. on Pure and Applied Math., Vol. XXI. 1968.

Jarvis, C. S. Flood Flow Characteristics. Trans. ASCE, Vol. 89, pp. 985-1032. 1926.

Kibler, D. F. and Woolhiser, D. A. The Kinematic Cascade as a Hydrologic Model. Hyd. Paper No. 39, Colorado State Univ., Fort Collins, Colorado, 27 p. 1970.

King, H. W. and Brater, E. F. Handbook of Hydraulics. McGraw-Hill Book Co., New York. 1963.

Lane, L. J. A Proposed Model for Flood Routing in Abstracting Ephemeral Channels. Hyd. and Water Res. in Arizona and the Southwest. Proc. of Joint AWRA and Arizona Acad. of Sci. Meetings, Prescott, Arizona, 2:439-453. 1972.

Lane, W. L. Personal Communication. 1974.

Langford, K. J. and Turner, A. K. Effects of Rain and Depression Storage on Overland Flow. Presented at Hyd. Conf. Inst. Eng. Aust., pp. 135-146. 1971.

Leopold, L. B. and Miller, J. P. Ephemeral Streams--Hydraulic Factors and Their Relation to the Drainage Net. USGS Prof. Paper 282-A, 37 p. 1956.

Lighthill, M. J. and Whitham, C. B. On Kinematic Waves: Flood Movement in Long Rivers. Proc. Royal Soc. (London) Series A, 229:281-316. 1955.

Markovic, R. D. Review of Recent Trends in the Analysis of the Development of River Networks. Colorado State Univ., Engr. Res. Center, Paper No. CER66-67RDM9, Fort Collins, Colorado, 50 p. 1966.

Minshall, N. E. Predicting Storm Runoff on Small Experimental Watersheds. Proc. ASCE, Jour. Hyd. Div., Vol. 86, No. HY8, pp. 17-38. 1960.

Murphey, J. B. et al. Using Geomorphic Parameters to Predict Hydrograph Characteristics in the Southwest. Unpub. Manuscript, submitted to the Bull. GSA. 1974.

Nash, J. E. The Form of the Instantaneous Unit Hydrograph. Inter. Assoc. Sci. Hyd., Pub. 45, No. 3, pp. 114-121. 1957.

Overton, D. E. Eigenvector Analysis of Geomorphic Interrelations of Small Agricultural Watersheds. Trans. ASAE, Vol. 12, No. 4, pp. 506-508. 1969.

Overton, D. E. Mechanics of Surface Runoff on Hillslopes. Proc. of Third Int. Seminar for Hyd. Prof., "Biological Effects in the Hydrological Cycle." pp. 186-210. Dept. of Agric. Engr., Agric. Exp. Sta., Purdue Univ., West Lafayette, Indiana. 1971.

Palmer, J. R. An Improved Procedure for Orthogonalizing the Search Vectors in Rosenbrock's and Swann's Direct Search Optimization Methods. Computer Jour., Vol. 12, pp. 29-42. 1969.

Parker, R. S. An Experimental Study of Basin Evolution and Its Hydrologic Impact. Dissertation, Colorado State Univ., Fort Collins, Colorado. 1975.

Philip, J. R. The Theory of Infiltration: 4. Sorptivity and Algebraic Infiltration Equations. Soil Sci., Vol. 84, pp. 257-264. 1957.

Ragan, R. M. and Duru, J. O. Kinematic Wave Nomograph for Times of Concentration. Proc. ASCE, Jour. of Hyd. Div., Vol. 98, No. HY10, pp. 1765-1771. 1972.

Renard, K. G. The Hydrology of Semiarid Rangeland Watersheds. U.S. Dept. of Agric. Pub. ARS 41-162, 26 p. 1970.

Rosenbrock, H. H. An Automatic Method for Finding the Greatest or Least Value of a Function. Computer Jour., Vol. 4, pp. 175-184. 1960.

Singh, V. P. A Nonlinear Kinematic Wave Model of Surface Runoff. Ph.D. Dissertation, Colorado State Univ., Fort Collins, Colorado, 282 p. 1974.

Smith, F. M. and Striffler, W. D. Pawnee Site Microwatershed: Selection, Description, and Instrumentation. Tech. Report No. 5, Grasslands BIOME, U.S.I.B.P., 29 p. 1969.

Smith, R. E. Mathematical Simulation of Infiltrating Watersheds. Ph.D. Dissertation, Colorado State Univ., Fort Collins, Colorado, 193 p. 1970.

Smith, R. E. and Woolhiser, D. A. Mathematical Simulation of Infiltrating Watersheds. Hyd. Paper, No. 47, Colorado State Univ., Fort Collins, Colorado, 44 p. 1971.

Strahler, A. N. Hypsometric (area-altitude) Analysis of Erosional Topography. Bull. Geol. Soc. Amer., Vol. 63, pp. 1117-1142. 1952.

Strahler, A. N. Quantitative Geomorphology of Drainage Basins and Channel Networks. Section 4, Part 2, pp. 4-39 to 4-76 in Handbook of Applied Hyd., ed. by V. T. Chow. McGraw-Hill Book Co., New York. 1964.

U.S.D.A. Hydrologic Data for Experimental Agricultural Watersheds in the United States, 1956-59 and Subsequent Years. U.S. Dept. of Agric., Misc. Pub. No. 945. 1963.

Wooding, R. A. A Hydraulic Model for the Catchment-Stream Problem: 1. Kinematic Wave Theory. Jour. Hyd. 3(3):254-267. 1965a.

Wooding, R. A. A Hydraulic Model for the Catchment-Stream Problem: 2. Numerical Solutions. Jour. Hyd. 3(3):268-282. 1965b.

Wooding, R. A. A Hydraulic Model for the Catchment-Stream Problem: 3. Comparison with Runoff Observations. Jour. Hyd. 4(1):21-37. 1966.

Woolhiser, D. A. Simulation of Unsteady Overland Flow. Chapter 12, Inst. on Unsteady Flow, Colorado State Univ., Fort Collins, Colorado, June 1974, Water Resources Pub., Fort Collins, Colorado. 1975.

Woolhiser, D. A. et al. Experimental Investigation of Converging Overland Flow. Trans. ASAE, Vol. 14, No. 4, pp. 684-687. 1971.

Yevjevich, V. et al. An Application of Multi-Variate Analysis in Hydrology. Completion Report Series, No. 35, Environmental Resources Center, Colorado State Univ., Fort Collins, Colorado, 39 p. 1972.

KEY WORDS: Runoff simulation, watershed geometry, rainfall-to-runoff models, overland flow, kinematic cascades model, parameter estimation, model testing:

ABSTRACT: For water flow on the surface of a watershed, geometric simplifications must be made. Consequences of such simplifications are examined. Objective procedures for geometric simplification of complex watersheds are developed. Watershed geometry is represented by a series of planes and channels in cascade, with the resulting "kinematic cascade model."

Planes are fitted to coordinate data from topographic maps by a least squares procedure. Channel elements are determined using Gray's method. An overall goodness-of-fit statistic is the drainage density ratio. The kinematic impulse response is the solution of the kinematic

KEY WORDS: Runoff simulation, watershed geometry, rainfall-to-runoff models, overland flow, kinematic cascades model, parameter estimation, model testing:

ABSTRACT: For water flow on the surface of a watershed, geometric simplifications must be made. Consequences of such simplifications are examined. Objective procedures for geometric simplification of complex watersheds are developed. Watershed geometry is represented by a series of planes and channels in cascade, with the resulting "kinematic cascade model."

Planes are fitted to coordinate data from topographic maps by a least squares procedure. Channel elements are determined using Gray's method. An overall goodness-of-fit statistic is the drainage density ratio. The kinematic impulse response is the solution of the kinematic

KEY WORDS: Runoff simulation, watershed geometry, rainfall-to-runoff models, overland flow, kinematic cascades model, parameter estimation, model testing:

ABSTRACT: For water flow on the surface of a watershed, geometric simplifications must be made. Consequences of such simplifications are examined. Objective procedures for geometric simplification of complex watersheds are developed. Watershed geometry is represented by a series of planes and channels in cascade, with the resulting "kinematic cascade model."

Planes are fitted to coordinate data from topographic maps by a least squares procedure. Channel elements are determined using Gray's method. An overall goodness-of-fit statistic is the drainage density ratio. The kinematic impulse response is the solution of the kinematic

KEY WORDS: Runoff simulation, watershed geometry, rainfall-to-runoff models, overland flow, kinematic cascades model, parameter estimation, model testing;

ABSTRACT: For water flow on the surface of a watershed, geometric simplifications must be made. Consequences of such simplifications are examined. Objective procedures for geometric simplification of complex watersheds are developed. Watershed geometry is represented by a series of planes and channels in cascade, with the resulting "kinematic cascade model."

Planes are fitted to coordinate data from topographic maps by a least squares procedure. Channel elements are determined using Gray's method. An overall goodness-of-fit statistic is the drainage density ratio. The kinematic impulse response is the solution of the kinematic

cascade model for an impulse input. For overland flow, peak discharge of the impulse response is affected by the surface shape.For overland flow, peak discharge of the impulse response is greater for parabolic than for uniform slope surfaces.

For a concave channel, the index of concavity is related to the error in peak discharge. Underestimating the drainage density results in overestimated time characteristics and underestimated peak discharge. The first moment of a linear instantaneous unit hydrograph decreases as drainage density increases. The degree of apparent nonlinearity is affected by drainage density.

REFERENCE: Lane, L. J., Woolhiser, D. A., and Yevjevich, V., Colorado State University Paper No. 81 (December 1975) "Influence of Simplifications in Watershed Geometry in Simulation of Surface Runoff."

cascade model for an impulse input. For overland flow, peak discharge of the impulse response is affected by the surface shape.For overland flow, peak discharge of the impulse response is greater for parabolic than for uniform slope surfaces.

For a concave channel, the index of concavity is related to the error in peak discharge. Underestimating the drainage density results in overestimated time characteristics and underestimated peak discharge. The first moment of a linear instantaneous unit hydrograph decreases as drainage density increases. The degree of apparent nonlinearity is affected by drainage density.

REFERENCE: Lane, L. J., Woolhiser, D. A., and Yevjevich, V., Colorado State University Paper No. 81 (December 1975) "Influence of Simplifications in Watershed Geometry in Simulation of Surface Runoff."

cascade model for an impulse input. For overland flow, peak discharge of the impulse response is affected by the surface shape.For overland flow, peak discharge of the impulse response is greater for parabolic than for uniform slope surfaces.

For a concave channel, the index of concavity is related to the error in peak discharge. Underestimating the drainage density results in overestimated time characteristics and underestimated peak discharge. The first moment of a linear instantaneous unit hydrograph decreases as drainage density increases. The degree of apparent nonlinearity is affected by drainage density.

REFERENCE: Lane, L. J., Woolhiser, D. A., and Yevjevich, V., Colorado State University Paper No. 81 (December 1975) "Influence of Simplifications in Watershed Geometry in Simulation of Surface Runoff."

cascade model for an impulse input. For overland flow, peak discharge of the impulse response is affected by the surface shape.For overland flow, peak discharge of the impulse response is greater for parabolic than for uniform slope surfaces.

For a concave channel, the index of concavity is related to the error in peak discharge. Underestimating the drainage density results in overestimated time characteristics and underestimated peak discharge. The first moment of a linear instantaneous unit hydrograph decreases as drainage density increases. The degree of apparent nonlinearity is affected by drainage density.

REFERENCE: Lane, L. J., Woolhiser, D. A., and Yevjevich, V., Colorado State University Paper No. 81 (December 1975) "Influence of Simplifications in Watershed Geometry in Simulation of Surface Runoff."